SUPPRESSION AND ENHANCEMENT OF BOILING ASSOCIATED WITH MULTIPLE DROPLET IMPINGEMENT

A Thesis

by

YUXUAN YANG

Submitted to the Office of Graduate and Professional Studies of
Texas A&M University
in partial fulfillment of the requirements for the degree of

MASTER OF SCIENCE

Chair of Committee,	Jorge L. Alvarado
Committee Members,	Michael Pate
	Hassan A. Yassin
Head of Department,	Andreas A. Polycarpou

May 2014

Major Subject: Mechanical Engineering

Copyright 2014 Yuxuan Yang

ABSTRACT

Spray cooling has proven to be efficient in managing thermal load in high power applications. Reliability of electronic products lies on the thermal management and understanding of heat transfer mechanisms of the most commonly used thermal management schemes such as spray cooling. Many experiments have been done to understand the heat transfer mechanisms associated with spray cooling. However, most of them have relied on comprehensive spray cooling experiments where multiple physical variables are at play simultaneously. Furthermore, experiments with single streams of droplets have not been able to elucidate the effects of the onset of boiling (ONB) during the droplet impingement process. Therefore, efforts have been undertaken to consider the effects of using three droplet streams arranged in a triangulated fashion. The effects of using triangulated multiple droplet impingements on the suppression or enhancement of boiling on heated surfaces has been investigated. Moreover, the effects of using screen laminated on the suppression of ONB during the droplet impingement process has been studied in detail. The main goal of this project is to study the effects of multiple droplet impingement on the flat heater surface in the spray cooling with and without the use of metallic screen laminates. Single and triple droplet impingement experiments have been performed to understand the droplet behavior in spray cooling systems where multiple droplets simultaneously impact a heated surface.

The experiments consisted of using a stainless steel screen laminate over a sample surface to observe the suppression or enhancement of pool boiling which tends to occur at the periphery of each droplet impingement zone. An infrared-based imaging technique was used to measure surface temperature during droplet impingement. The heat transfer performance has been evaluated in terms of heat flux, droplet frequency and volume flow rate. The results indicate that droplet stream spacing and the use of copper meshes can enhance surface cooling significantly. Specifically, droplet stream spacing of 1000 μm with copper meshes with a 6 mm hole and gap of 0.2 mm lead to enhanced surface cooling during the multiple droplet impingement process. It is expected that the results and conclusions of this study will be useful in understanding the physics of spray cooling which should help design better spray cooling system.

DEDICATION

To Dr. Jorge L. Alvarado for his inspiration, support and patience

To my family for their unconditional love

ACKNOWLEDGEMENTS

I would like to thank my advisor, Dr. Jorge L. Alvarado, and my committee members, Dr. Michael Pate and Dr. Yassin A. Hassan, for their guidance and support throughout the this research.

I would also like to thank my friends, the colleagues and the department faculties and staff for making my time at Texas A&M University a great experience. I appreciate Taolue Zhang, Ph.D. student, for his support throughout this research. Finally, thanks to my parents for their encouragement and to my girlfriend for her company and love.

NOMENCLATURE

A	Area
C	Heat capacity
D	Digital count of infrared camera
D	Diameter
$d_{32.}$	Sauter-mean diameter
f	Frequency
h.	Heat transfer coefficient
h_{fg}	Latent heat of vaporization
I	Current
k.	Thermal conductivity
L	Distance between droplets
M”	Mass flowrate
Nu	Nusselt number ((hd)/k)
P	Power
q	Heat
q”	Heat flux
Q”	Volumetric flowrate
Re	Renolds number ((ρvd/μ))
S	Droplet spacing
St	Strouhal number ((fd)/v
T	Temperature

T	Liquid film thickness
U	Uncertainty
V	Voltage
v.	Velocity
W	Irradiance
We	Weber number ($(\rho v^2 d)/\sigma$)
η	Fluid cooling efficiency
μ	Dynamic viscosity
ρ	Density
τ	Transmissivity

TABLE OF CONTENTS

Page

LIST OF FIGURES

Page

LIST OF TABLES

Page

1. INTRODUCTION

1.1 Motivation

With the development of electronic and computational systems, high speed calculations and high reliability of such system are needed eagerly. Due to these requirements, new cooling technologies should be developed to reduce very high heat flux in many industrial applications including electronic cooling. Conventional air- and water-based technologies have been developed to handle these problems, but they can only deal with low heat flux, which is in the range of 5 to 20 W/cm^2. Therefore, new phase change cooling technologies should be proposed that can handle high heat flux values as high as 1000 W/cm^2. Among the most promising phase change–based cooling schemes, spray cooling is thought to be the most appropriate because of its reliability, uniformity and heat transfer capacity.

Compare to pool boiling, spray cooling can handle higher heat flux values because of its ability to dissipate heat at higher critical heat flux (CHF) values than in pool boiling. Furthermore, the surface temperature distribution found in spray cooling systems is more uniform than that of jet cooling, which makes spray cooling much more reliable than jet cooling, especially in applications where precise electronic devices are needed.

Heat dissipating capability in spray cooling is determined by numerous correlated factors including coolant type, nozzle type, nozzle-to-surface distance, droplet diameter, droplet frequency, droplet velocity and volumetric flow rate. The study of each parameter independently using a spray cooling set-up is difficult to carry out. In this project, surface heat flux, droplet frequency and liquid volume flow rate were considered independently in order to compare the heat transfer performance of multiple droplet spray cooling including the effects of the screen laminates.

1.2 Objectives

The objective of this study is to observe multiple stream droplets impinging on a surface when it is subjected to constant heat flux. This is the first study when the effects of using triangulated multiple droplet streams have been considered. Single and triple stream droplet impingement cooling experiments have been performed in an effort to minimize the number of physical parameters necessary to elucidate the main mechanisms in droplet impingement. In this project, triple streams of droplets impacting a heated surface arranged in an equilateral triangle shape was used since it represents the most basic impingement pattern in a possible spray cooling system. The used patterned in very repeatable, which should be easy to extend into other multiple stream droplet impingement schemes. The effects of screen laminates on pool boiling of the surface area was also

studied. The screen laminates were used to suppress and enhance pool boiling. The following is a brief summary of the tasks that were undertaken as part of the study.

1.3 Organization of this work

Section 2 provides a detail literature review of current research about spray cooling, which includes single droplet impingement, multiple droplets impingement and screen laminates application in the boiling field. The present research was based on the knowledge gap found in these former studies.

Section 3 describes the experimental setup that was used to perform the heat transfer and visualization experiments. The fluid delivery system, heating system, data acquisition system, high-speed imaging system, infrared imaging system are represented in detail. Finally, experiments were conducted to decide the appropriate droplet frequency, volume flow rate and heat flux.

Section 4 presents the results including heat transfer performance of triangulated triple stream droplet impingements and the effects of screen laminates on pool boiling of the surface area.

Section 5 includes the conclusions and future work.

2. LITERATURE REVIEW

2.1 Spray cooling review

For the last few decades, numerous studies have been done in order to characterize the dominating parameters responsible for high heat transfer in spray cooling.

In the work of Monde [2] and Mudawar et al. [1], [3], several parameters of spray cooling were studied and they concluded that CHF was the mostly dependent on volumetric flow rate. Mudawar [3] also suggested that Sauter mean diameter (d_{32}) and nozzle-to-surface distance also have strong influence on spray cooling.

Kopchikov et al. [4] found that CHF in film boiling are several times larger than those in pool boiling. They used distilled water, ethanol, carbon tetrachloride and benzene as the test fluids. They have changed some of the fluid supply conditions such as: nozzle-to-surface distance, jet inclination to the heated surface and spray nozzle diameter; but they suggested that these mentioned characteristics have no effect on the heat transfer process within a certain range.

Toda [5, 6] obtained a heat transfer curve using distilled water for a wide range of surface temperatures, generating a heat flux temperature plot similar to pool boiling curve. Nucleate boiling, transitional, and film boiling were identified in their study. They also estimated droplet diameter which was 117μm, with droplet impact velocities of 72.4m/s

and the Weber number was calculated to be 8,750. But all the data were not measured directly. They showed that spray volume flow rate has the strong effect on cooling performance, while subcooling of the spray liquid hardly had any effect.

Other researchers [7, 8, 9, 10] used pressure-atomized nozzles in their liquid delivery systems. Tilton [7] used water as the test fluid and an1cm×1cm copper sample as the heated surface. Droplet diameters ranges from 50 to 100μm and the velocity was 9 m/s. Tilton [7]indicated that heat transfer was dependent on droplet velocity and droplet diameter which were used to determine Weber number. Smaller droplets were also suggested due to the formation of a thinner film during impingement.

Navedo [8] found that droplet impinging frequency and droplet velocity were proportional to Critical Heat Flux (CHF) and heat transfer coefficient (h) at CHF. Also the Sauter Mean Diameter (d_{32}) was found to be inversely proportional to heat transfer coefficient at CHF but has no directly effect on CHF value.

Ortiz et al. [9] used distilled water as the cooling fluid. Mass flow rate, surface roughness, subcooling temperature, and spray impact angle were considered and investigated because they may have influence on the stable two phase flow behavior. Their experiment results showed that heat flux would increase with mass flow rate and surface roughness, but heat flux would decrease with the impact angle increasing.

Estes et al. [10] used different working fluid such as FC-72, FC-87 and water. The research team presented a correlation between heat transfer performance and Sauter Mean

Diameter (d32) of droplets. The results also suggested that CHF increased with the increasing of mass flow rate and subcooling. Most significant contribution part was the postulation of correlation (2.1) which could accurately predicts CHF for FC-72, FC-87 and water and many different full cone nozzles within a wide range of flow rate and subcooling.

$$\frac{qc''}{\rho_q h_{fg} Q''} = 2.3\left(\frac{\rho_f}{\rho_g}\right)^{0.3}\left(\frac{\rho_f Q''^2 d_{32}}{\sigma}\right)^{-0.35}\left(1 + 0.0019\frac{\rho c_f \Delta T_{sub}}{\rho_g h_{fg}}\right)^{0.98} \quad (2.1)$$

Cho et al. [11] showed that heat transfer rate was a function of superheat temperature and the Weber number defined in terms of the Sauter Mean Diameter (d_{32}) as indicated in Equation (2.2).

$$\frac{q''H}{\mu_f h_{fg}} = 93.8 We_{d_{32}}{}^{0.43}\left(\frac{c_f \Delta T_{sup}}{h_{fg}}\right)^{0.98} \quad (2.2)$$

Tao et al. [12] used dionized water as the working fluid and they found out that non-boiling spray cooling system can remove high heat flux from a small surface while maintaining the surface at desirable low temperatures. Increasing the liquid volume flow rate or reducing the liquid inlet temperature would increase the heat transfer coefficient (h). The most significant contribution from their work is the effect of the nozzle-to-surface distance on the heat transfer coefficient as shown in Figure 1.In the article, the reported

nozzle to surface distance ranged from 7 to 22 mm, and the maximum liquid volume flow rate of each nozzle was 8.67×10^{-6} m^3/s.

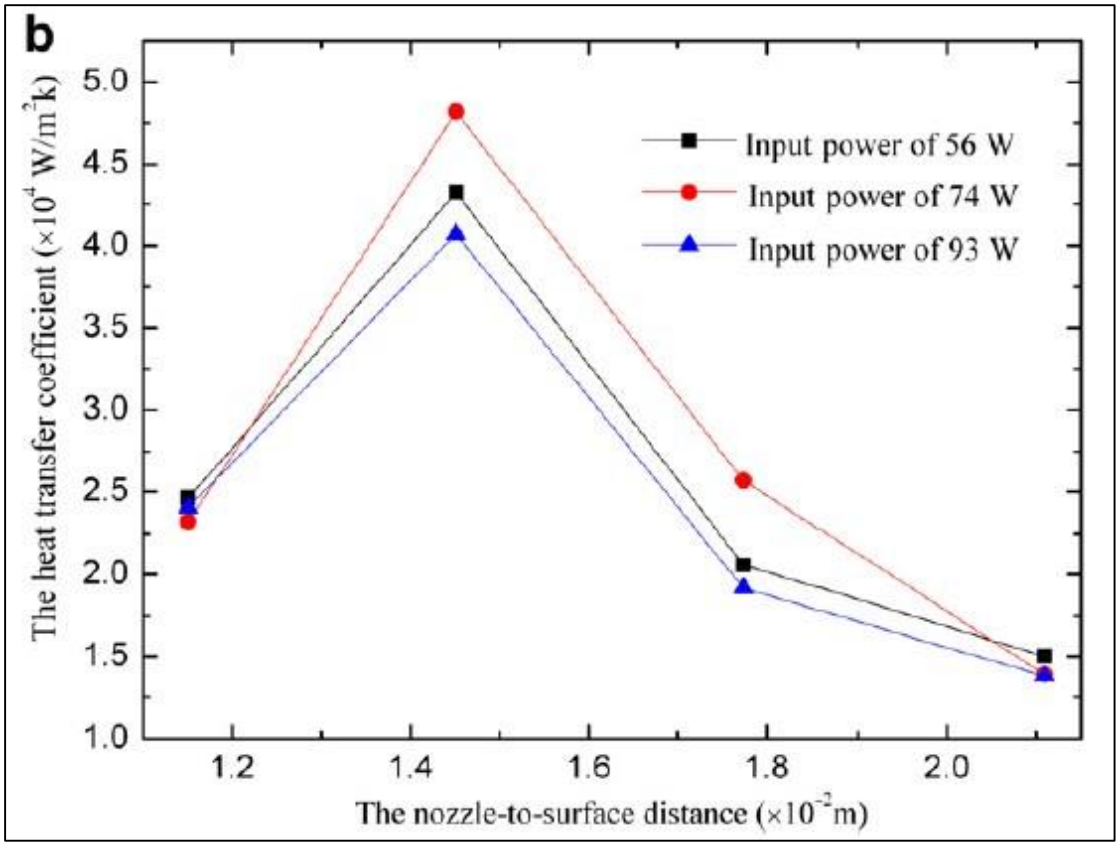

Figure 1. Heat transfer coefficient as a function of nozzle-to-surface distance [12]

Zhang et al. [13] also presented optimal orifice-to-surface distance results in their article. Deionized water was also used as the cooling fluid in the study using both flat and enhanced surface as heater surfaces. The volumetric flow rate ranged from 22.2L/h to 60.8L/h, and the orifice-to-surface distance varied from 0.5 cm to 3.0 cm with spray

inclination angles from 0to 45°. They found out that the best orifice-to-surface distance for spray cooling when using flat surfaces was 1.5cm. Another helpful conclusion was that the optimal inclination angle was 0° in terms of heat transfer performance.

Yan et al. [14] used normal and inclination sprays to show the effects of inclination on thermal performance for the same spray coverage area and flow conditions. The results from their study indicate that normal sprays lead to uniform surface temperature distribution at different flowrates as shown as Figure 2. I summary, normal sprays are better than inclined sprays in terms of temperature distribution.

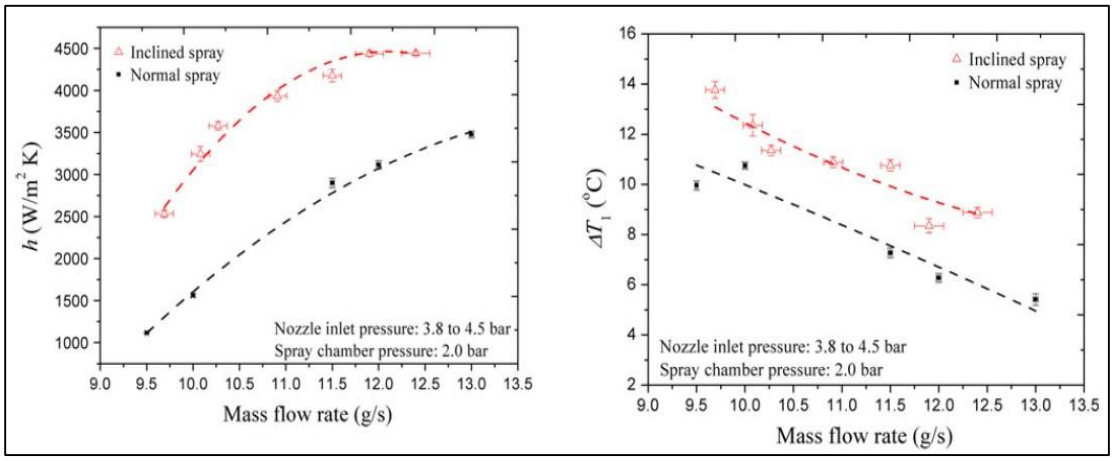

Figure 2. Normal spray and inclined spray at different flowrates [14]

Fabris et al. [15] indicated that drops impinging on a liquid film, spread without splashing leading to high-efficiency and stable heat transfer behavior. Distilled water was used in their experiment when using both single and dual nozzles in their experimental

setup. The droplet impingement frequency ranged from 2 kHz to 8 kHz. They determined that the heat flux is proportional to mass flow rate but not directly related with the wetted area. The most significant conclusion from the point of view of the current study was the effect of droplet velocity on the occurrence of splashing. It was concluded that at low velocities, splashing is not likely to happen when droplets impacting the thin liquid film.

Tsai [16] studied single stream droplet impingent cooling at different impact angle, and also double streams droplet impingement cooling with different spacing and impact angles. The author suggested that for spray cooling, a 0° impact angle leads to the best heat transfer performance. From the double stream droplet impingement cooling test results, the optimum spacing of multiple droplet impingement was given, which was also found to be proportional to the flow rate per droplet stream. In addition, for fixed flow rate, dryout was found between adjacent impacts when the spacing was larger than a critical spacing value, which caused large temperature variation within the two adjacent craters. On the other hand, fluid collision was observed when the spacing became smaller than the critical spacing, which led to the spreading-splashing mode and lower heat transfer.

2.2 Multiple nozzles spray cooling review

Pautsch et al. [17] studied the effects of multiple nozzle arrays of spray cooling on heat transfer. The cooling performance was evaluated by calculating its spray efficiency.

Spray efficiency is limited by the area first exposed to CHF. This area often occurs at the center region of the heater due to flow interactions from adjacent nozzles. Moreover, a stagnation region in the liquid film could exist between neighboring spray zones at the surface where heat transfer is adversely affected. The authors suggested that heat transfer performance was sensitive to nozzle spacing and the arrangement of spray nozzles.

Hou et al. [18] simulated the multiple nozzles spray cooling with CFD method based on the fundamentals of air flow and liquid droplet collision dynamics. They concluded that the main multiple nozzles spray variables should include the Sauter Mean Diameter (d_{32}) of droplets and the mass weight average droplet velocity since they are significantly influenced by the nozzle inlet pressure, the nozzle-to-surface distance, and the number of nozzles. Water was used as the simulated cooling fluid. They indicated that the droplet Sauter Mean Diameter increases linearly with mass flux. Also, it was found that the average droplet velocity also increases with the mass flux. Hou [18] found that with a linear arrangement of nozzles, increasing nozzle number should decrease the average droplet velocity without affecting the droplet size. They also concluded that with an increase in the number of nozzles, the distributions of droplet size and droplet velocity will be improved greatly.

Soriano [19] studied single and triple droplet impingements under constant heat flux conditions. From his single stream tests, the author suggested that forced heat convection is the main heat transfer mechanism inside the crown formation formed by droplet

impingement. Impact regimes also play an important role on heat transfer behavior. Spacing among adjacent droplets was found to be the most important factor for multiple droplet stream heat transfer behavior.

Lin [20] studied spray cooling over a bare and a nano-structured surface with single and triple stream droplets. He used FC-72 as the cooling fluid, silicon as the material of the heater for both bare and nano-structured heater surfaces. Lin [20] measured heat transfer performance with single and triple droplets, and also adjusted the spacing of the triple streams. His results showed that for triple streams, larger spacing (2000μm) leads to a uniform temperature distribution than smaller (500μm) spacing as shown in Figure 3. The results clearly indicate that larger spacing could provide better heat transfer performance by maintaining lower minimum wall temperature and more uniform surface temperature distribution especially at high heat flux condition than at smaller spacings.

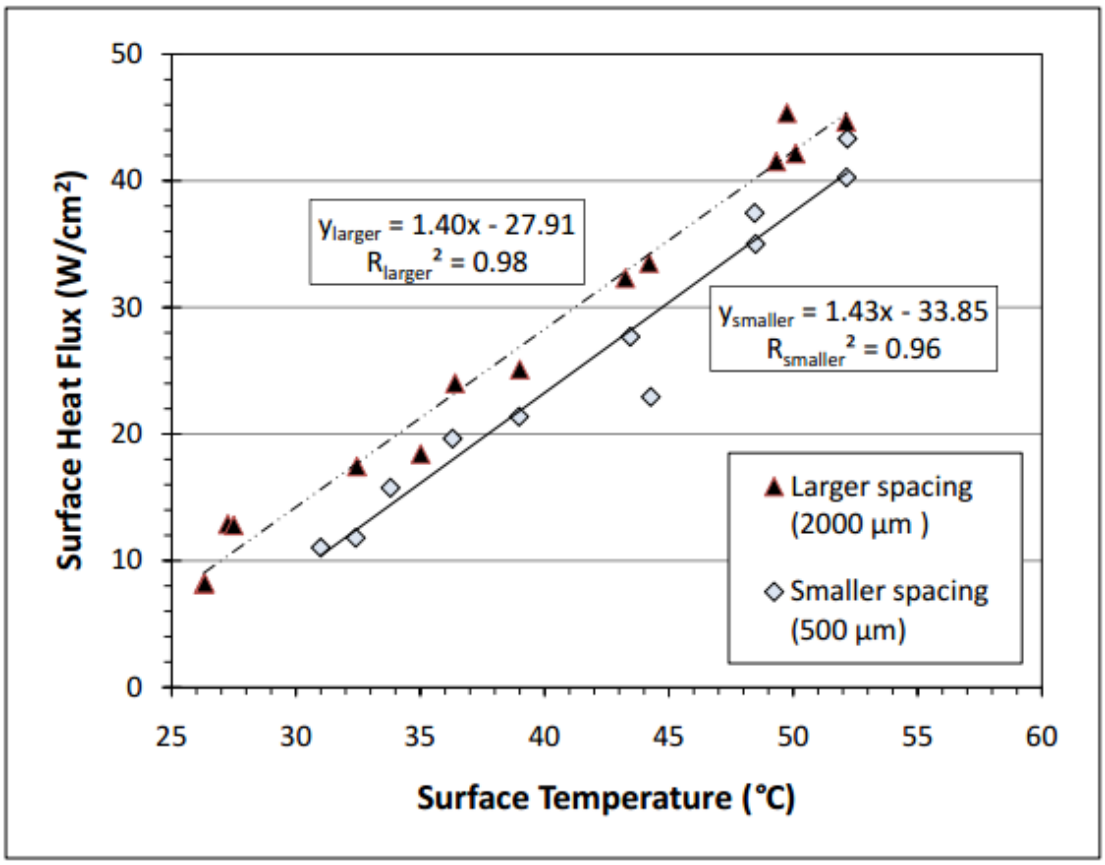

Figure 3. Minimum wall temperature for triple droplet stream cooling with 500 µm and 2000 µm stream spacing [20]

On the other hand, droplet streams with smaller spacing showed a wide and flat local temperature distribution, which indicate the advantage of moderating temperature gradient within a small area. Curves in Figure 4and 5 showed that smaller spacing between droplet streams can provide a more intensive cooling in a small area.

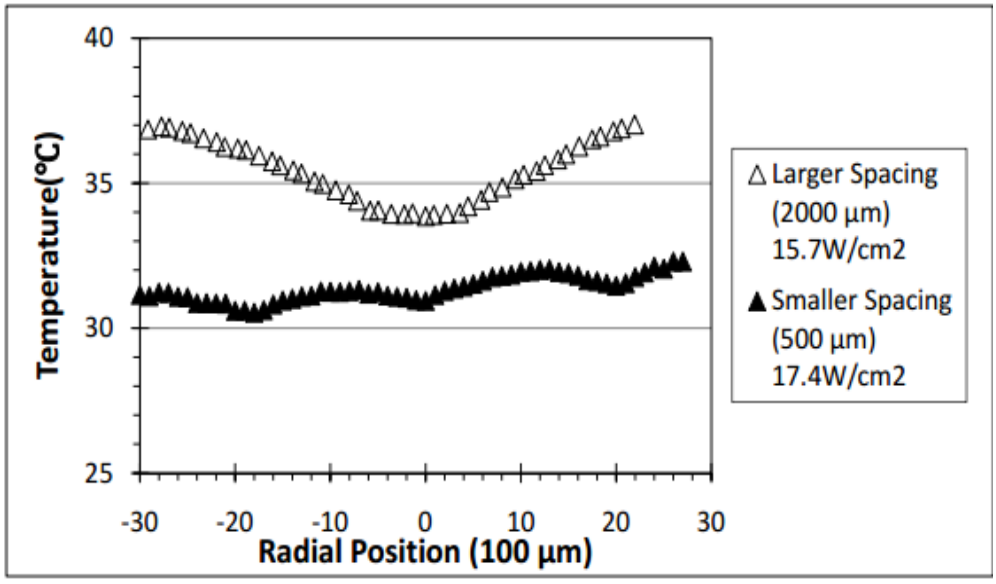

Figure 4. Radial temperature distribution for triple droplet stream cooling with different stream spacing (500 µm and 2000 µm) under low heat flux condition [20]

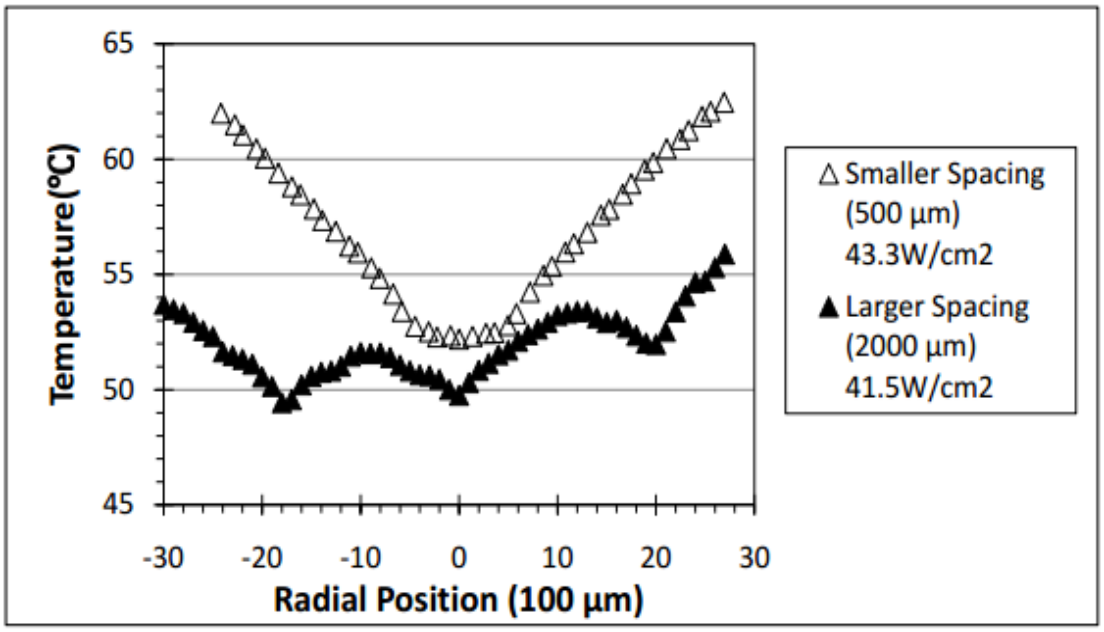

Figure 5. Radial temperature distribution for triple droplet stream cooling with different stream spacing (500 µm and 2000 µm) under high heat flux condition [20]

2.3 Mesh laminates review

Holland et al. [21] studied flow boiling with multi-layered screen laminates using porous extended surface matrices (ESMs). The authors suggested that screen laminates can effectively enhance heat transfer over a surface in terms of both surface temperature and heat flux.

Sloan et al. [22] used copper mesh laminates in their study with three different sizes including 50, 80 and 145 (Number of filaments per inch). They used deionized distilled water as the working fluid. Figure 6 shows that the unenhanced surface experiences on set of boiling (ONB) at a 7K superheat, while the surface with screen laminates experiences ONB at only 2K superheat.

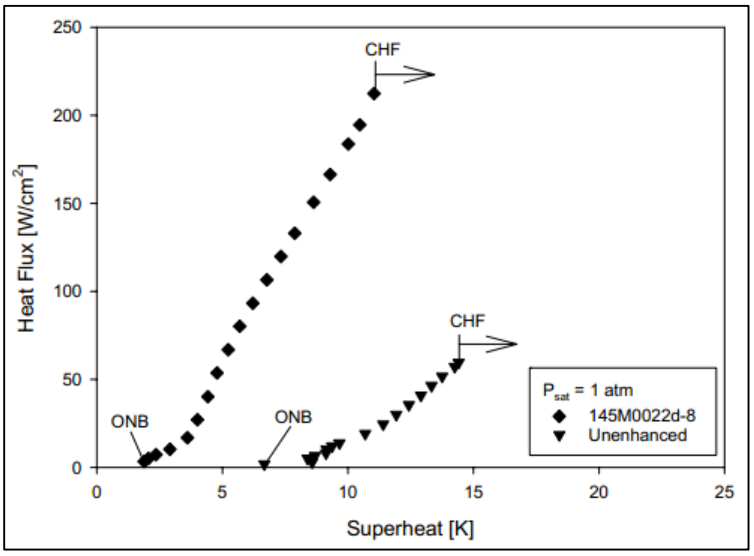

Figure 6. Comparison of Onset of Nucleate Boiling (ONB) using mesh laminates on enhanced and unenhanced surfaces [22]

They studied the lamination sublayer and concluded that the laminates may preheat the working fluid next to the edge of the test surface. Although the lamination sublayer might not be hot enough to induce local boiling, it could still provide some heat to the fluid. After comparing all the surfaces with different sizes of screen laminates, Sloan [22] presented that the best enhancement surface in terms of boiling performance was the finest mesh, thickest lamination surface at all pressures. For this surface, a CHF of 212 W/cm^{2}at a superheat of 11 K and 1 atm of pressure was obtained.

In general, this research was very helpful in the current study since it facilitated the selection of screen laminates that could enhance and suppress boiling within the droplet impingement region. Based on their results, heat transfer performance improved as the pore hydraulic diameter decreased and the thickness (number of layers) of the lamination was increased. The rapid coalescence of departing bubbles on the lower part of the test surfaces help swept the upper area of the test surfaces, possibly contributing to improved heat transfer. Also, increased contact between the mesh layers and the heater surface led to an increased in effective thermal conductivity, which also contributed to improved heat transfer.

Li and Peterson [23] showed experimentally that in pool boiling, having multiple layers of screen laminates leads to enhanced thermal performance.

2.4 Identification of gaps in current knowledge base

In the multiple arrays spray cooling studies conducted by Pautsch [17], Hou [18], Soriano [19] and Lin [20], only linearly arranged orifices were considered in their experiments. Pautsch [17] suggested that heat transfer performance is sensitive to nozzle spacing and the arrangement of spray nozzles. Lin [20] indicated that larger spacing in the case of droplet impingement could provide more uniform surface temperature distribution and better heat transfer performance. So understanding how the spacing and arrangement of droplet stream affect surface cooling heat transfer performance is very important to better explain the spray cooling mechanisms in the future.

In the studies for screen laminates in cooling or boiling, Holland [21], Sloan [22], Li and Peterson [23] suggested that screen laminates could improve heat transfer performance on a heated surface. Li and Peterson [23] used multiple layers of screen laminates over a heated surface, and claimed that multiple layers are more efficient than a single layer. However, the effects of screen laminates on heat transfer performance over a heated surface in spray cooling have not been explained clearly, and the suppression effect of screen laminates on boiling surrounding the droplet impingement zone still has to be considered and evaluated experimentally.

3. EXPERIMENTAL SETUP AND METHODOLOGY

In order to achieve the proposed objectives of this research project, an experimental setup was designed, built and calibrated accordingly. The experimental setup consisted of three main parts, which are: Fluid Delivery System, Heater System and Data Acquisition System as shown in Figure 7.

The Fluid Delivery System comprised of a syringe pump, a droplet generator and a frequency generator. The Heater System consisted of a power supply and the assembled heater. The Data Acquisition System included a computer, a high speed camera and an infrared camera.

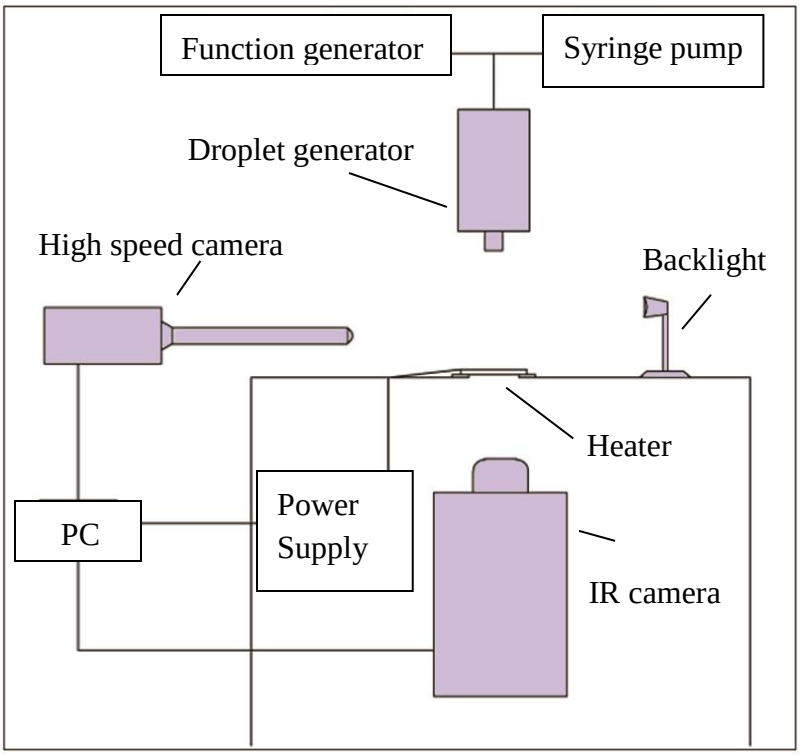

Figure 7. Experimental setup (schematic)

3.1 Fluid delivery system

In this research project, 3M™ Novec™ Engineered Fluid HFE-7100 was chosen as the coolant. HFE-7100 has been used in many applications as cleaning fluid, deposition solvents and heat transfer fluid. It is the appropriate coolant for this project because of its relatively low boiling point (61℃) and non-electrical conductivity. Some of physical and chemical properties are shown in Table 1(all properties specified at 25 ℃).

Table 1. Physical and chemical properties of HFE-7100

Physical Property	**Value**
Boiling Point (℃)	61 (@760mmHg)
Freezing Point (℃)	-135
Density (g/ml)	1.5
Latent Heat (J/g)	111.6
Specific Heat (J/kg.℃)	1183
Surface Tension (dynes/cm)	13.6

The HFE-7100 fluid was filled into the syringe always after being filtered using a 20 μm filter to avoid small particles from blocking or clogging the orifice plate hole. The syringe with a liquid volume of 120 ml was place in the syringe pump which was used to

provide precise volume flow rate. The end of the syringe was connected to the piezoelectric droplet generator using a 1.6mm plastic tubing. The piezoelectric droplet generator was made by TSI, model MDG100. Square waves were delivered by the frequency generator (Model 401A by BK Precision).

A three (triangulated) hole orifice plate was attached at the end of the droplet generator to dispense three identical droplet streams. The orifice plate was made of BeCu with a thin layer of Ni, and the hole was etched to ensure a smooth perimeter around each hole. Two orifice plates were used in this research project with different hole center-to-center distance. The plates had center-to-center distance and hole diameter of 1000 μm and 150 μm, and 750 μm and 150 μm, respectively. Figure 8 shows the orifice plates used in the study. Theoretically, the three streams of droplets should be parallel to each other and the droplets should have the same velocity. The gravity effect on the velocity was found to be less than 4%, so the droplet velocity was assumed to be constant in this project.

750 µm center to center orifice plate 1000 µm center to center orifice plate

Figure 8. Orifice plates

3.2 Heater system

Silicon was chosen as the substrate of the heater because of its IR range (1 µm to 10 µm) which makes translucent from the IR camera's point of view. The dimension of the substrate was 15 mm by 10mm, and its thickness was 0.5 mm. A 100 nm thick Indium Tin Oxide (ITO) coating was placed on the top surface of the Silicon substrate to serve as heating element. Two copper wires were attached on the very edge of the surface using an electrically conductive epoxy. The effective area for heat transfer testing was about 0.9 cm^2. The wires were connected to the Power Supply (Lambda GEN600-2.6). The Power Supply was controlled by the computer using the Microsoft HyperTerminal. The Silicon substrate was attached on top of the Teflon-based sample holder using insulation epoxy. The heater system is shown in Figure 9.

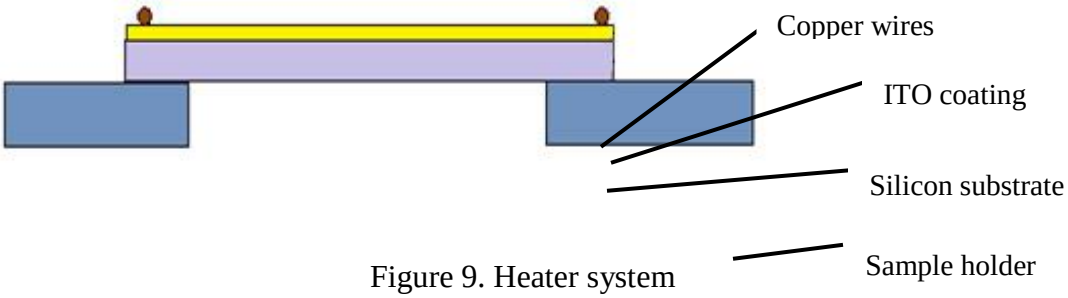

Figure 9. Heater system

3.3 Infrared imaging system

Temperature was measured using an IR camera (FLIR SC7000) located below the heater system. The distance from the IR camera to the sample surface was about 90 mm, and the field of view was about 18.2 mm by 12.9 mm. The resolution of the lens was 25 μm/pixel. The temperature range of this model IR camera is between 5 °C to 300 °C with an accuracy of ±1 ℃. Figure10 shows a typical IR example image for the three triangulated droplets impact case.

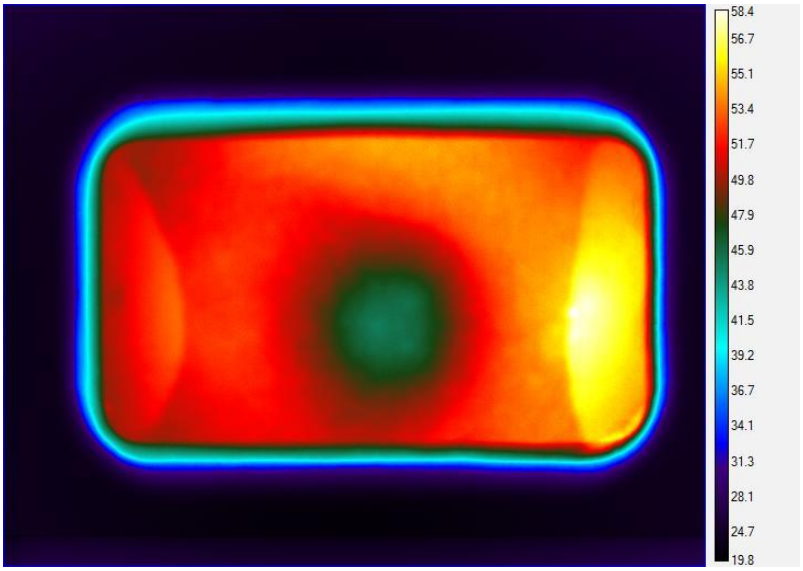

Figure 10. IR example image

3.4 High-speed imaging system

A Photron SA3 high speed camera was used in this research project. The maximum image capture rate was set to 60,000 frames per second. The maximum vision of this camera was 1024 by 1024 pixel. However, the resolution was varied as the lens and the film rate were changed. The camera was located both on the left side of the droplet generator to capture the images of droplets or at 60° with respect to the vertical axis for capturing images at the impact craters during the droplet impingement process. A 250W backlight was used for illumination in order to capture better images with the high-speed camera. Figure 11 shows the Photron AS3 model of the high-speed camera and Figure 12 shows the positions of the camera used during the experiments.

Figure 11. Photron AS3 model of high-speed camera

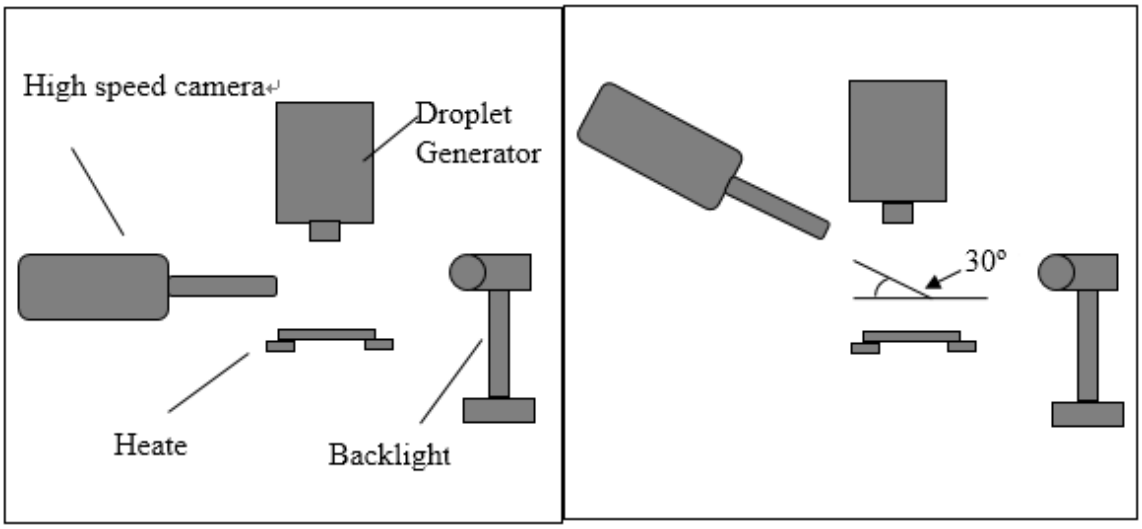

Figure 12. Two positions of the high-speed camera

3.5 Data acquisition system

For the infrared camera, we used the Thermal Vision Examine IR as the imaging software. Through changing the variables such as surrounding (reflective) temperature, environmental temperature, emissivity, measuring distance and environmental humidity, the temperature distribution image can be obtained using the software. Then CSV format

files could be exported as comma-separated values, which were analyzed using a Matlab code for calculating average temperature, minimum temperature, maximum temperature and some other relative information.

For the high-speed camera, we used the Photron FASTCAM Viewer to record and export the images and movies. The high speed camera was also used for measuring droplet diameter and droplet velocity, and also the impact craters.

3.6 Multiple droplets impingement experiment

Before running the heat transfer experiments, the high-speed camera was used to observe the multiple droplet streams to determine the optimal flowrates and impingement frequencies that would results in stable streams.

The experimental setup was adjusted as shown in Figure 7. Discrete and stable, and unstable droplet streams were imaged to determine the effect of droplet frequency, flowrate, and spacing on stream stability. Two different sets of experiments were conducted to determine the effect of center-to-center hole distance within the orifice plate on stream behavior.

The first test considered a center-to-center distance of 750 μm. With this orifice plate, droplet stream movies were recorded at flowrates of 450 ml/hr, 480 ml/hr and 510

ml/hr. For each flowrate, several droplet generation frequencies were considered. Figure 13, 14 and 15show multiple droplet streams at different frequencies and flowrates.

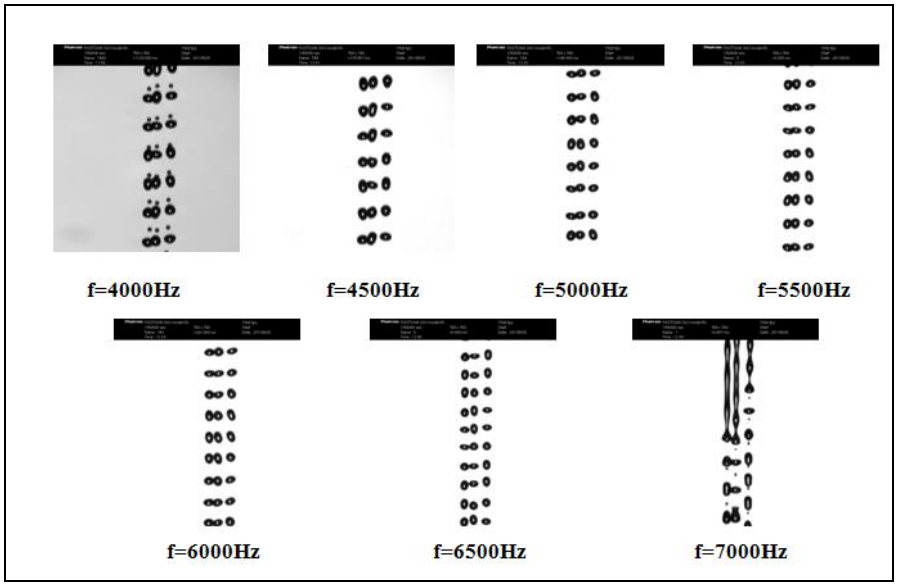

Figure 13. Image for multiple droplet streams with 750µm center-to-center hole distance within the orifice plate at a flowrate of 510ml/hr

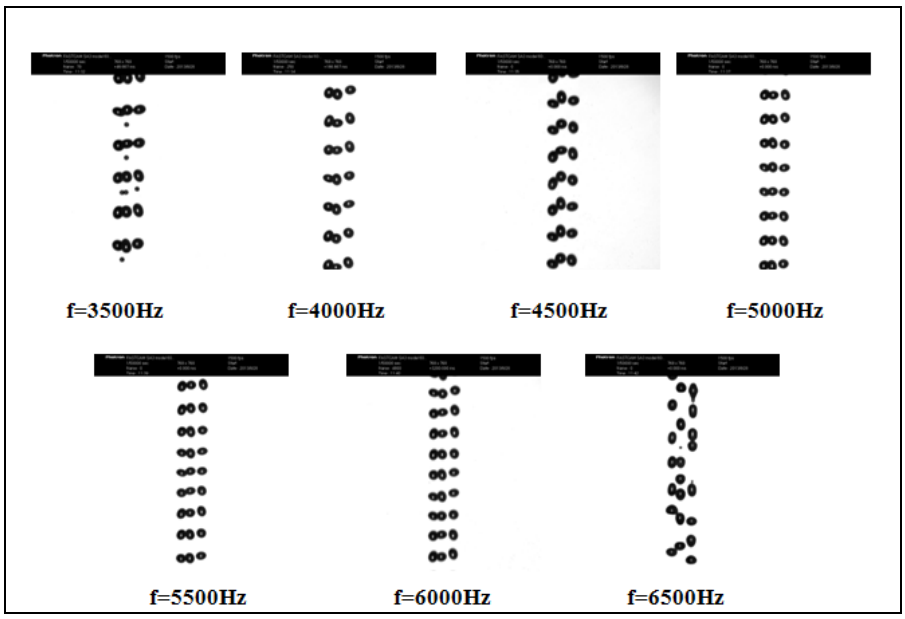

Figure 14. Image for multiple droplets with 750µm center-to-center hole distance within the orifice plate at a flowrate of 480ml/hr.

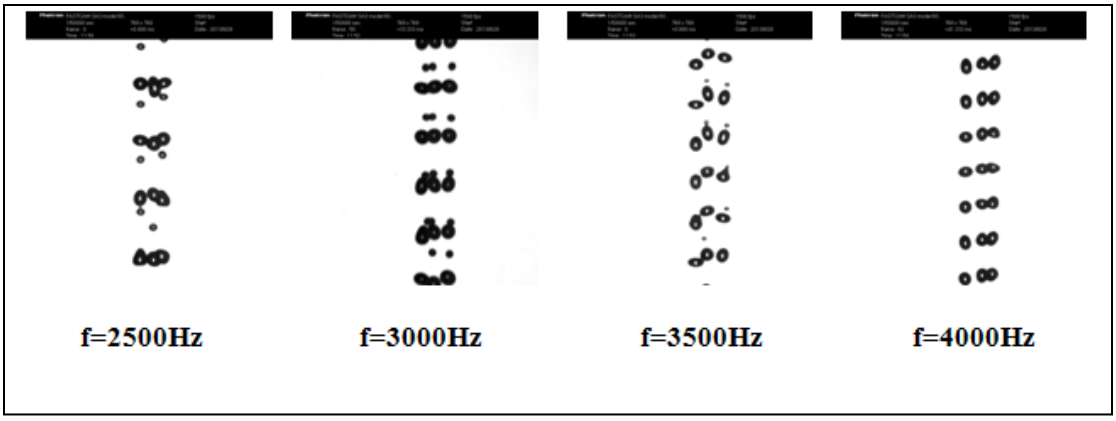

Figure 15. Image for multiple droplets with 750μm center-to-center hole distance within the orifice plate at a flowrate of 450ml/hr.

As seen in Figure 13, some droplets collided or coalesced with neighboring droplets at a flowrate of 510ml/hr and frequencies less than or equal to 4000Hz. The same behavior was observed at a flowrate of at 480ml/hr and frequencies less than or equal to 3500Hz as seen in Fig. 14. Also at frequencies as high as 7000 Hz, droplets were observed to fall down discontinuously at a flowrate of 510ml/hr. The same behavior was observed at 6500 Hz at a flowrate of 480ml/hr. For a flowrate of 450ml/hr, droplet streams oscillated with respect to the vertical axis slightly, so those conditions were not used for any heat transfer test. In summary, the flowrate and droplet frequency had to be adjusted to avoid unstable behavior.

The tests were repeated when the center-to-center hole distance within the orifice plate was set at 1000 μm for the same flowrates. Results of those tests are shown in Figure 16, 17 and 18.

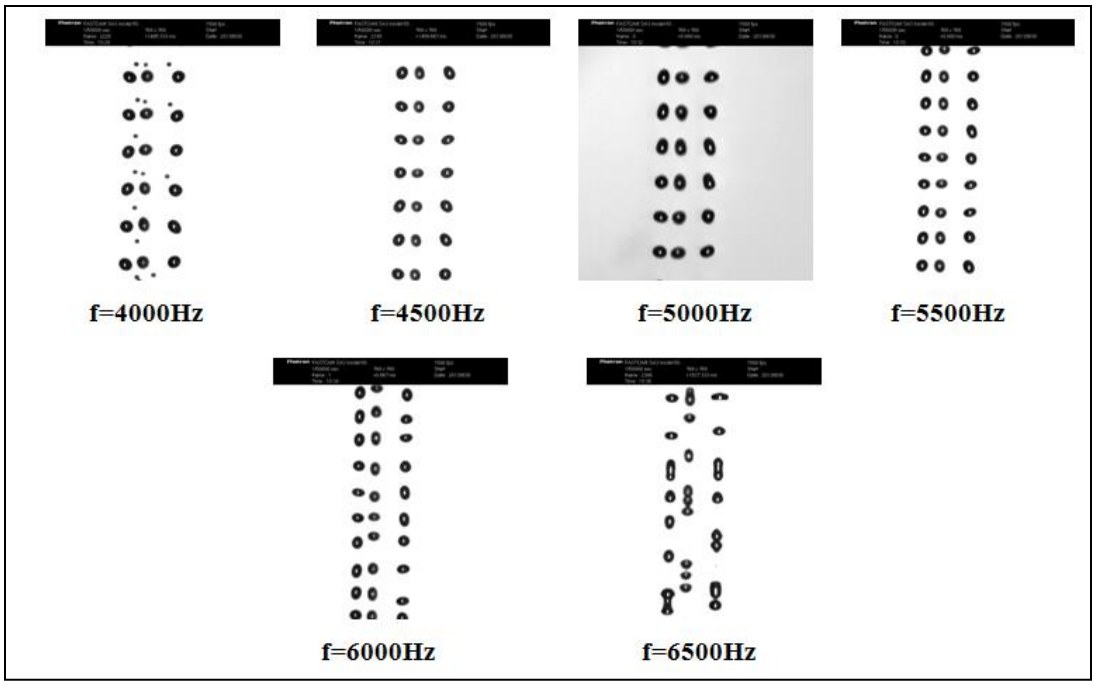

Figure 16. Image for multiple droplets with 1000µm center-to-center hole distance within the orifice plate at a flowrate of 510ml/hr.

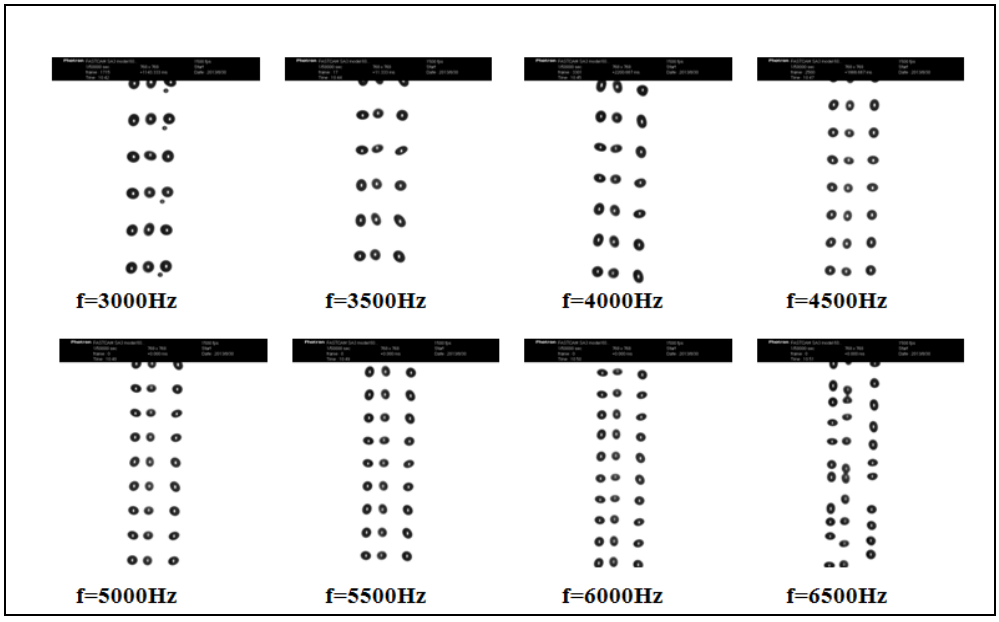

Figure 17. Image for multiple droplets with 1000µm center-to-center hole distance within the orifice plate at a flowrate of 480ml/hr

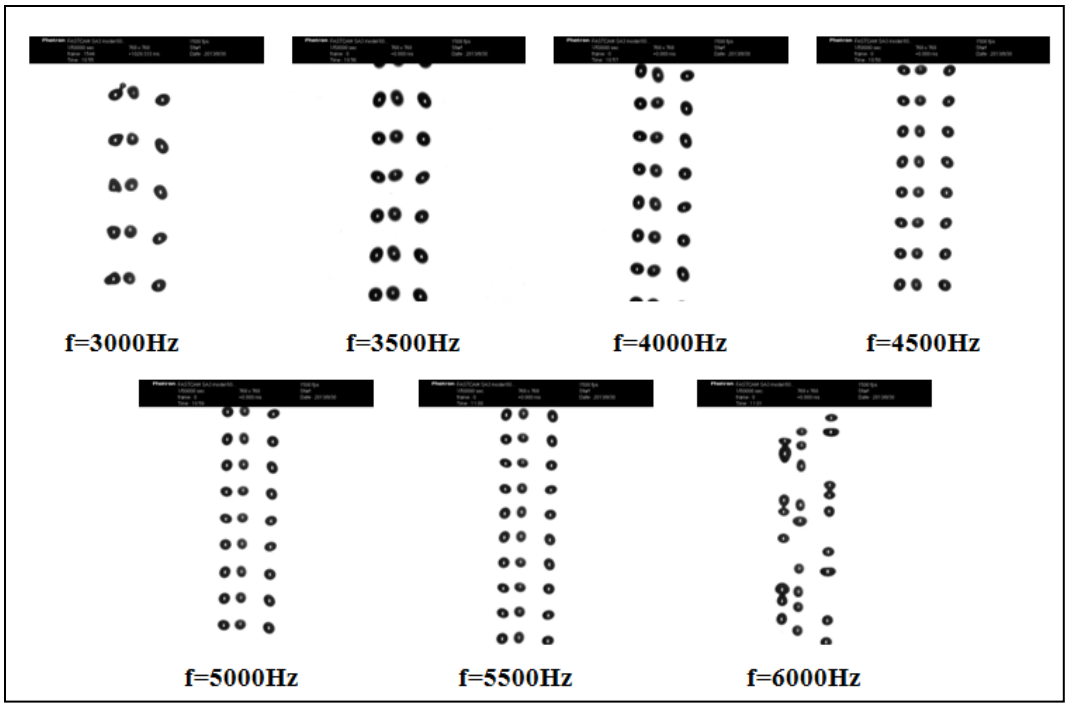

Figure 18. Image for multiple droplets with 1000µm center-to-center hole distance within the orifice plate at a flowrate of 450ml/hr

For the 1000µm center-to-center hole distance, oscillations of the droplet streams were not observed.

In conclusion, the flowrates and frequencies had to be adjusted to ensure stable and discrete droplet streams for all the heat transfer experiments. Table 2 shows the acceptable conditions considered during the heat transfer tests.

Table 2. Flowrate and relative frequencies selection

750μm center-to-center hole distance						
Flowrate(ml/hr)	Frequency (Hz)					
510	4500	5000	5500	6000	6500	
480	4000	4500	5000	5500	6000	
100μm center-to-center hole distance						
Flowrate(ml/hr)	Frequency (Hz)					
510	4500	5000	5500			
480	3500	4000	4500	5000	5500	6000
450	3500	4000	4500	5000	5500	

Once the fluid delivery system conditions that would ensure the formation and delivery of stable droplet streams were identified, the focus of the study shifted to the use of droplet streams for surface cooling. Before each heat transfer test, the heater surface was inspected and cleaned. Isopropyl alcohol was used to wipe the surface before drying it using an air duster. The IR camera was also used to check whether the top surface showed any hot spots caused by possible particle contamination or sample damage.

After making sure the heater surface was clean, the thermal distribution of the sample was assessed using the infrared camera. For each orifice plate case, the sample heated up until it reached a certain heat flux value under each combination of flowrate

and droplet frequency. The results of the heat transfer experiments are discussed in section 4.

3.7 Screen laminates experiment

Screen laminates were made of copper and aluminum with different sizes to be able to determine their effects of surface cooling and suppression of pool boiling in droplet impingement experiments. Screen laminates were cut into 0.7 mm by 35 mm sections which were suitable for the size of heating sample. Then, different holes were cut of different sizes to make sure the screen laminates did not obstruct the impinging streams. The sizes of the holes were based on the dimension of the impact craters. Because the dimension of the impact craters were 1000 μm and 500 μm, respectively, the hole diameters were 2.5 mm, 4.5 mm and 6 mm. Table 3 presents the screen laminates properties. Table 4 presents the properties of copper and aluminum.

After cutting the screen laminates, wooden stages were built to ensure the laminates could rest on them to avoid any direct contact with the heater surface. The gap between each screen laminate and the heater surfaces was fixed accordingly. Figure 19 shows the screen laminates setup used in the experiments.

Table 3. Properties of copper and aluminum screen laminates or meshes

	Mesh Size (filaments per inch)	Opening Size, mm (inch)	Open Area	Wire Diameter mm (inch)
aluminum	50x50	0.28 (0.011)	30%	0.23 (0.009)
	120x120	0.11(0.0043)	27%	0.1(0.004)
copper	60x60	0.23(0.009)	30%	0.19(0.0075)
	100x100	0.15(0.006)	30%	0.11(0.0045)

Table 4. Properties of copper and aluminum at 300 K

	ρ (kg/m^3)	c_p ($J/kg \cdot K$)	k ($W/m \cdot K$)	$\alpha \cdot 10^6$ (m^2/s)
aluminum	2702	903	237	97.1
copper	8933	385	401	117

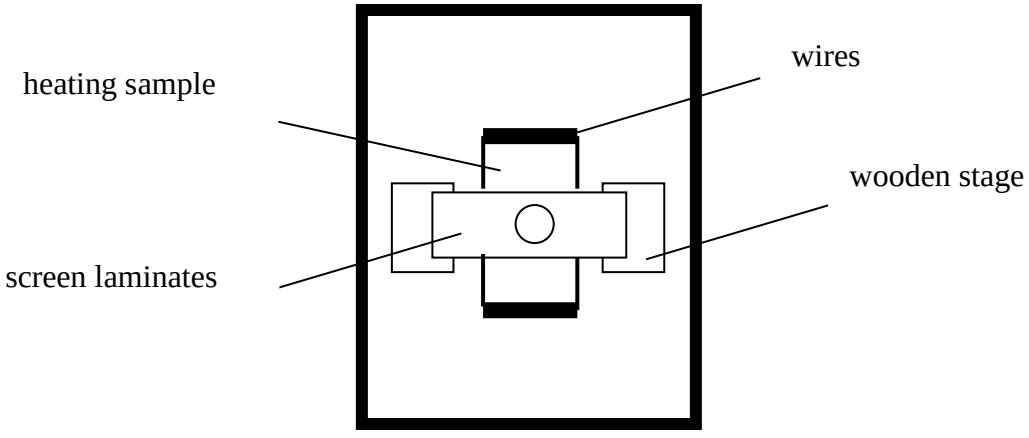

Figure 19. Heater setup

Heat transfer experiments were undertaken by considering the same variables as in the multiple droplets impingement experiments. Results and plots for the screen laminate cases are presented and compared in Section 4.

4. RESULTS AND DISCUSSION

In this section, heat transfer performance and droplet characterization of droplets impinging on a heated surface are presented based on data acquired using IR and high speed imaging systems. First, single stream droplet and three triangulated arranged stream droplets tests were undertaken and heat transfer results under conditions of different frequency, flow rate and spacing are presented. Weber number and Strouhal number are presented along with surface temperature. The relationship between surface temperature and radial distance along the impinged liquid film is presented graphically. Then, heat transfer data for cases where metallic screen laminates were used are presented as well.

4.1 Droplet characterization

As piezo-electric droplet generator was used in this research to produce monodispersed stream of droplets. The streams were characterized using a high-speed camera. The effect of drag force and gravity at the point of impact can be neglected because of the small size of the droplets used in the experiments. As a result, initial droplet velocity measured at the outlet of droplet generator was assumed to be the same as the impact velocity. Droplet diameter (d_d) and droplet velocity (v_d) were measured and their theoretical values were calculated using Equations 4.1and 4.2.

$$d_d = \left(\frac{6\dot{Q}}{\pi f}\right)^{1/3} \tag{4.1}$$

$$v_d = \left({v_j}^2 - \frac{12\sigma}{\rho d_d}\right)^{1/2} \tag{4.2}$$

Where the $\dot{Q}$ is flow rate, f is frequency, v_j is initial velocity of droplet stream which is calculated using Equation4.3,σ is surface tension of HFE7100 (which is 13.6 dynes/cm), ρ is the density of HFE7100 (which is 1.5 g/ml).

$$v_j = \frac{4\dot{\mathrm{V}}}{\pi \mathrm{d_j}^2} \tag{4.3}$$

Where d_j is the diameter of orifice. Droplet diameter and droplet velocity of both three droplet streams were measured and are presented in Table 5 and 6. In the table, the experimental value of droplet velocity was calculated using Equation 4.4.

$$v_d = Lf \tag{4.4}$$

Table 5. Average droplet diameter and average velocity for 1000 μm center to center horizontal spacing.

Flowrate(ml/hr)	Frequency (Hz)	Theoretical d_d(μm)	Experimental d_d(μm)	Theoretical v_d(m/s)	Experimental v_d(m/s)
510	4500	271.7	259.6	2.60	2.81
510	5000	262.3	268.5	2.59	2.95
510	5500	254.1	247.8	2.59	2.76
480	5000	257.1	241.9	2.43	2.57
480	5500	249.0	236.0	2.43	2.60
480	6000	241.9	230.1	2.42	2.58

Table 6. Average droplet diameter and average velocity for 500 μm center to center horizontal spacing.

Flowrate (ml/hr)	Frequency (Hz)	Theoretical d_d(μm)	Experimental d_d(μm)	Theoretical v_d(m/s)	Experimental v_d(m/s)
510	5000	262.3	253.7	2.59	2.68
510	5500	254.1	250.75	2.59	2.73
510	6000	246.8	253.7	2.59	2.80
480	5000	257.1	253.7	2.43	2.60
480	5500	249.0	241.9	2.43	2.56
480	6000	241.9	247.8	2.42	2.55

Table 7 and 8 shows the comparison between experimental value and theoretical value including percent difference and standard deviation. Most differences of theoretical and experimental values on droplet diameter and velocity fall below 10%. The percent difference (% diff) was calculated taking into account the theoretical and experimental values.

Table 7. Comparison of droplet diameter and velocity for 1000 μm center to center horizontal spacing

Theoretical d (μm)	Experimental d (μm)	Std Dev	%diff	Theoretical v (m/s)	Experimental v (m/s)	Std Dev	%diff
271.7	259.6	8.5	-4.4	2.60	2.81	0.15	8.4
262.3	268.5	4.3	2.3	2.59	2.95	0.25	13.7
254.1	247.8	4.5	-2.5	2.59	2.76	0.12	6.4
289.5	277.3	8.6	-4.2	2.44	2.64	0.14	8.4
257.1	241.9	10.7	-5.9	2.43	2.57	0.10	5.6
249.0	236.0	9.2	-5.2	2.43	2.60	0.12	7.0
241.9	230.1	8.3	-4.9	2.42	2.58	0.11	6.6

Table 8. Comparison of droplet diameter and velocity for 500μm center to center horizontal spacing

Theoretical d(μm)	Experimental d(μm)	Std Dev	%diff	Theoretical v(m/s)	Experimental v(m/s)	Std Dev	%diff
262.3	253.7	6.1	-3.3	2.59	2.68	0.06	3.5
254.1	250.75	2.4	-1.3	2.59	2.73	0.10	5.2
246.8	253.7	4.9	2.8	2.59	2.80	0.15	8.0
257.1	253.7	2.4	-1.3	2.43	2.60	0.12	6.8
249.0	241.9	5.0	-2.9	2.43	2.56	0.10	5.6
241.9	247.8	4.2	2.4	2.42	2.55	0.09	5.1

4.2 Single stream droplets experiments without screen laminates

In this section, the basic physical phenomenon of droplet impingement is presented using IR images. Three main parameters were considered for the single stream droplets experiments, which were flowrate, frequency and heat flux. The relationship between minimum surface temperature and heat flux is also presented graphically.

4.2.1 Effect of heat flux and flowrate

While the sample was heated at different heat flux values, surface temperature would be different. Temperature distribution for single droplet stream under different heat fluxes condition with the same frequency, two different flowrates are shown in Figure 20 and 21.

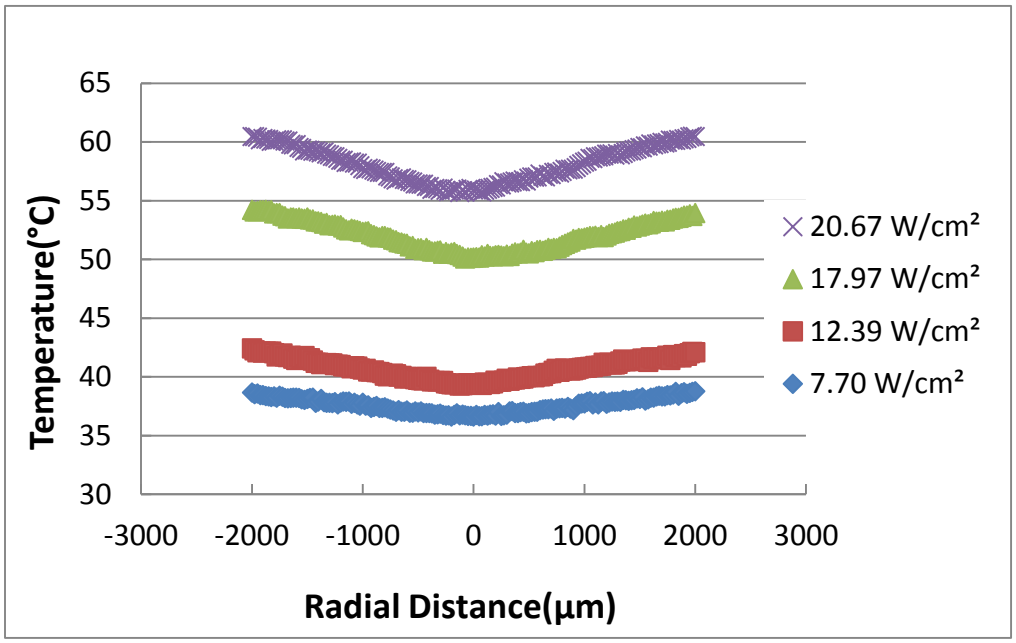

Figure 20. Single stream droplets with flowrate at 160 ml/hr, frequency at 5000 Hz and different heat fluxes

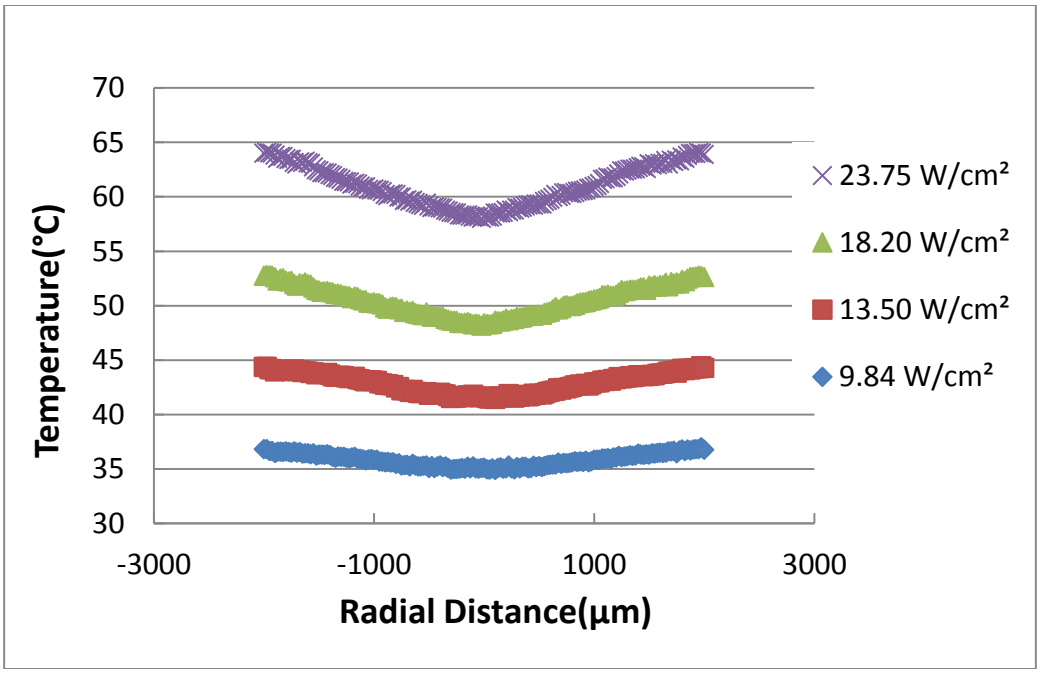

Figure 21. Single stream droplets with flowrate at 170 ml/hr, frequency at 5000 Hz and different heat fluxes

As presented in the figures, when the heat flux is higher, the temperature curve shifts upwardly. In Figure 20, the maximum temperature difference within the temperature profile at 7.7 W/cm^2 is within 2 ºC, but increases over 5 ºC at 20.7 W/cm^2. The temperature difference increased when the heat flux increased because of a greater surface tension gradient effect at higher temperature. Furthermore, the temperature within the impact crater at high heat flux is below the boiling point of HFE (60 °C), indicating that the droplet streams impinging on the surface suppresses the onset of boiling within the impact crater.

Surface temperatures at two different flowrates were measured to determine its effect on heat transfer performance. Temperature were compared at different heat fluxes. Minimum surface temperature for different flowrates under different heat fluxes conditions are shown in Figure 22. Linear correlations have been added on the profile to indicate that most of the heating that takes place is single phase in nature, which can be found in the inner area of the impingement zone. Furthermore, at higher flowrates, lower surface temperatures can be obtained as indicated by the intercept of the correlated equations.

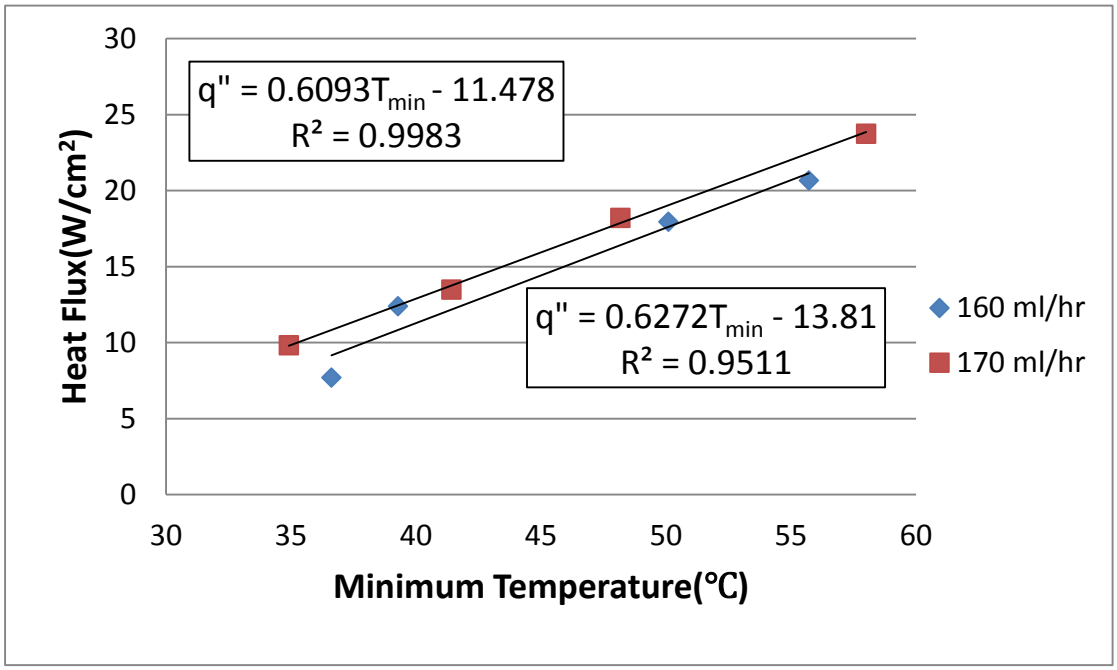

Figure 22. Minimum wall temperature of single droplet stream with different flowrates under different heat flux conditions

4.2.2 Effect of frequency

Frequency is a significant parameter in the experiment, although it is believed to have small effect on heat transfer performance in spray cooling applications. Experiments were undertaken to study the effects of droplet impingement frequency by maintaining the heat flux and flowrate constant. Figures 23, 24 and 25 present the temperature distribution for the different heat flux and flowrate conditions.

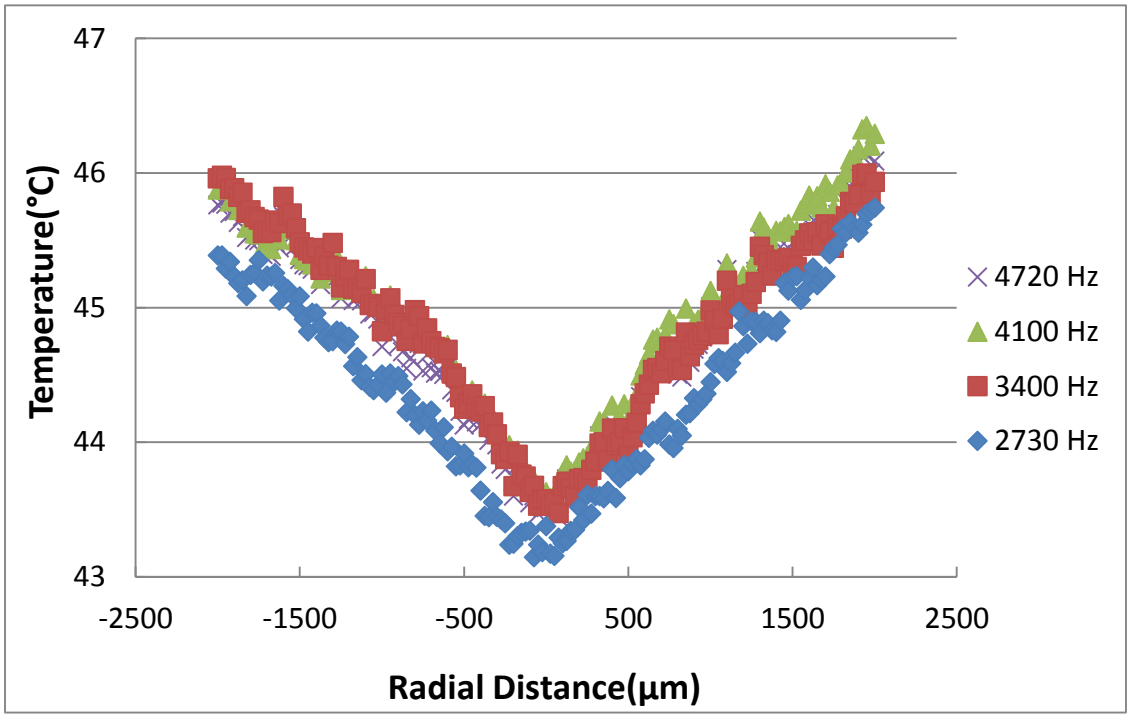

Figure 23. Temperature distribution of single droplet stream with 120 ml/hr flowrate, 11 W/cm^2 heat flux under different frequency conditions

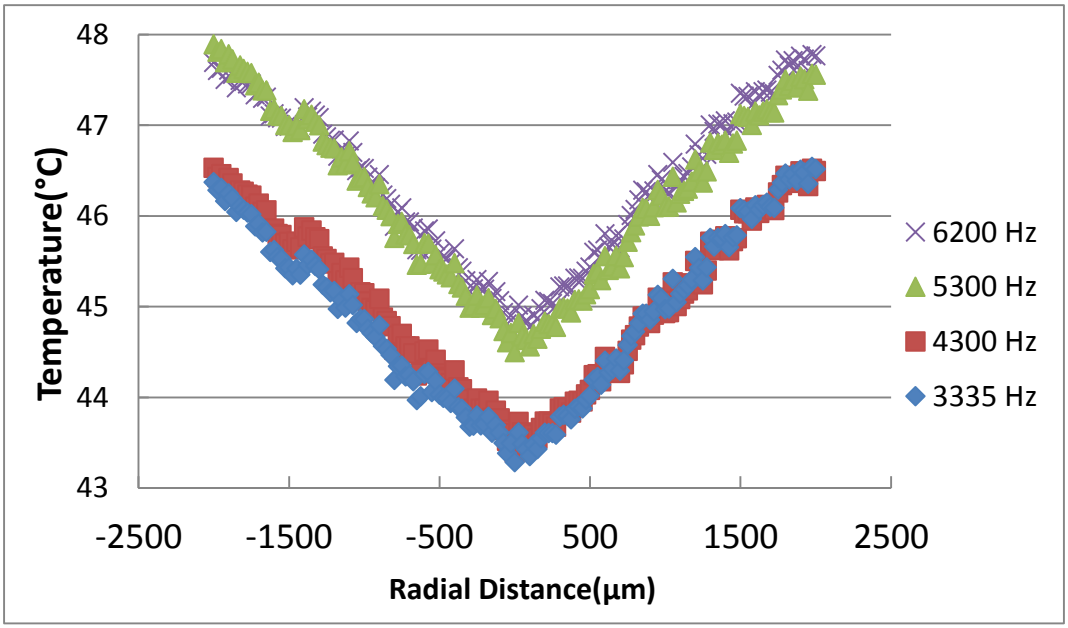

Figure 24. Temperature distribution of single droplet stream with 150 ml/hr flowrate, 13.2 W/cm2 heat flux under different frequency conditions

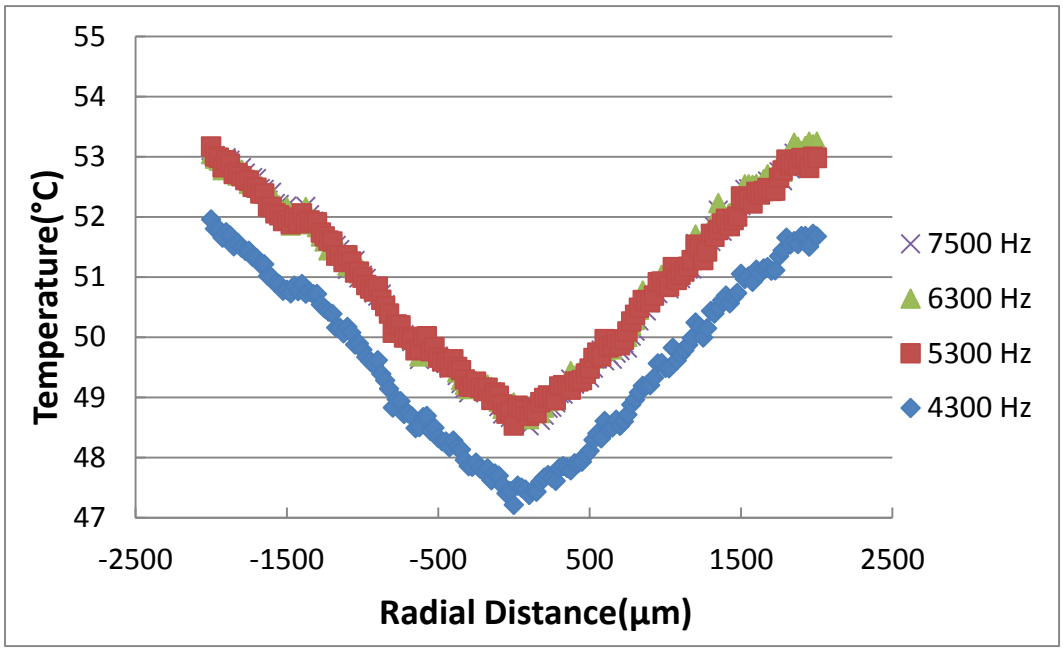

Figure 25. Temperature distribution of single droplet stream with 180 ml/hr flowrate, 18.2 W/cm2 heat flux under different frequency conditions

As mentioned in Section 2, frequency has an optimal range which increases with flowrate. For each case, flowrate and heat flux were set to be constant, while frequencies were varied as shown in Table 9.

Table 9. Droplet Diameter, Weber number and minimum temperature for different flowrates and frequencies

Flowrate ml/hr	Frequency Hz	D µm	We	St	T_{min} °C	$T_{min,\ highest} - T_{min,\ lowest}$
120	4720	238.0	80.4	0.654	43.44	0.4
	4100	249.5	84.3	0.595	43.55	
	3400	265.5	89.7	0.525	43.38	
	2730	285.7	96.5	0.454	43.15	
150	6200	232.9	134.2	0.649	44.70	1.41
	5300	246.7	141.4	0.584	44.50	
	4300	264.5	151.6	0.508	43.40	
	3335	287.9	165	0.430	43.29	
180	7500	233.5	201	0.639	48.52	1.43
	6300	247.5	213	0.568	48.64	
	5300	262.2	225.7	0.508	48.53	
	4300	281.1	242	0.441	47.21	

In all three cases, the lowest frequency and higher Weber number depict the lowest temperature profile. For 120 ml/hr case, the difference between minimum temperatures was within 1°C, and the difference was about 1 °C for 150 ml/hr case then increased at about 1.5 °C for 180 ml/hr case. This indicated that frequency and Weber number have an effect on the heat transfer performance and this effect grows with flowrate. Furthermore, the results suggest that the interaction between larger impinging droplets and the fluid at the surface could be playing a significant role in terms of surface cooling. Pointedly, it could be inferred that larger droplets lead to greater microscale capillary waves at the solid-liquid interface as seen in the study by Trujillo et al [24]. Similar studies have been undertaken by Zhang et al [25] where the effects of frequency and Weber number have been discussed.

4.3 Triple stream droplets experiments without screen laminates

In this section, the effects of multiple droplet impingement spacing, flowrate and frequency on heat transfer performance are presented.

4.3.1 Effect of flow rate on the temperature distribution

In the study of triple streams experiments, firstly, a high-speed camera was used to measure the center-to-center distance of droplet impact craters two different orifice sizes.

Because the substrate which was made of silicon was not transparent in the optical range, ZnSe was used as substrate to be able to measure impact crater spacing among the three impact craters. The ZnSe sample was only used for imaging the impact craters without applying any heat transfer to the surface. All the other experiments were conducted using the Silicon samples since they could be used to measure surface temperature during each heat transfer experiment. A 45º mirror was located just below the ZnSe sample which allowed the high-speed camera to record images of the impact craters through the mirror. Then ImageJ software was then used to calculate the center to center distance on the sample surface. Figure 26 shows the image taken by high-speed camera. From the image, impact crowns could easily be recognized, the impact points were seems to be forming an equilateral triangle. Ejection of fluid along the inner perimeters of the impact craters was also observed through the image. The ejection area were circled in Figure 26 to facilitate identification of the maim features of triple droplet impingement.

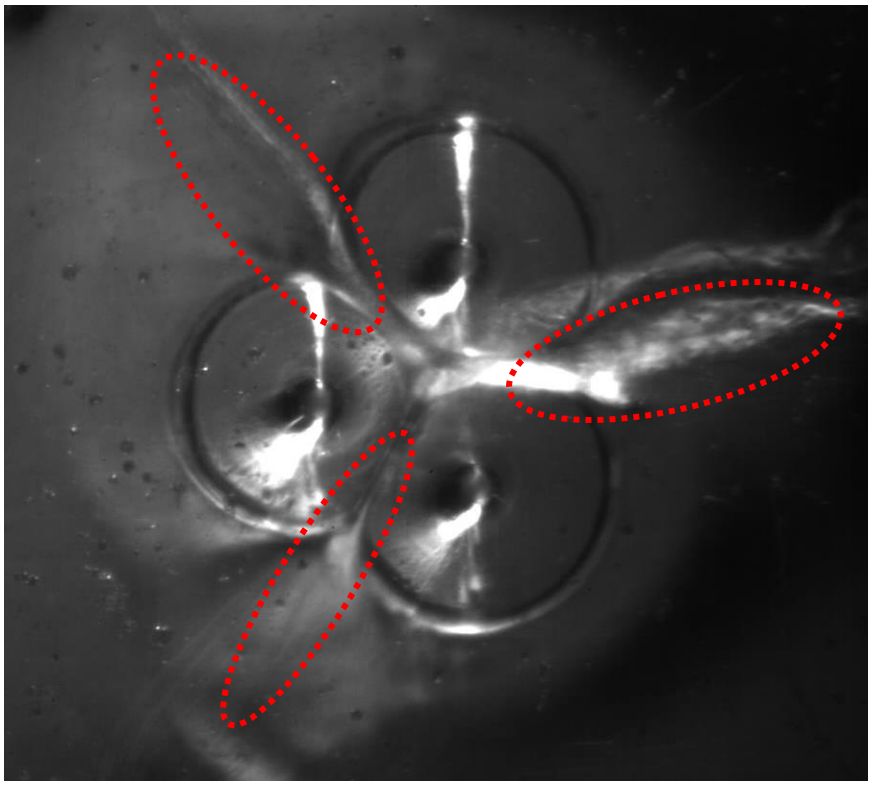

Figure 26. Image taken by high speed camera through a ZnSe sample at 540 ml/hr flowrate, 7200 Hz frequency and 1000 µm center to center distance

As images show, when the orifice center-to-center distance was 1000 µm, the craters center to center distance was about 1000 µm, but when the 750 µm center-to-center distance on the orifice plate was used, it resulted in a 500 µm center-to-center distance. Temperature distribution images were recorded using the IR camera as shown in Figure 27. From the image, the lowest temperature was approached within the impact craters. Matlab software was used to obtain the temperature distribution data along different directions and areas.

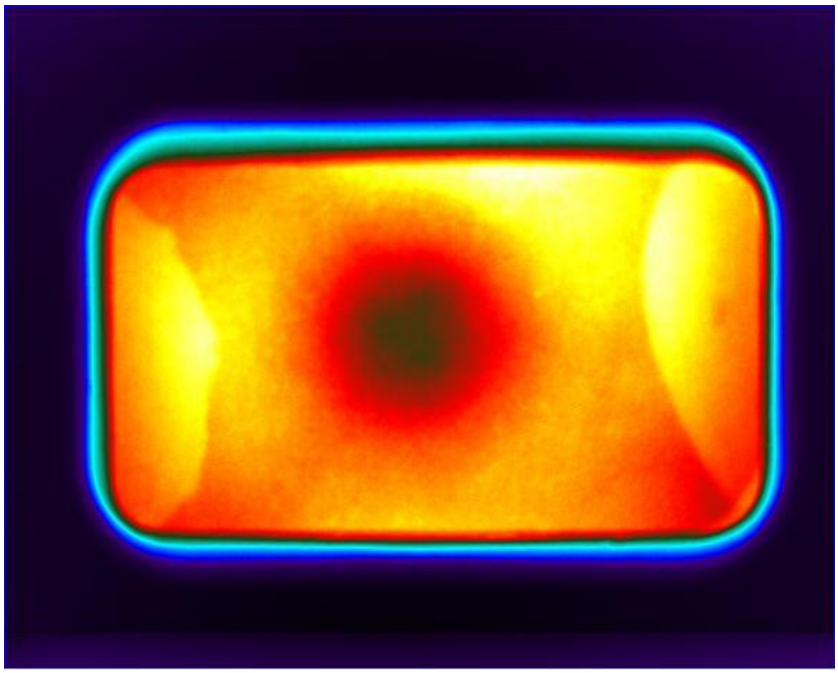

Figure 27. IR image through a Silicon sample, with droplets impinging a flowrate of 480 ml/hr, 5000 Hz frequency and 1000 μm center-to-center spacing

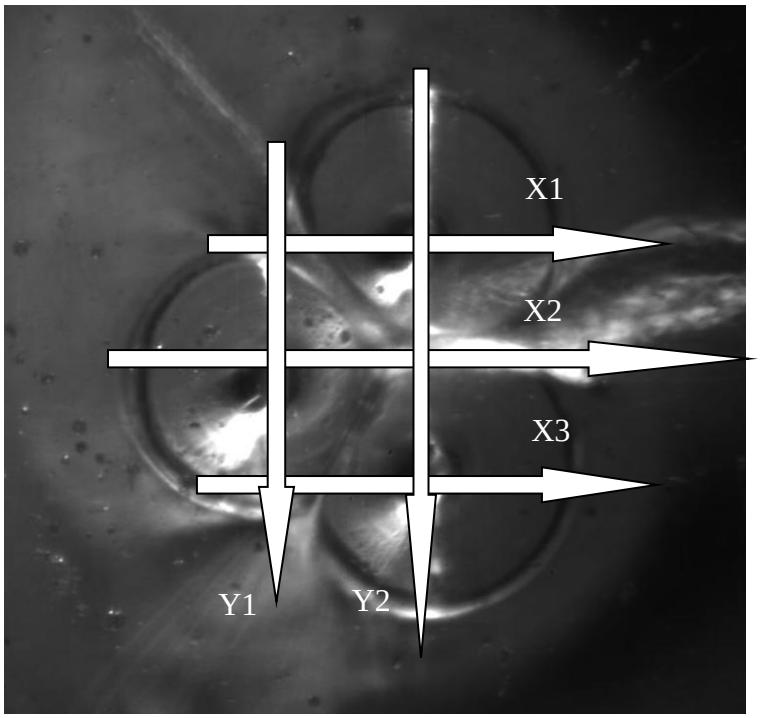

Figure 28. Temperature distribution directions

As shown in Figure 28, five different directions and lines were drawn on the impacting area. X1, X3 and Y1 crossed both three impact craters. X2 crossed one crater and the ejection area and Y2 crossed both two impact craters and the ejection area. With Matlab, temperature data could be plotted as a function of radial position. Figure 29-32 show the temperature distribution on the heated surface at heat flux values.

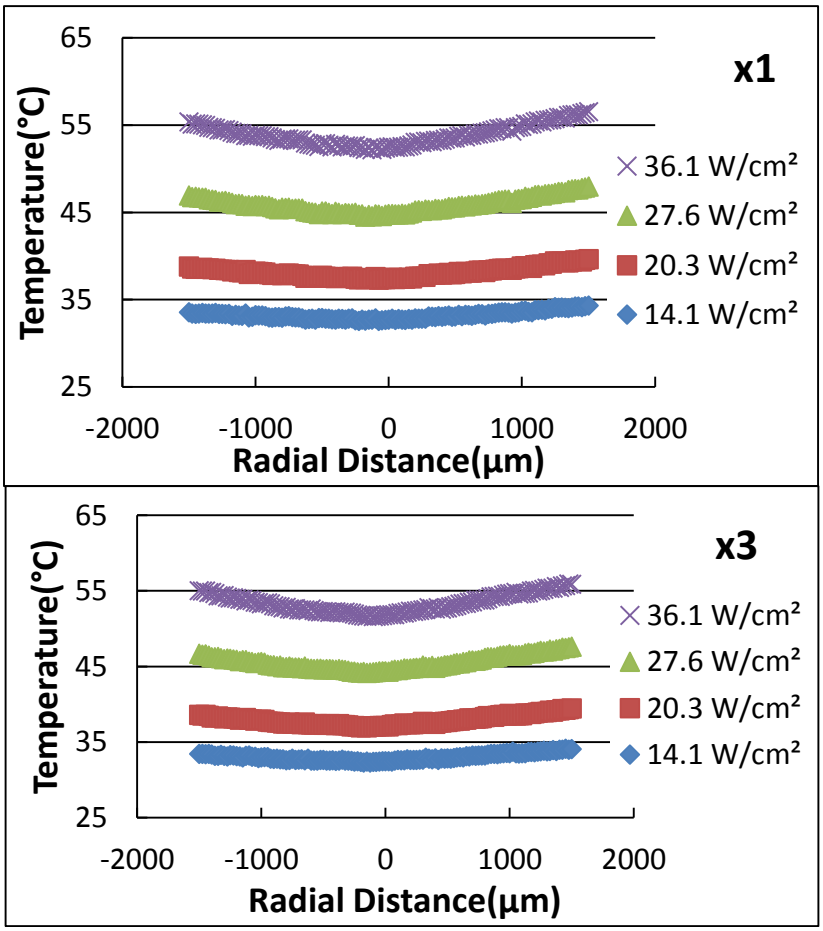

Figure 29. Images for X1 and X3 directions at 480 ml/hr flowrate, 5000Hz frequency and 1000 µm impact spacing and different heat fluxes

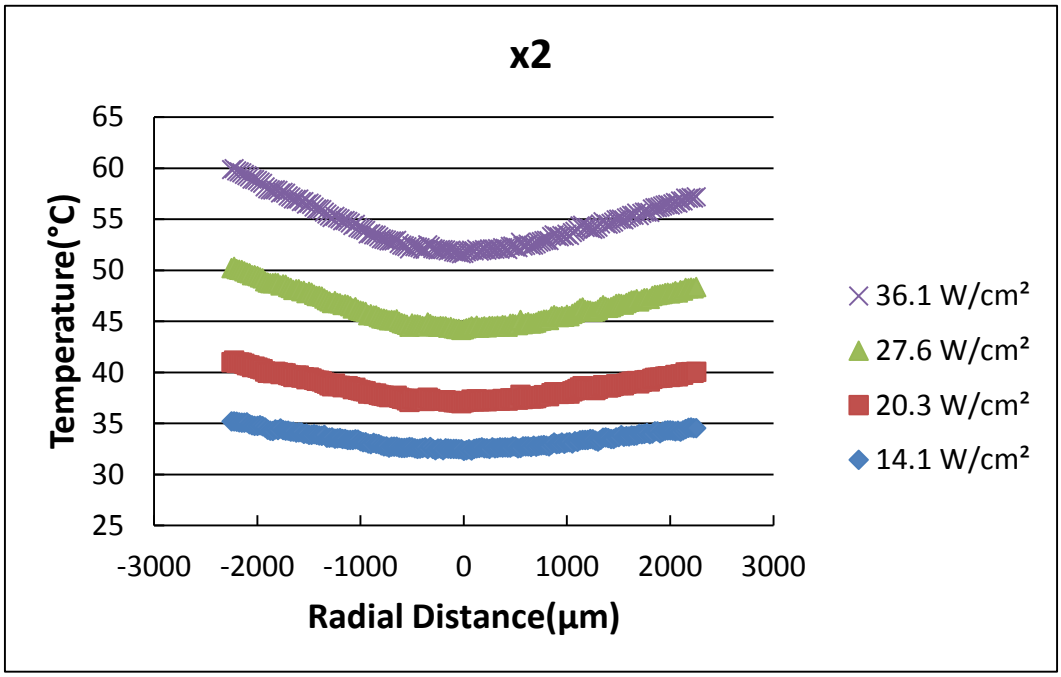

Figure 30. Images for X2 direction at 480 ml/hr flowrate, 5000Hz frequency and 1000 µm impact spacing and different heat fluxes

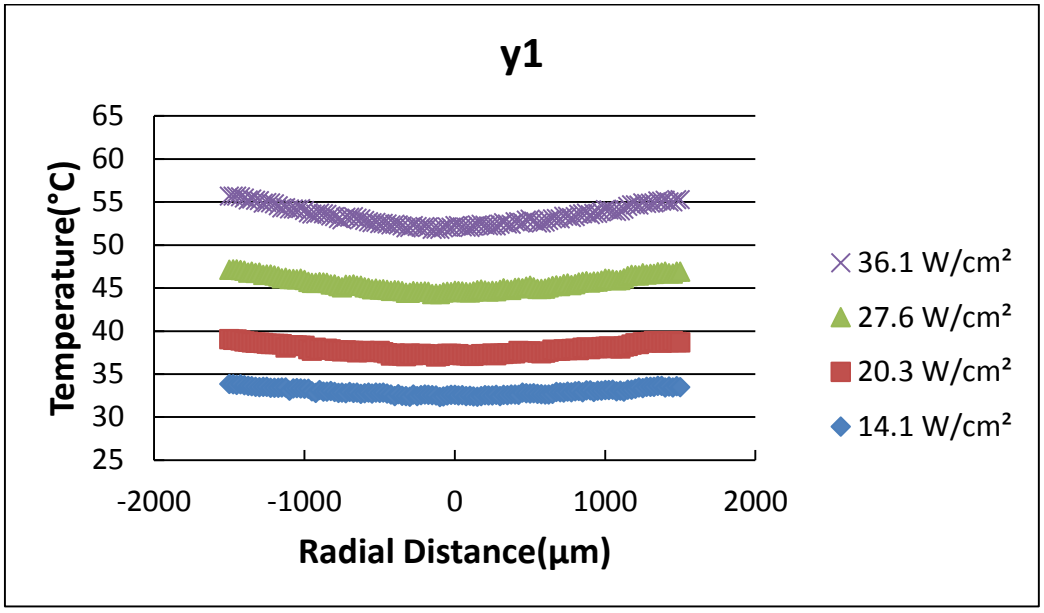

Figure 31. Images for Y1 direction at 480 ml/hr flowrate, 5000Hz frequency and 1000 µm impact spacing and different heat fluxes

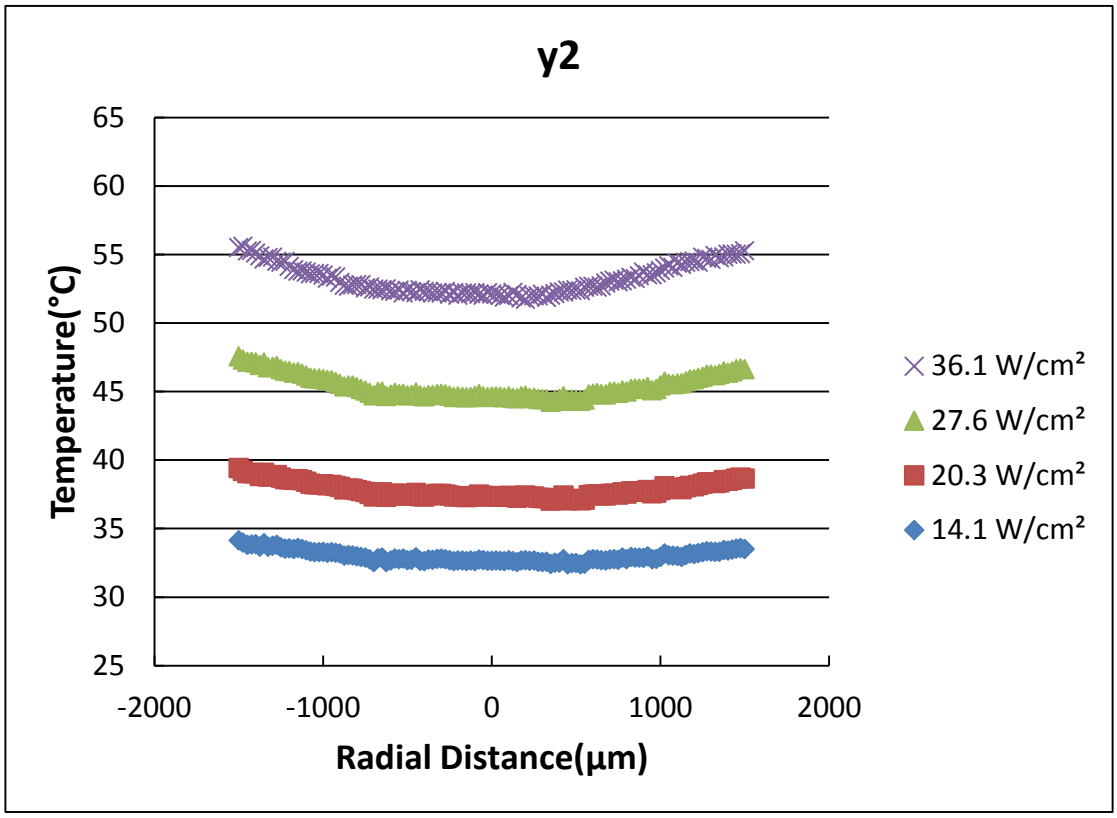

Figure 32. Images for Y2 direction at 480 ml/hr flowrate, 5000Hz frequency and 1000 µm impact spacing and different heat fluxes

In Figure 29, the temperature distribution at X1 and X3 directions are almost identical. The temperature slope was a little bit lower in the negative direction because of the impact crater and the ejection of fluid in the negative direction. In Figure 30 for the X2 direction, temperature slope was lower in the positive direction because of the two impact craters and the ejection flow was in the positive direction. In Figure 31 for Y1 direction, temperature slope was almost symmetric and the temperature at the end of both negative and positive directions are equally to the temperature at negative direction of X1 and X3, because they were both in the ejection area. In Figure 32 for Y2 direction, the

temperature at the end of both negative and positive direction appears to be identical. A flat slope was observed in the center area which can be attributed to the adjacent area between two craters and the ejection area. The temperature distribution in this area was very stable which may be very suitable in temperature sensitive applications. Furthermore, all the results indicate that at higher heat flux values, the whole temperature profile shifts upwardly.

Experiments were also performed at higher flowrate (510 ml/hr) but same frequency and same impact spacing. Figure 33 shows the minimum wall temperature for the above cases but with different flowrates.

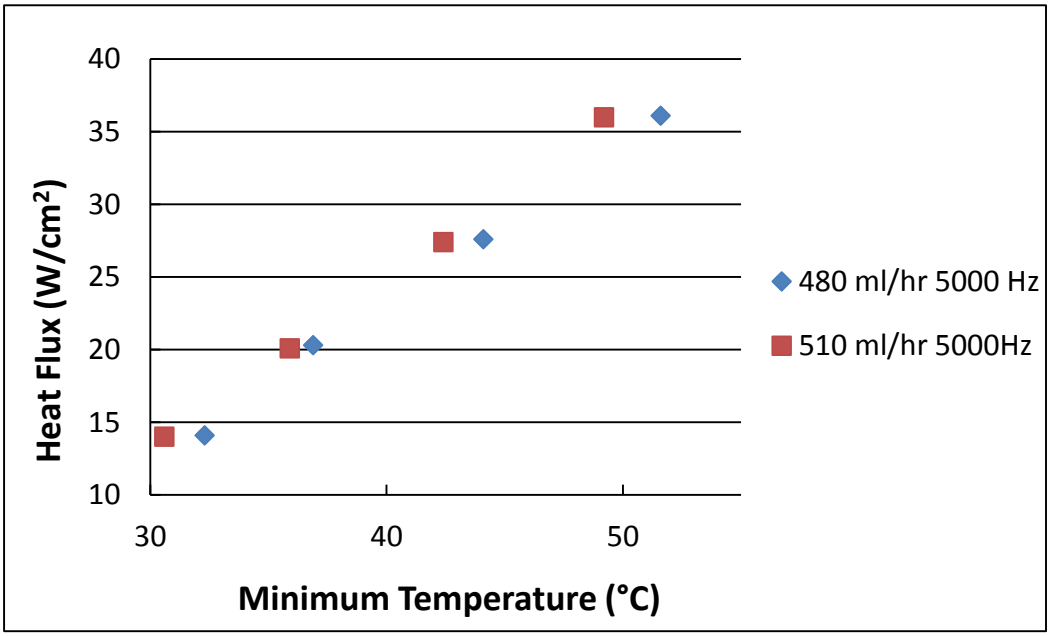

Figure 33. Minimum wall temperature of triple droplets stream with different flowrates under same frequency conditions

Figure 33 indicates that minimum temperature decreases with flowrate at the same heat flux. Figure 34-38 shows the temperature distribution comparison profiles for the highest heat flux cases, from which the temperature difference is presented more clearly.

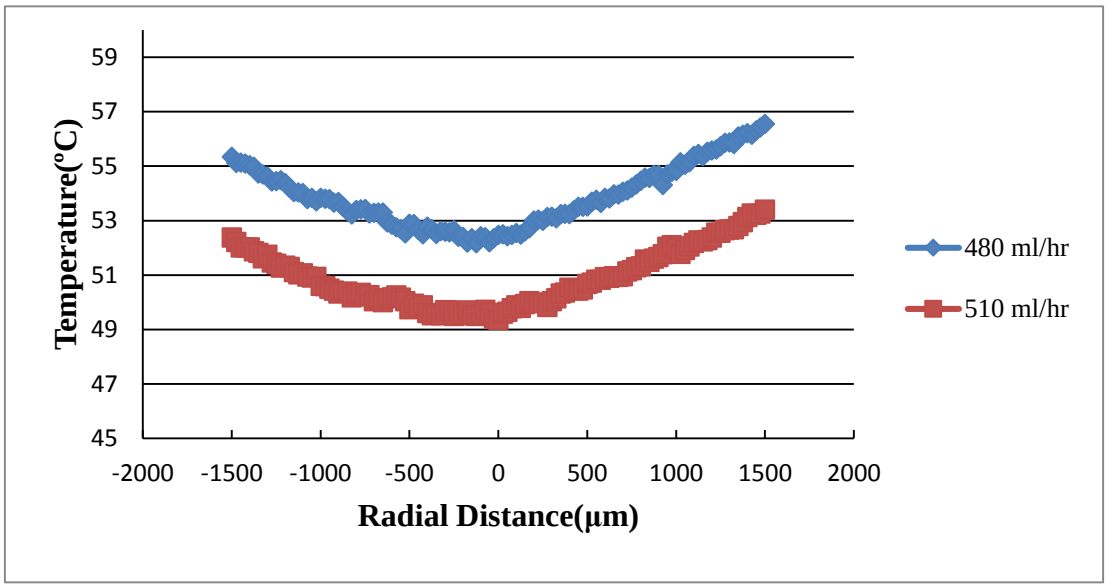

Figure 34. Temperature distribution comparison on X1 direction for flowrate at 480 ml/hr (Heat flux at 36.1 w/cm^2) and 510 ml/hr (Heat flux at 36.0 w/cm^2), frequency at 5000Hz, 1000 µm impact spacing

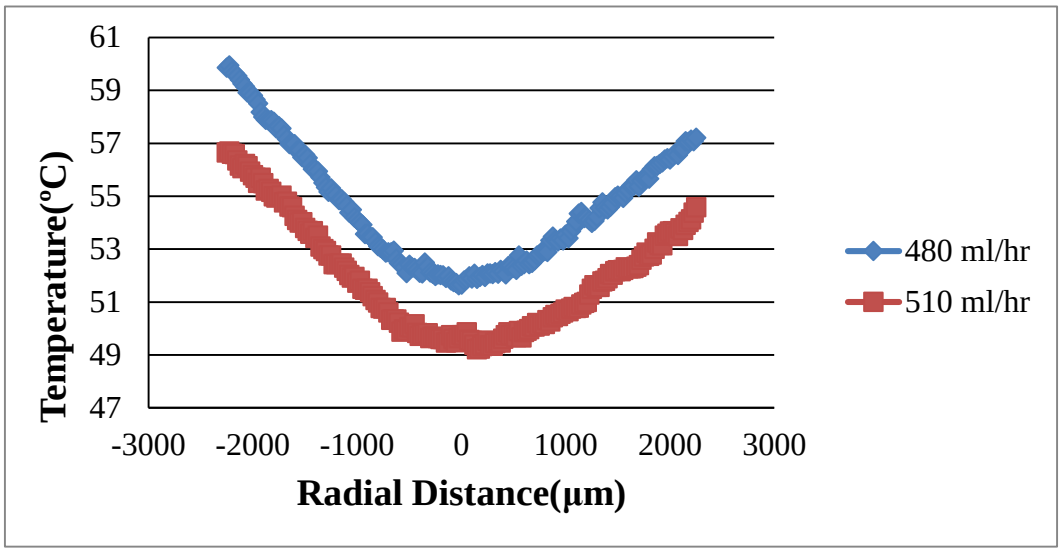

Figure 35. Temperature distribution comparison on X2 direction for flowrate at 480 ml/hr (Heat flux at 36.1 w/cm^2) and 510 ml/hr (Heat flux at 36.0 w/cm^2), frequency at 5000Hz, 1000 µm impact spacing

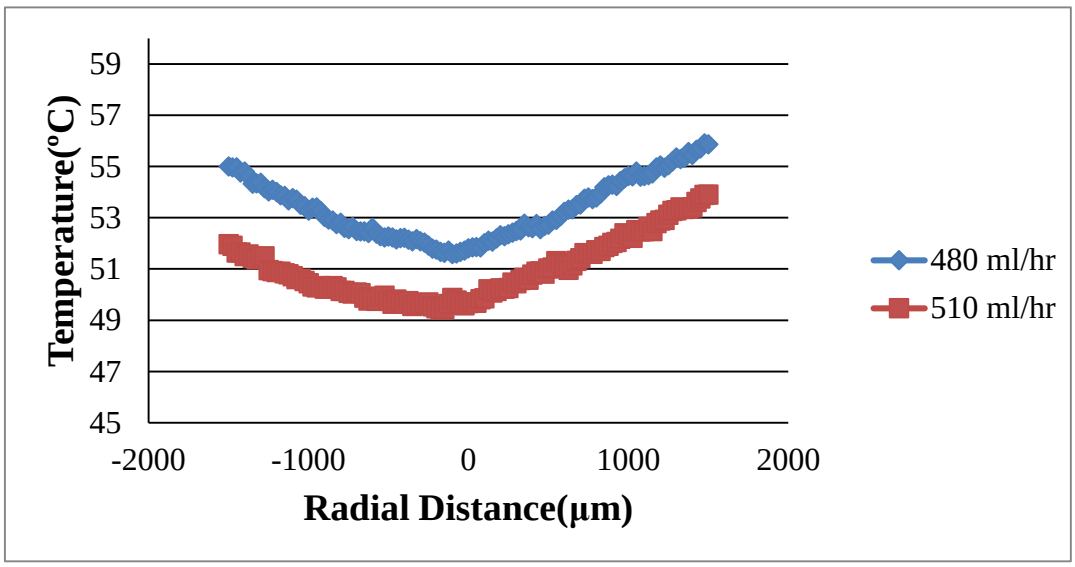

Figure 36. Temperature distribution comparison on X3 direction for flowrate at 480 ml/hr (Heat flux at 36.1 w/cm^2) and 510 ml/hr(Heat flux at 36.0 w/cm^2), frequency at 5000Hz, 1000 µm impact spacing

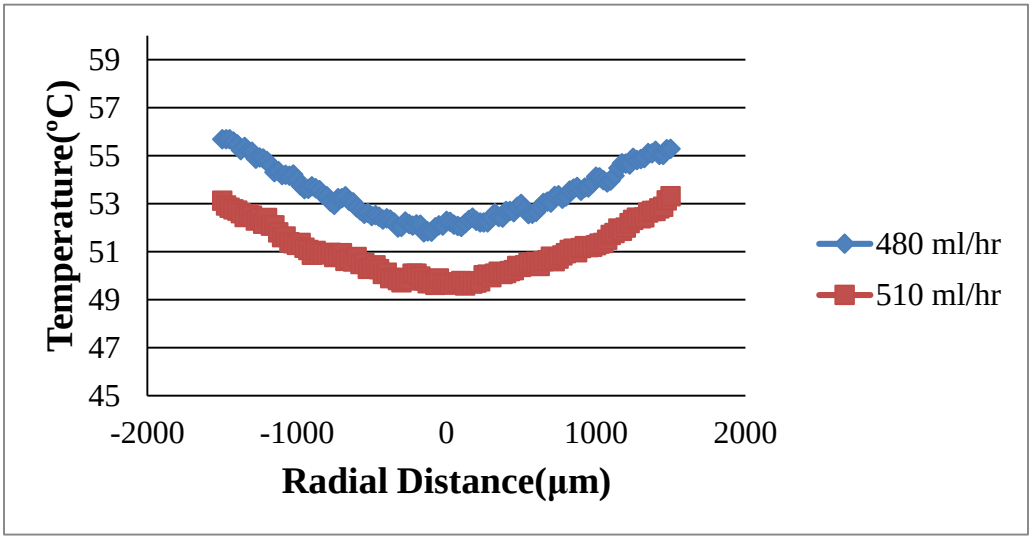

Figure 37. Temperature distribution comparison on Y1 direction for flowrate at 480 ml/hr (Heat flux at 36.1 w/cm^2) and 510 ml/hr (Heat flux at 36.0 w/cm^2), frequency at 5000Hz, 1000 µm impact spacing

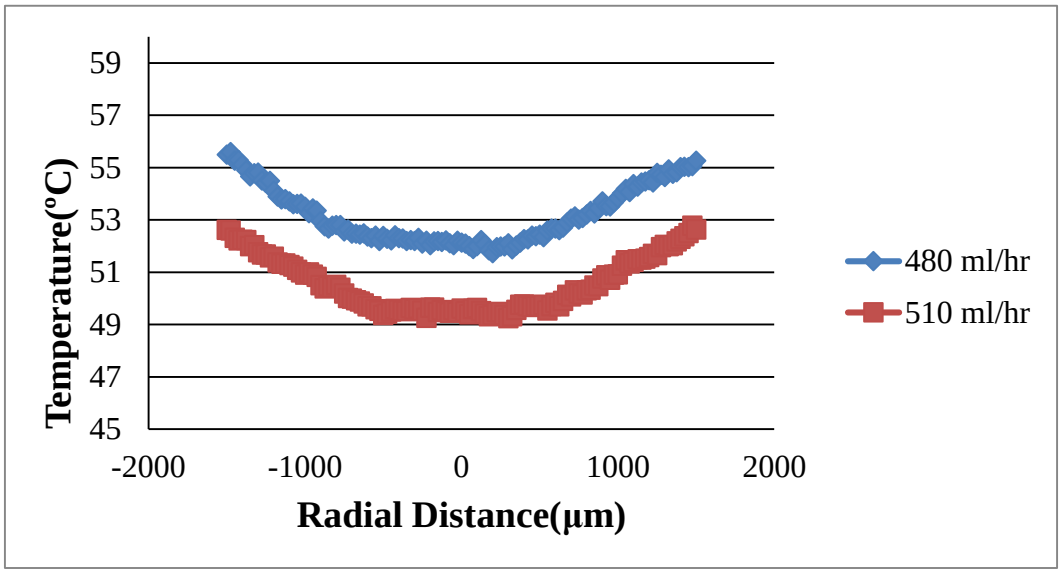

Figure 38. Temperature distribution comparison on Y2 direction for flowrate at 480 ml/hr (Heat flux at 36.1 w/cm^2) and 510 ml/hr (Heat flux at 36.0 w/cm^2), frequency at 5000Hz, 1000 µm impact spacing

From Figure 34 - 38, flowrate is shown to be a very significant parameter which affects the cooling on a heated surface. The minimum temperature was about 3 ºC lower when the flowrate increased by only 30 ml/hr. However, as mentioned before, flowrate has an optimal range where no splashing takes place when droplets impact the heated surface. Moreover, previous results show that splashing should be avoided to improved heat transfer performance [19].

4.3.2 Effect of impact spacing

Experiments were performed under same conditions but different impact spacing. Figures 39 - 43 show the comparison for the effect of different spacing under the same flowrate, frequency and heat flux.

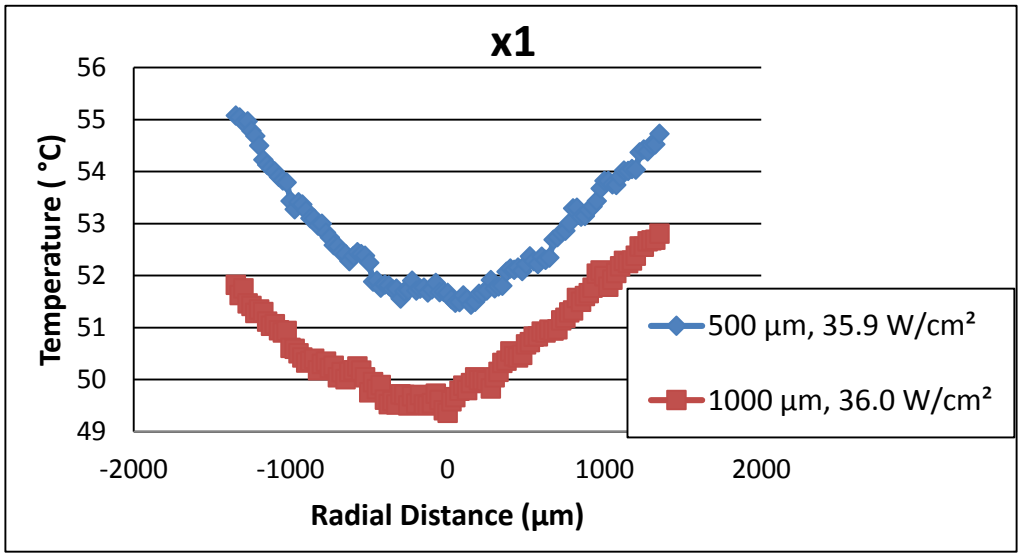

Figure 39. Temperature distribution comparison on X1 direction for 1000 µm and 500µm impact spacing, flowrate at 510 ml/hr, frequency at 5000Hz

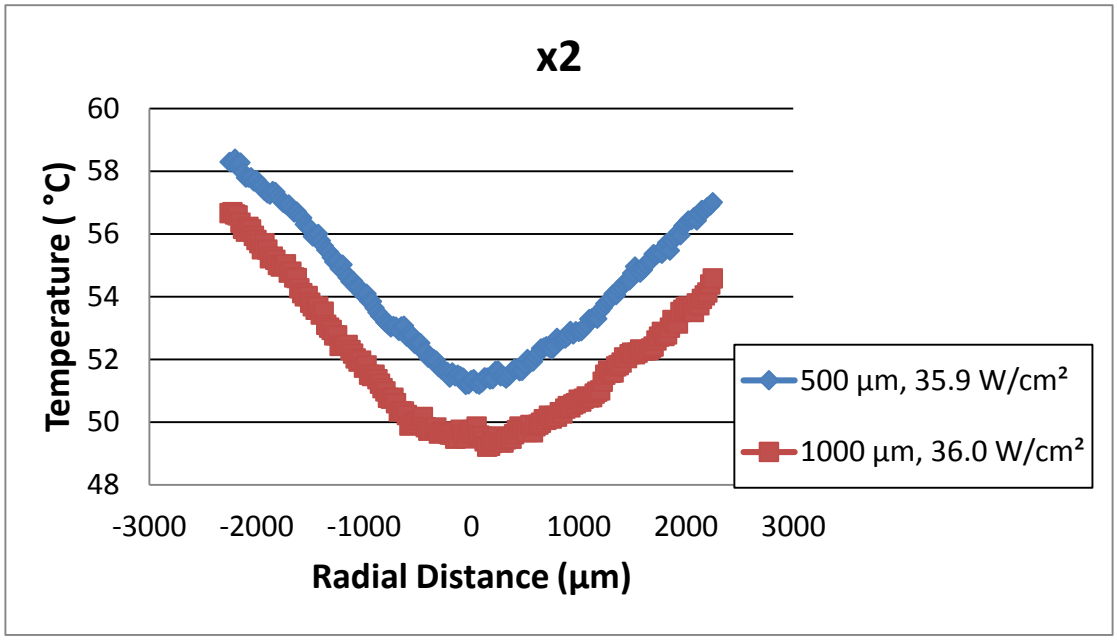

Figure 40. Temperature distribution comparison on X2 direction for 1000 µm and 500µm impact spacing, flowrate at 510 ml/hr, frequency at 5000Hz

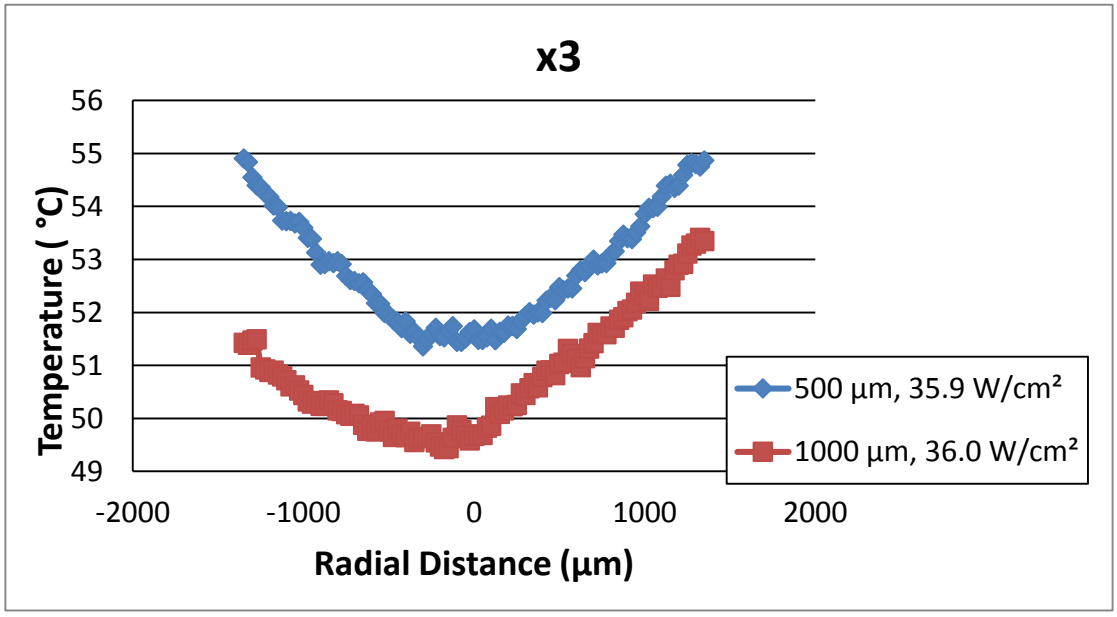

Figure 41. Temperature distribution comparison on X3 direction for 1000 µm and 500µm impact spacing, flowrate at 510 ml/hr, frequency at 5000Hz

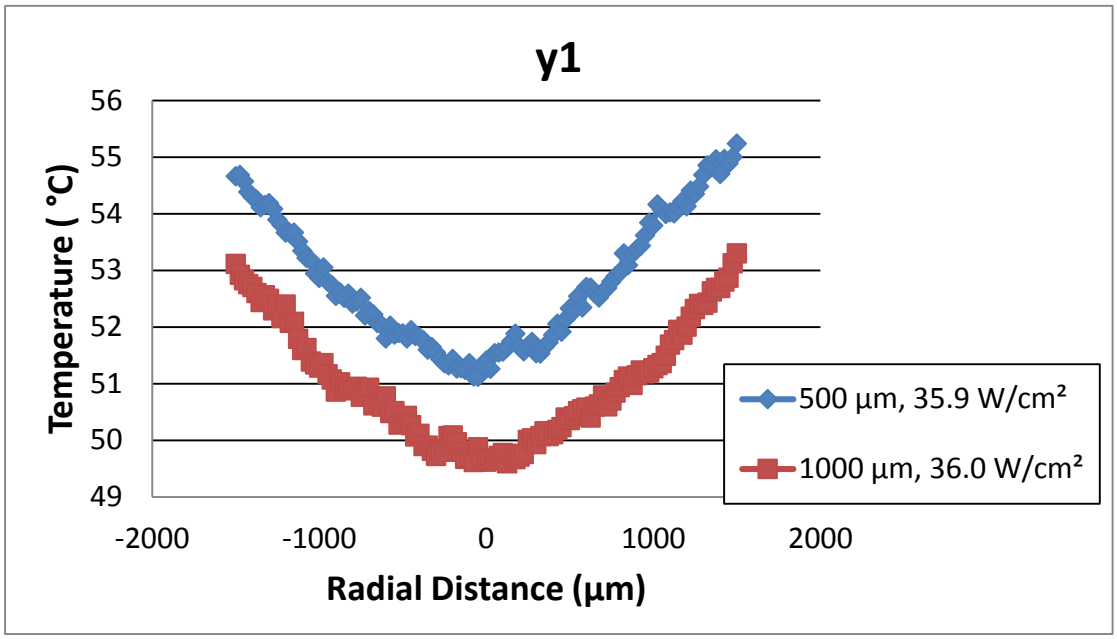

Figure 42. Temperature distribution comparison on Y1 direction for 1000 µm and 500µm impact spacing, flowrate at 510 ml/hr, frequency at 5000Hz

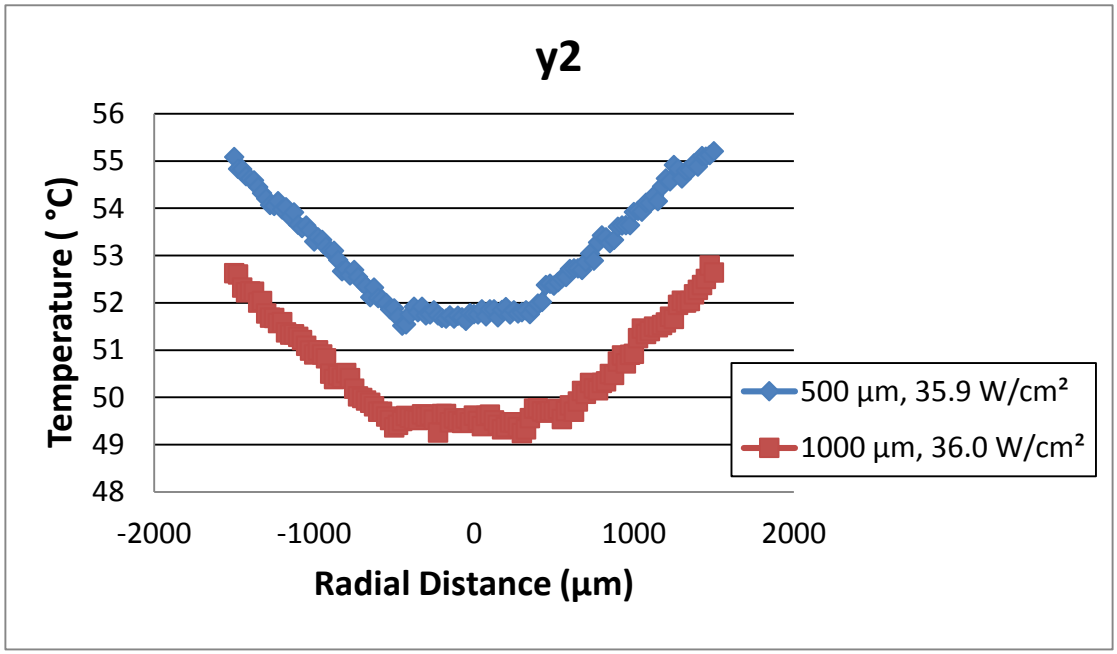

Figure 43. Temperature distribution comparison on Y2 direction for 1000 µm and 500µm impact spacing, flowrate at 510 ml/hr, frequency at 5000Hz

From Figures 39 - 43, 1000 µm spacing depicts better cooling performance than the 500 µm spacing case since the minimum surface temperature was about 3 ºC lower. High-speed camera were used to record the 500 µm and 1000 µm spacing impact process with ZnSe substrate. Figure 44 shows the comparison for both of them.

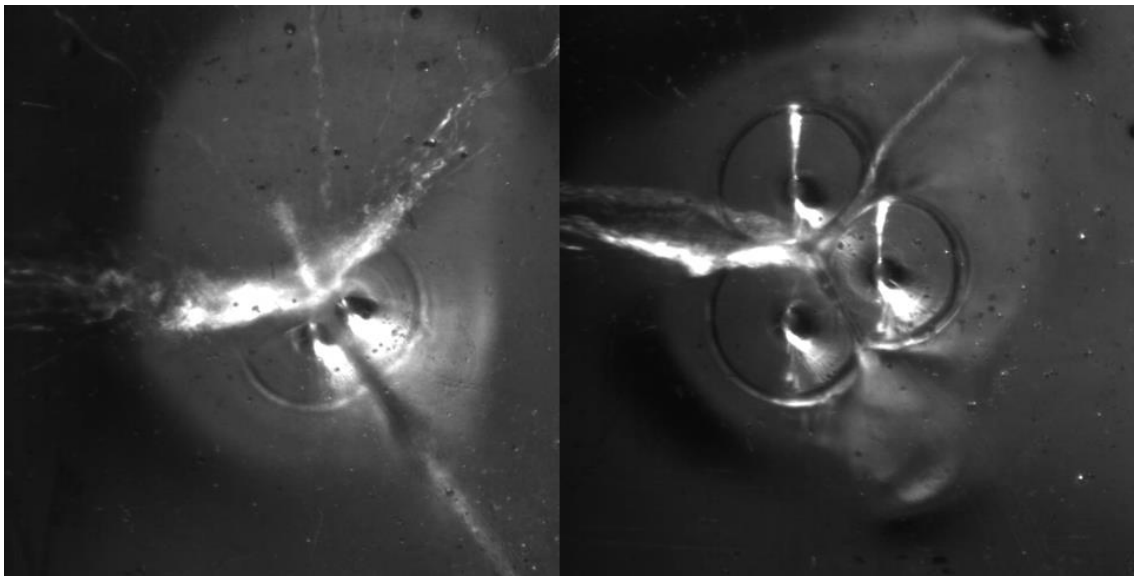

Figure 44. Comparison of 500 µm and 1000µm impact spacing at 540 ml/hr for flowrate, frequency at 7200 Hz.

From Figure 44, the left side shows an image for a 500 µm impact spacing, where overlapping of the impact craters was observed on the impinging surface, which may lead to thicker film thickness. The ejection phenomena in 500 µm spacing case is considered to be significant when compared with the 1000 µm impact spacing case. For the 1000 µm case, three impact craters never overlapped at all which led to the optimal ejection effect.

In summary, bigger impact spacing (1000 µm) led to better cooling performance in this research study.

In general, impact spacing was found to be very important for multiple droplet streams spray cooling arranged in triangulated shape.

4.3.3 Effect of frequency on the temperature distribution

Frequency was proven to be an influential parameter for cooling performance in Section 4.2.2 when using single streams of droplets. In this section, the results from experiments conducted using triple streams of droplets are presented to show how they affect cooling performance. Figure 45-49 show temperature distribution results under different frequencies, but at the same flowrate, same heat flux and same impact spacing.

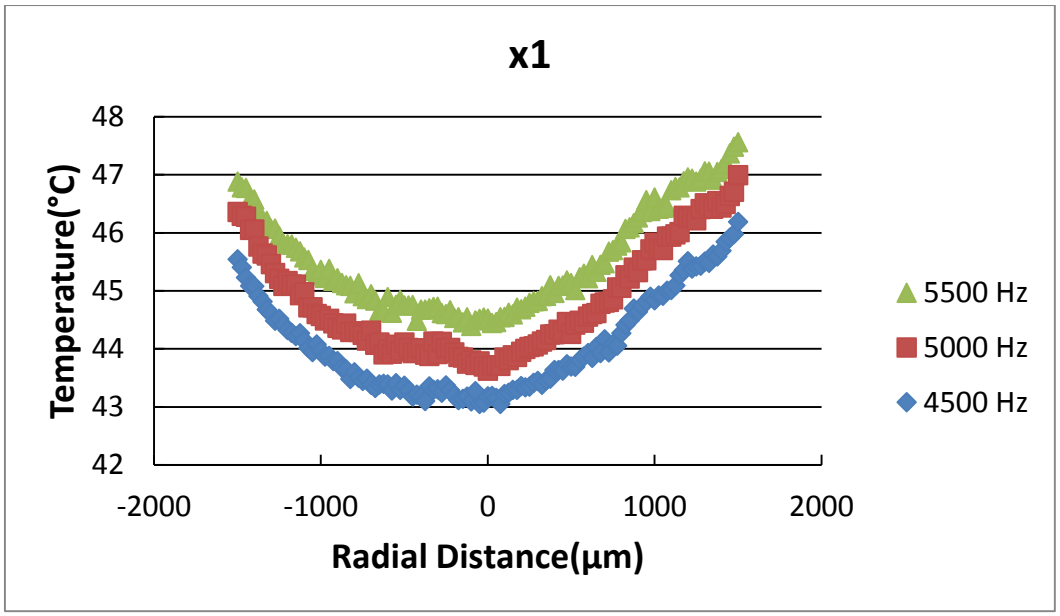

Figure 45. Temperature distribution on X1 direction under different frequencies, flowrate at 480 ml/hr, impact spacing at 1000 µm and heat flux at 26.5 W/cm^2

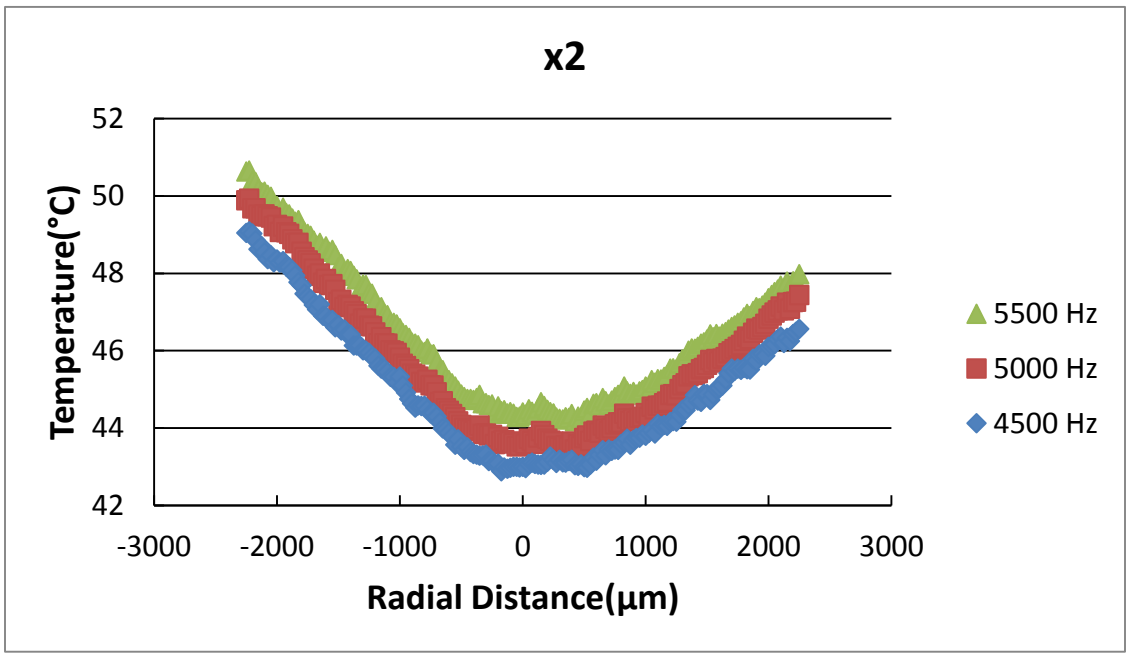

Figure 46. Temperature distribution on X2 direction under different frequencies, flowrate at 480 ml/hr, impact spacing at 1000 µm and heat flux at 26.5 W/cm^2

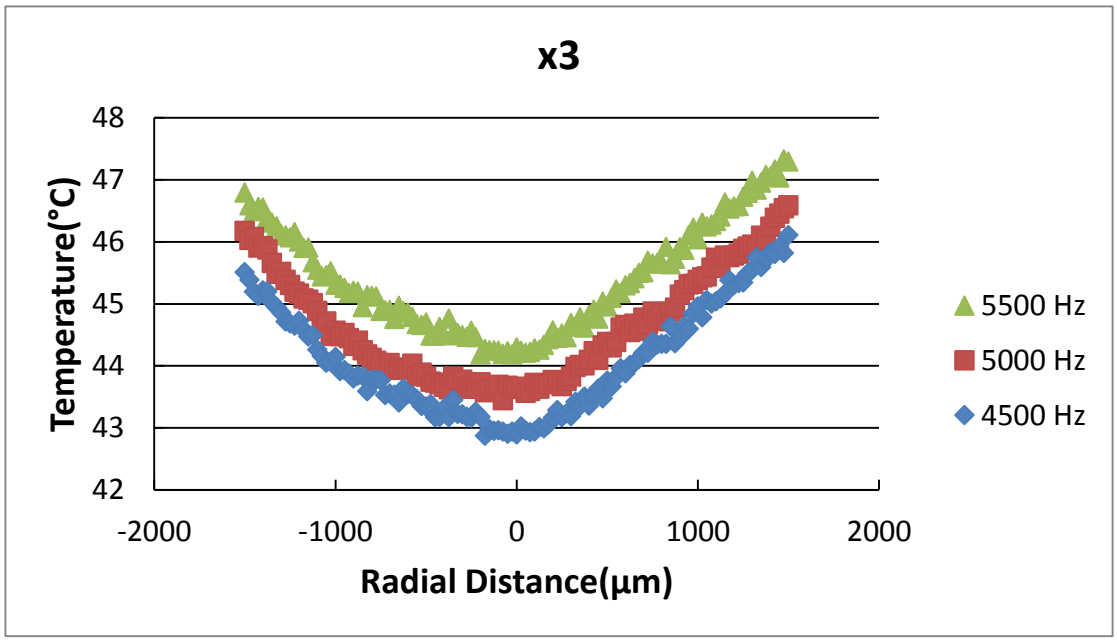

Figure 47. Temperature distribution on X3 direction under different frequencies, flowrate at 480 ml/hr, impact spacing at 1000 µm and heat flux at 26.5 W/cm^2

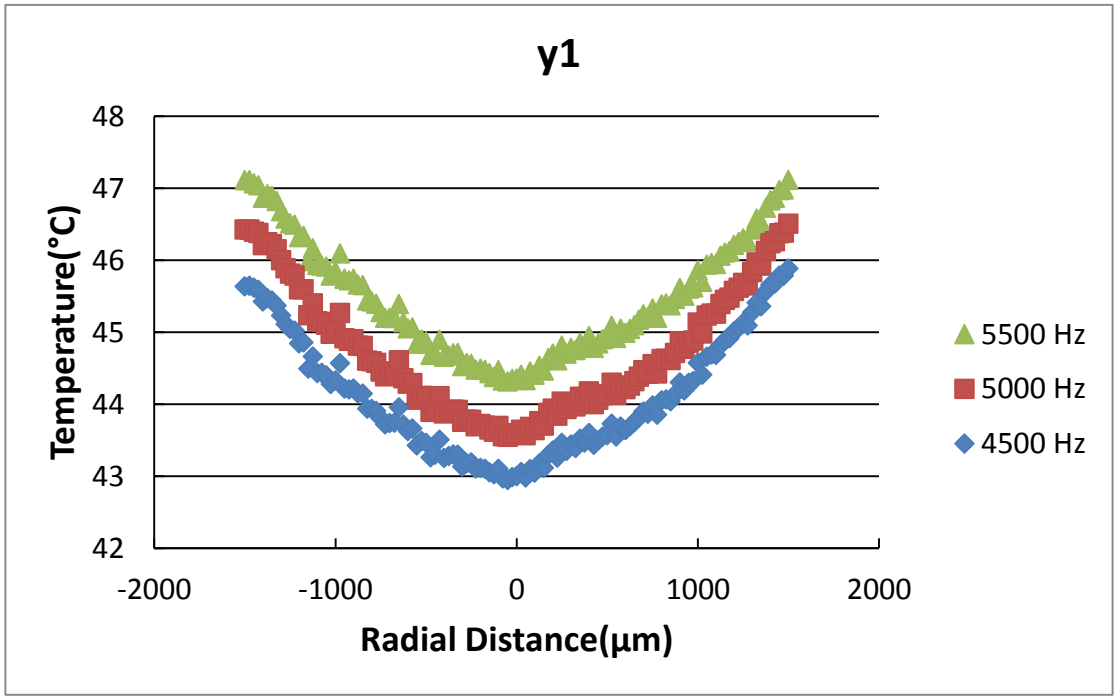

Figure 48. Temperature distribution on Y1 direction under different frequencies, flowrate at 480 ml/hr, impact spacing at 1000 µm and heat flux at 26.5 W/cm^2

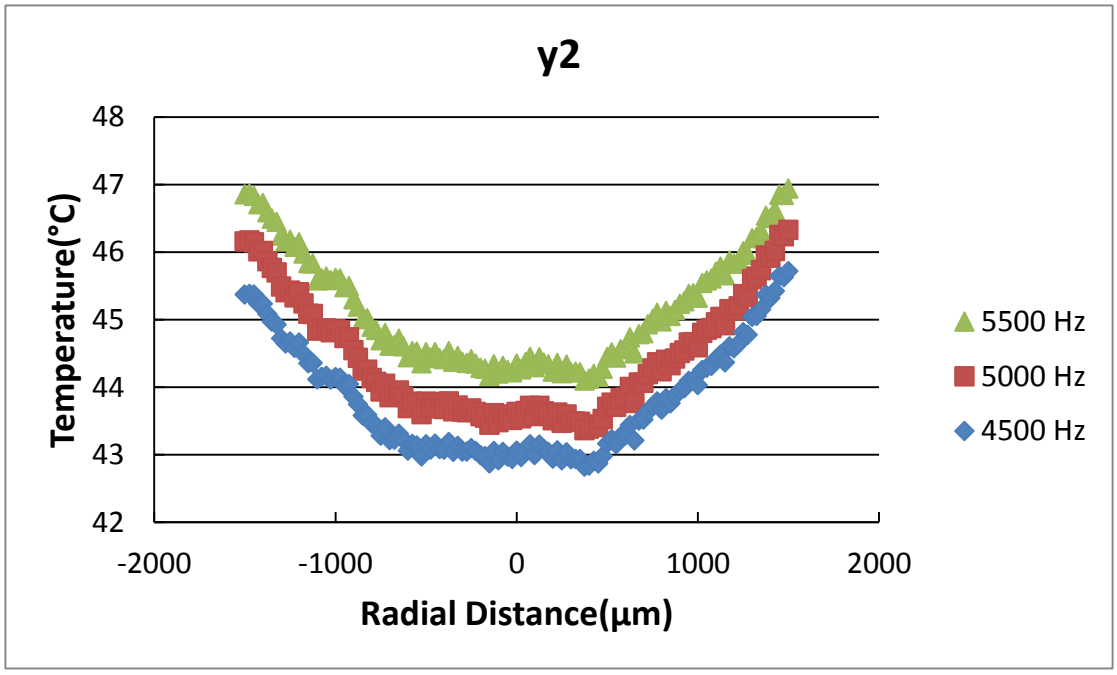

Figure 49. Temperature distribution on Y2 direction under different frequencies, flowrate at 480 ml/hr, impact spacing at 1000 µm and heat flux at 26.5 W/cm^2

Through Figure 45-49, the temperature profiles shift upwardly with impingement frequency. The figures also show that the temperature profiles are relatively flat within the droplet impingement zones. The difference of minimum temperature between 4500 Hz and 5500 Hz cases was only about 1 ºC. This means that within the optimal frequency range, lower frequency should lead to better cooling performance, which is consistent with the results presented in Section 4.2.2. Furthermore, frequency determines the droplet diameter and droplet impacting velocity at a fixed flowrate. Moreover, droplet diameters increased as frequency decreased, but the droplet impacting velocity would increase a little bit. Table 10 shows how droplet velocity, droplet diameter, Weber number and Strouhal number at different frequencies but the same impact spacing, same flowrate.

Table 10. Triple stream droplet properties under different frequencies and flowrate at 480 ml/hr, impact spacing at 1000 μm

frequency (Hz)	velocity (m/s)	droplet diameter (μm)	Weber	Strouhal
4500	2.433	266.2	171.5	0.493
5000	2.430	257.1	165.1	0.529
5500	2.427	249.0	159.6	0.564

From the Table 10, the percent difference of velocity was only 0.1% which can be neglected. As a result, droplet velocity in this research project could be assumed to be

constant under same flowrate but with different frequencies. On the other hand, percent differences of droplet diameter were about 3.5% which was not too big, this number could be an explanation of the 1 ºC temperature difference from 4500 Hz to 5500 Hz.

4.4 Experiments with screen laminates

For this section, results from screen laminates experiments are presented. Effects of the height between screen and heating surface, material of screen laminates and sizes of center hole on heat transfer performance have been investigated.

4.4.1 Effect of screen laminates material, size and stage height

As indicated in the literature review section of this thesis, screen laminates have been used to enhance the performance of boiling processes. Since some level of pool boiling takes place near the impact crates of the impingement zone, it was decided to investigate the effect of screen laminates on heat transfer performance when using single and triple streams of droplets. In order to select the right material and mesh size, small center holes were cut on both aluminum and copper meshes. Single stream droplets tests were run using the difference meshes or screen laminates. For the aluminum mesh, the mesh sizes were 50x50 (filaments per inch) and 120x120 (filaments per inch); and for copper mesh, the mesh sizes were 60x60 (filaments per inch) and 100x100 (filaments per inch).

Figure 50-53 show the temperature distribution results with aluminum meshes at different mesh sizes and gap distances.

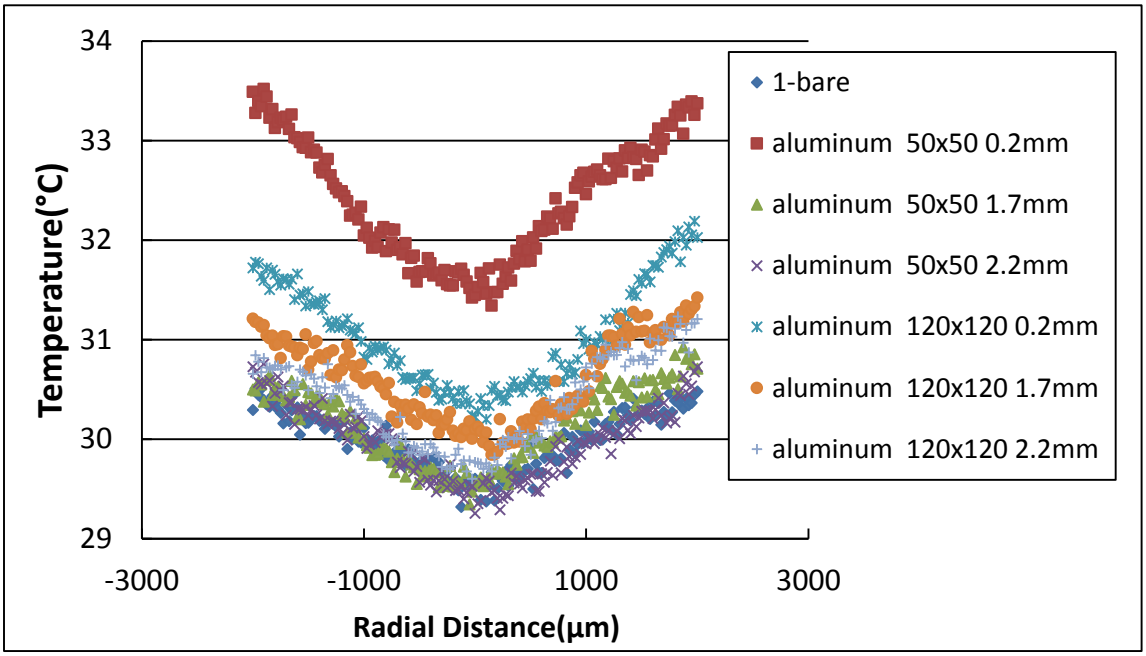

Figure 50. Temperature distribution with aluminum meshes under hole size of 2.5 mm of screen laminate, flowrate at 160 ml/hr, frequency at 5000 Hz and heat flux at 6.0 W/cm^2

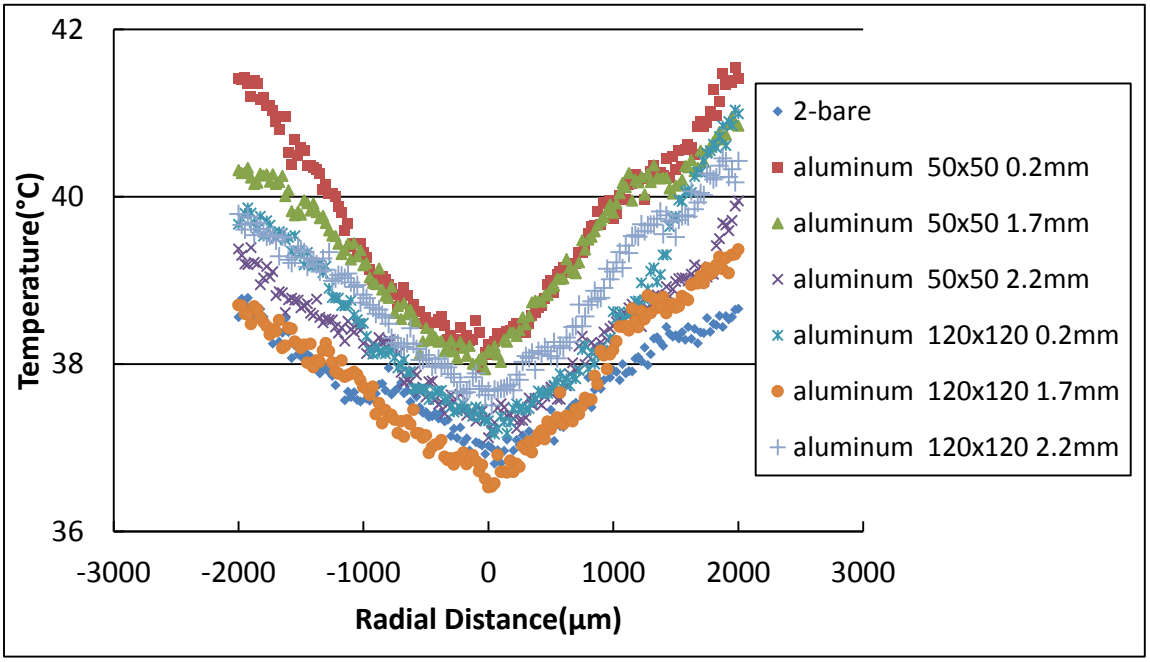

Figure 51. Temperature distribution with aluminum meshes under hole size of 2.5 mm of screen laminate, flowrate at 160 ml/hr, frequency at 5000 Hz and heat flux at 9.22 W/cm^2

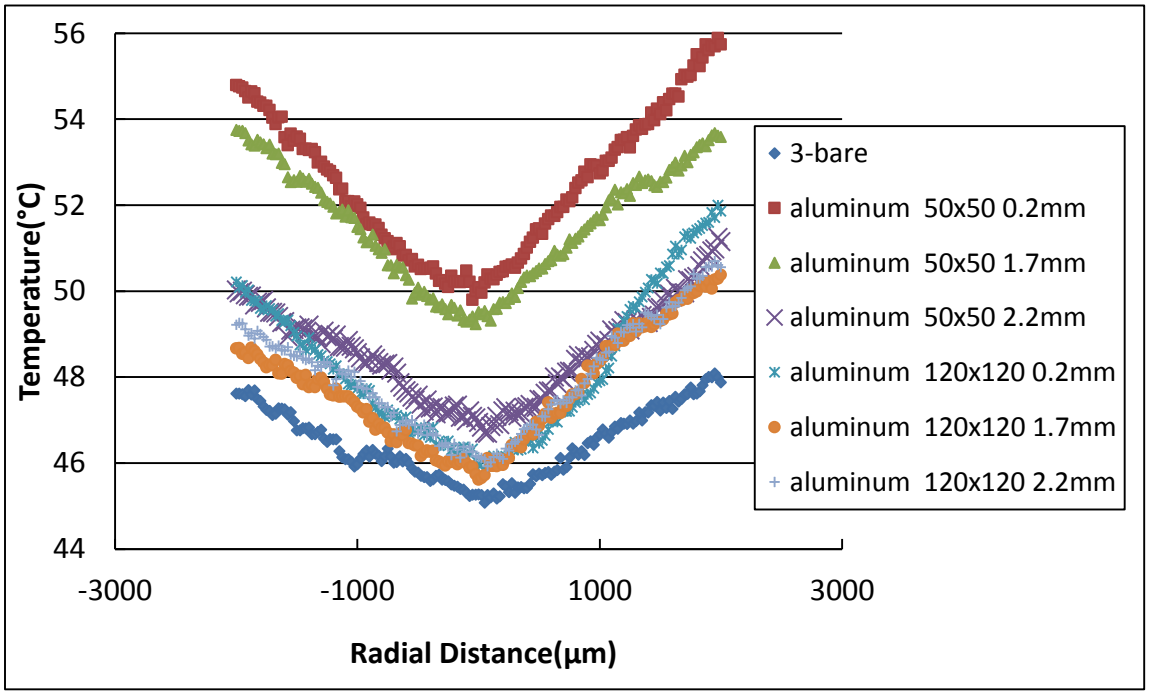

Figure 52. Temperature distribution with aluminum meshes under hole size of 2.5 mm of screen laminate, flowrate at 160 ml/hr, frequency at 5000 Hz and heat flux at 13.12 W/cm^2

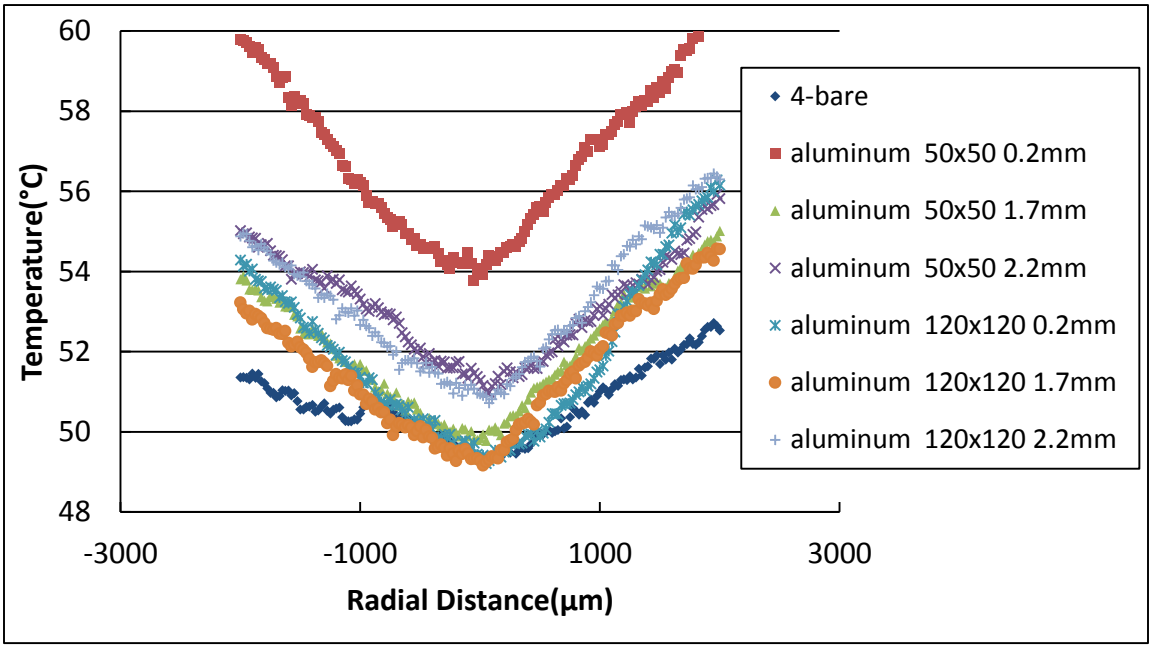

Figure 53. Temperature distribution with aluminum meshes under hole size of 2.5 mm of screen laminate, flowrate at 160 ml/hr, frequency at 5000 Hz and heat flux at 14.96 W/cm^2

From Figures 50, 51, 52 and 53, the bare surface temperature profiles are always the lowest compared to all the other mesh surface profiles, which indicates that screen laminates reduced the cooling efficiency. It is inferred that aluminum meshes interrupt the evaporation of cooling fluid on the heating surface. Moreover, it appears that the relatively high specific heat of aluminum (903 J/kg-k) which is comparable to the specific heat of HFE-7100, reduce the fluids ability to dissipate heat effectively. Furthermore, the thermal conductivity of aluminum is about 237 W/m-K which is 40% less than for copper. The results also show that coarse meshes at close proximity to the heater surface are detrimental in terms of heat transfer. This suggests that coarser meshes could be trapping air or vapor bubbles close to the surface without providing additional routes for heat transfer through metal phase. This effect seems to be ameliorated when

finer meshes are used because of the better thermal network available for heat transfer especially at small gap distance.

Figure 54-57 show the temperature distribution experimental results with copper meshes. In general, a fine mesh (100x100) at small gap distance (0.2 mm) performs better than under the other conditions. The enhanced performance can be explained by taking into account the thermal properties of copper as well as the high surface density of the fine mesh which allowed heat to flow unimpededly throughout the mesh structure.

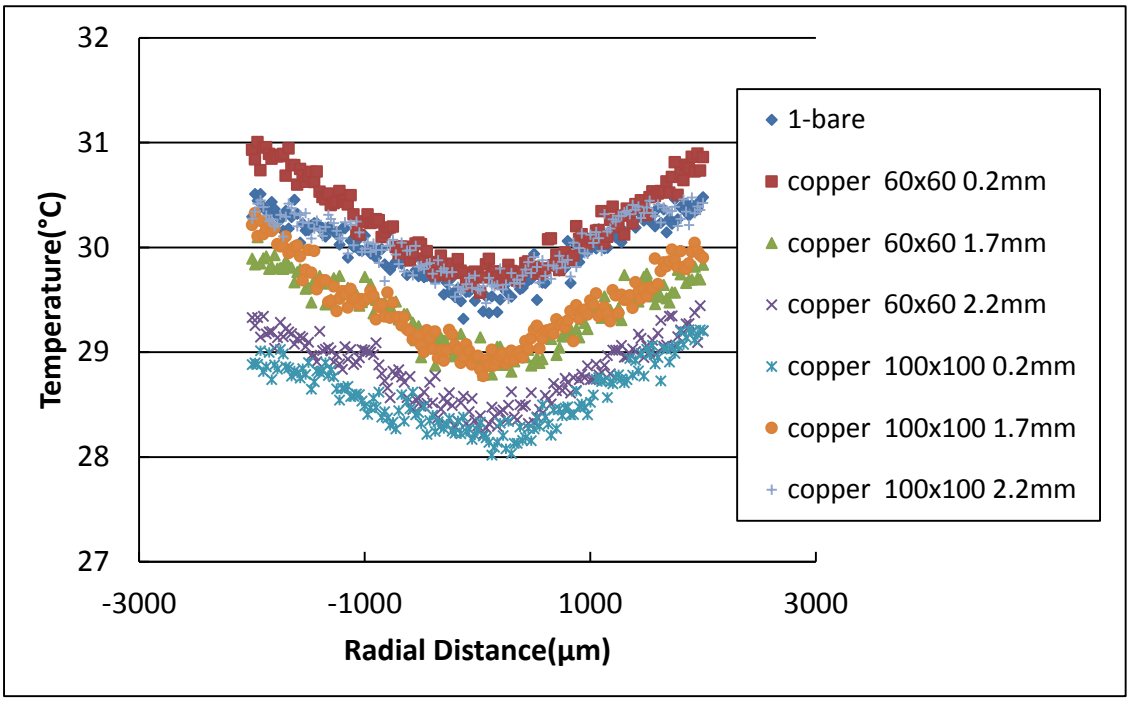

Figure 54. Temperature distribution with Copper meshes under hole size of 2.5 mm of screen laminate, flowrate at 160 ml/hr, frequency at 5000 Hz and heat flux at 5.75 W/cm^2

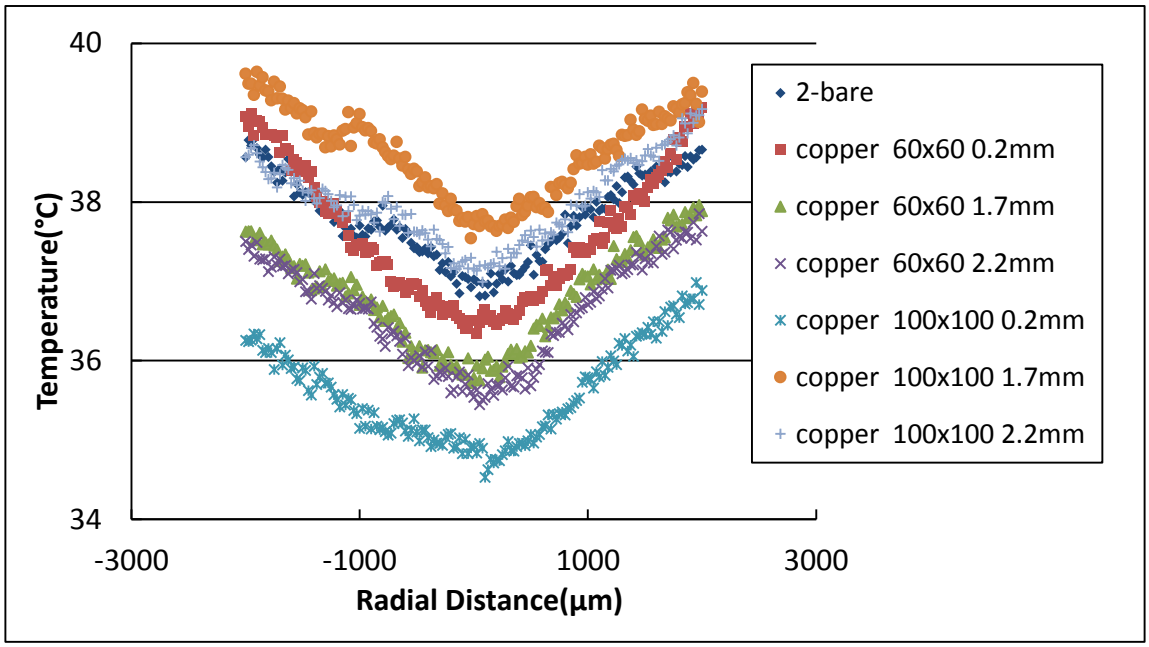

Figure 55. Temperature distribution with Copper meshes under hole size of 2.5 mm of screen laminate, flowrate at 160 ml/hr, frequency at 5000 Hz and heat flux at 8.9 W/cm^2

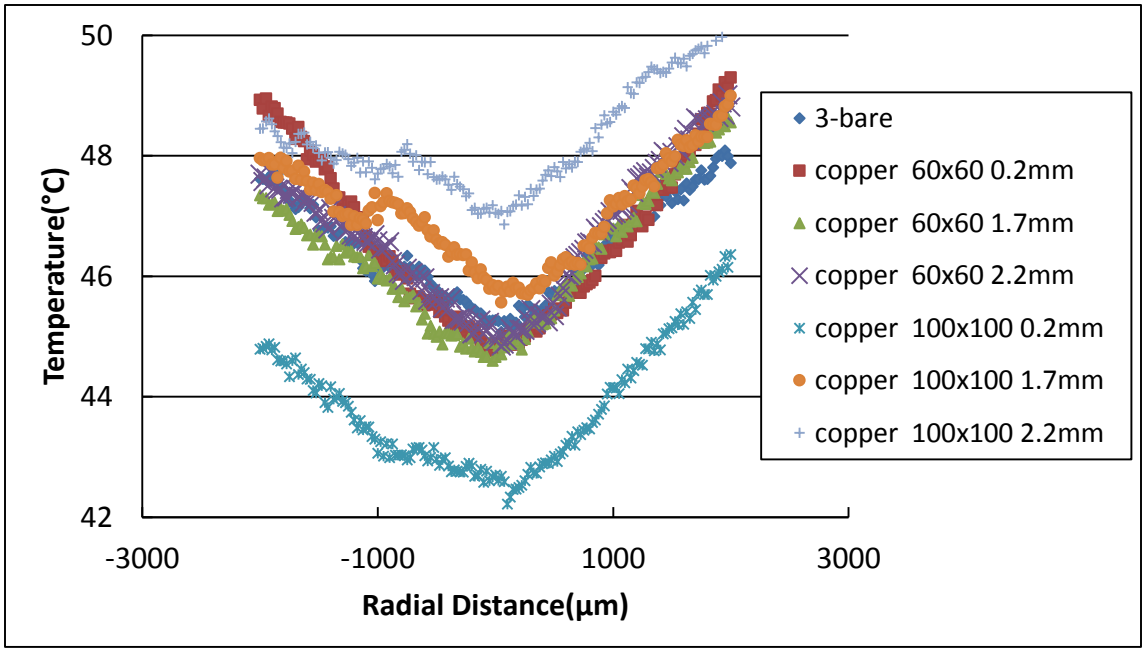

Figure 56. Temperature distribution with Copper meshes under hole size of 2.5 mm of screen laminate, flowrate at 160 ml/hr, frequency at 5000 Hz and heat flux at 12.86 W/cm^2

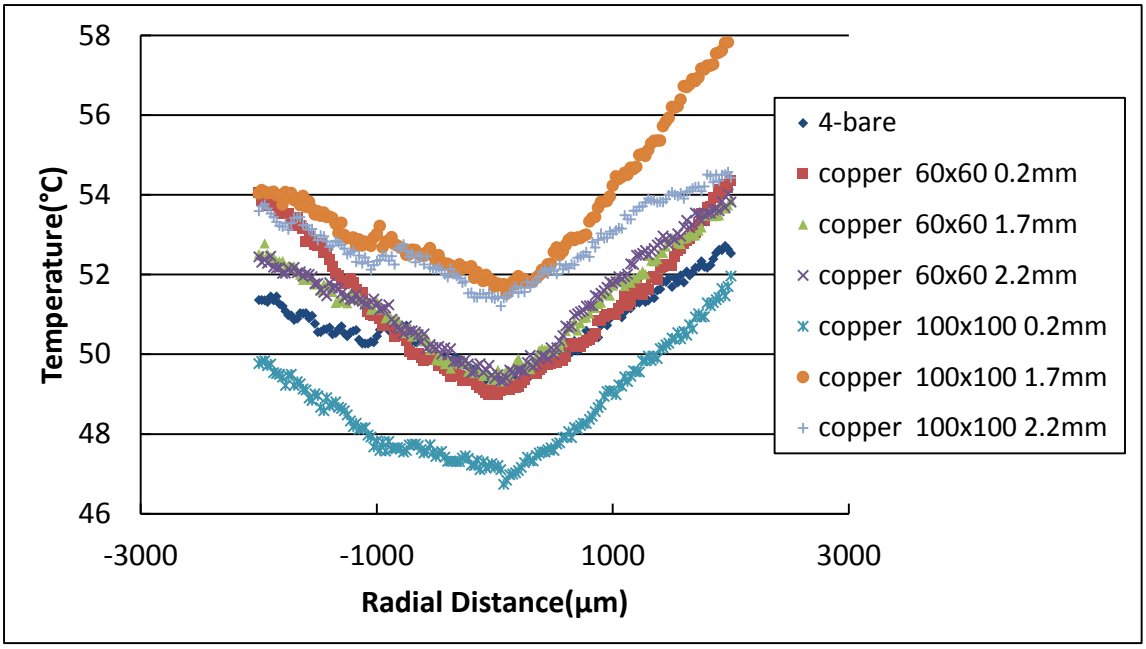

Figure 57. Temperature distribution with Copper meshes u under hole size of 2.5 mm of screen laminate, flowrate at 160 ml/hr, frequency at 5000 Hz and heat flux at 14.64 W/cm^2

From Figures 54 - 57, the copper mesh with size of 100x100 and the gap distance at 0.2 mm worked the best, for which the minimum temperature was lower than that of the bare surface and also the lowest among all the tested laminates or meshes. The results indicate that the finest filaments could provide the best cooling performance. Furthermore, the high thermal conductivity of copper should have also contributed to the high heat transfer rate as mentioned above. Furthermore, when the gap between mesh and heating surface was decreased, the temperature profile moved downwardly. In the case of single droplet stream, the film thickness was measured to be about 80 µm by Tsai [16], so it appears that the a small gap distance (0.2 mm or 200 µm) of the fine screen laminate could ensure adequate contact with the liquid layer outside the impingement zone but it was high enough not to disrupt the formation of the thin liquid film within the

impingement zone. In summary, surface density and gap distance of the screen laminate can enhance heat transfer under the right conditions.

4.4.2 Effect of screen laminates center hole sizes in triangulated droplet streams experiments

The effect of screen laminate hole size on droplet stream cooling was also considered by using copper as mesh material. A copper mesh of 100x100 size with gap distance at 0.2 mm (200 μm) was used.

For triple stream droplets experiments, both 500 μm and 1000 μm droplet spacing were used because droplet spacing effect on cooling varies with different center hole sizes.

Figure 58-60 are temperature distribution of 1000 μm impact craters spacing, and Figure 61-63 are 500 μm impact craters spacing.

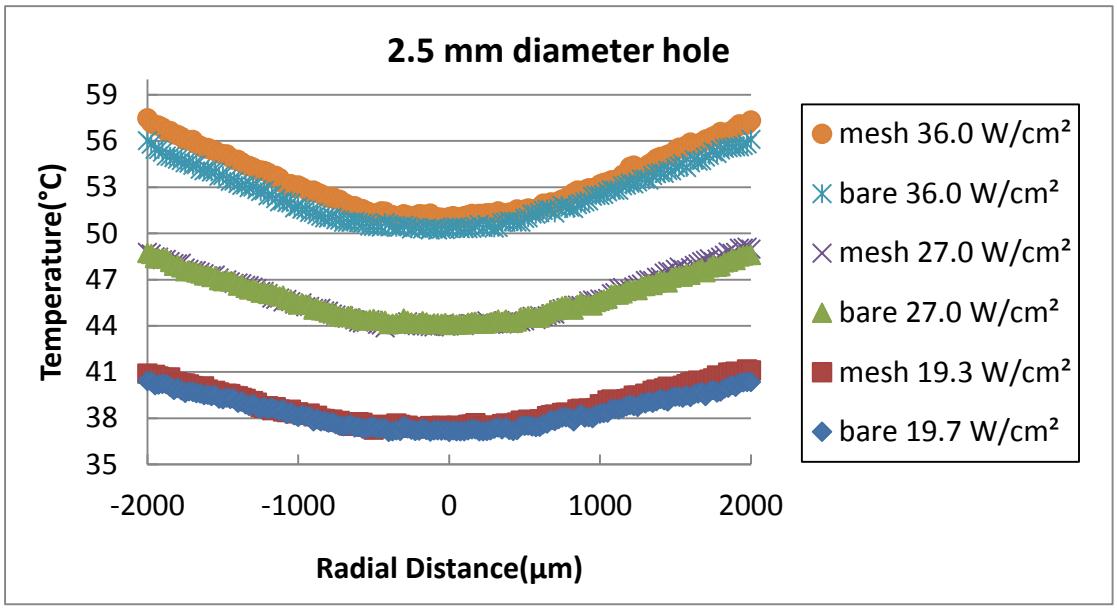

Figure 58. Temperature distribution of triangulated droplet steam with Copper meshes with a center hole at 2.5mm, size at 100x100 and gap distance at 0.2 mm, flowrate at 480 ml/hr, frequency at 5000 Hz, spacing of 1000 µm and different heat fluxes

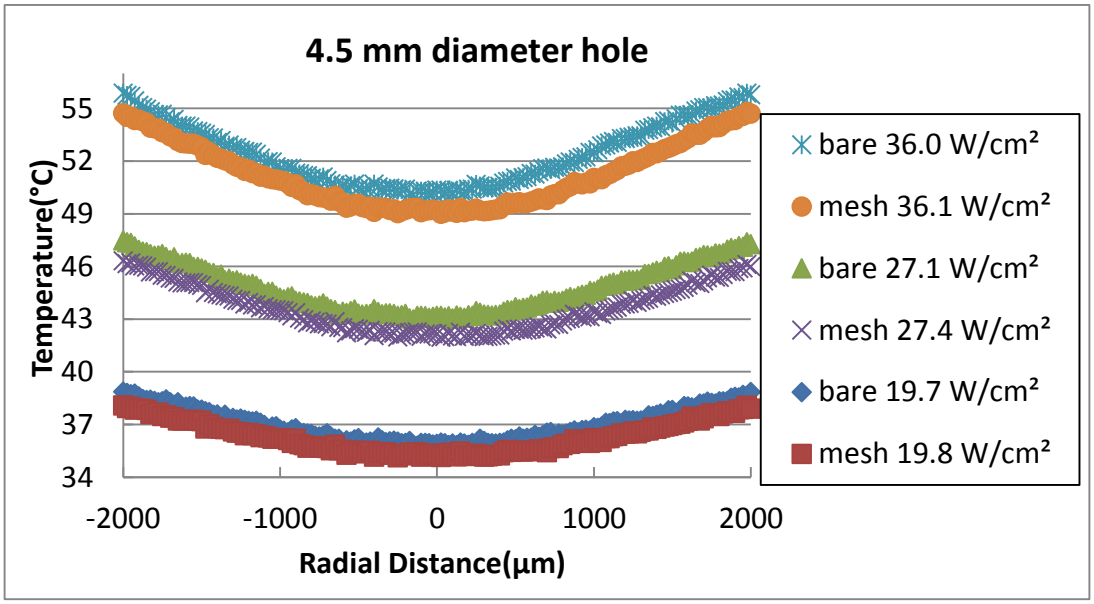

Figure 59. Temperature distribution of triangulated droplet steam with Copper meshes with a center hole at 4.5mm, size at 100x100 and gap distance at 0.2 mm, flowrate at 480 ml/hr, frequency at 5000 Hz, spacing of 1000 µm and different heat fluxes

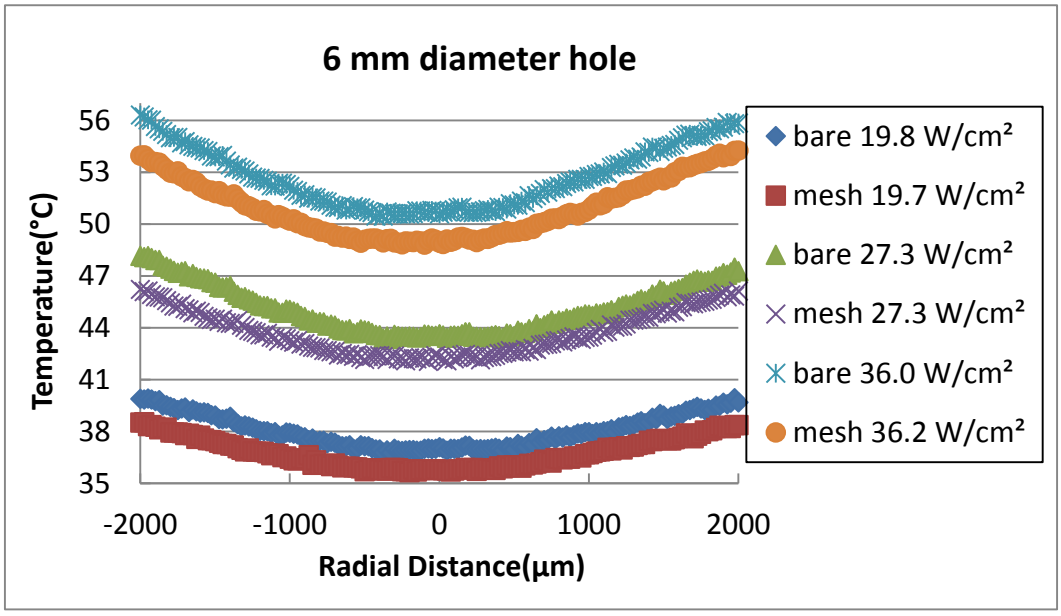

Figure 60. Temperature distribution of triangulated droplet steam with Copper meshes with a center hole at 6 mm, size at 100x100 and gap distance at 0.2 mm, flowrate at 480 ml/hr, frequency at 5000 Hz, spacing of 1000 µm and different heat fluxes

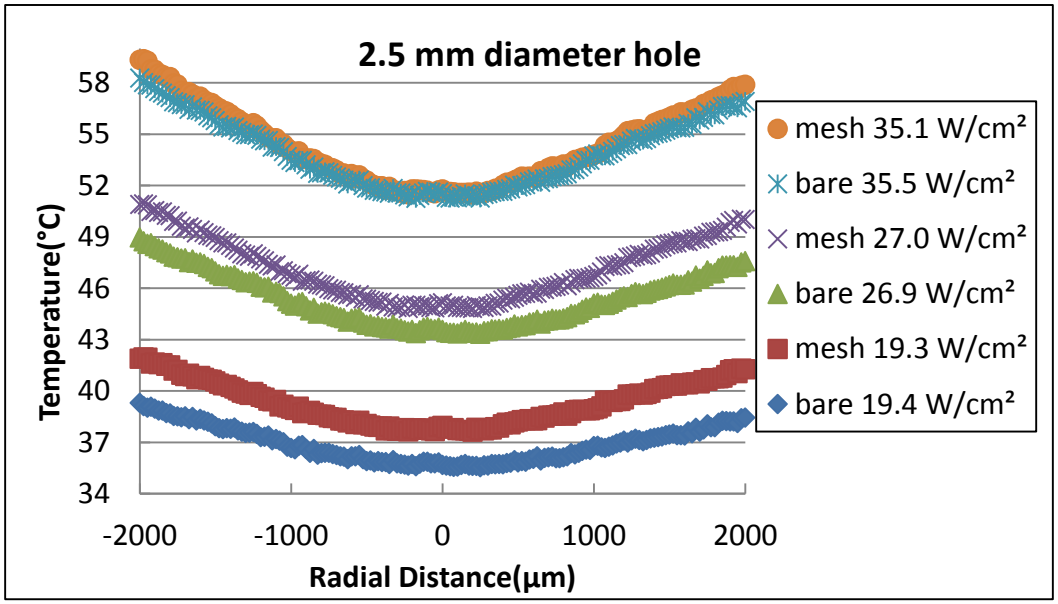

Figure 61. Temperature distribution of triangulated droplet steam with Copper meshes with a center hole at 2.5mm, size at 100x100 and gap distance at 0.2 mm, flowrate at 480 ml/hr, frequency at 5000 Hz, spacing of 500 µm and different heat fluxes

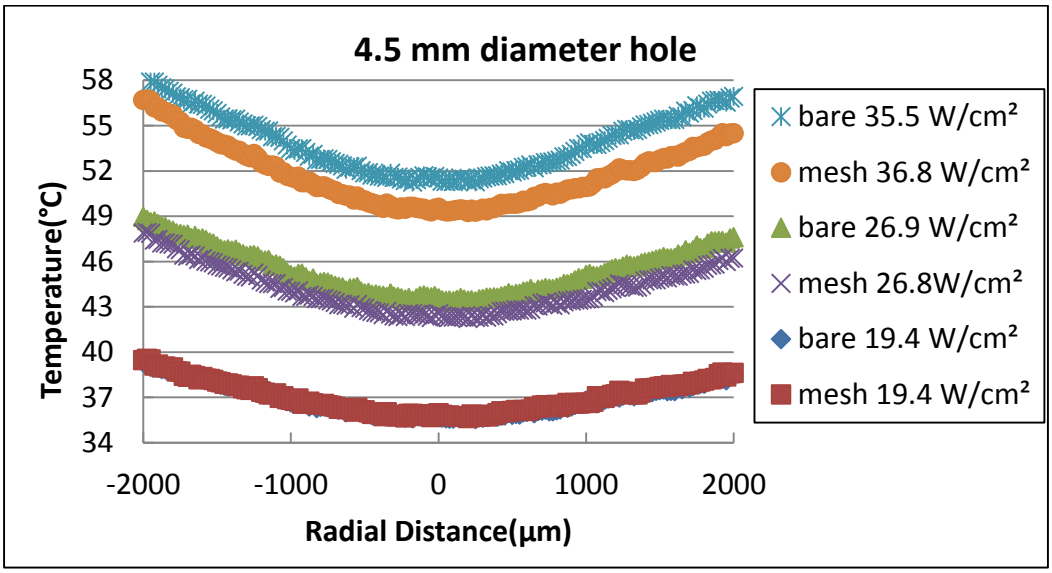

Figure 62. Temperature distribution of triangulated droplet steam with Copper meshes with a center hole at 4.5mm, size at 100x100 and gap distance at 0.2 mm, flowrate at 480 ml/hr, frequency at 5000 Hz, spacing of 500 µm and different heat fluxes

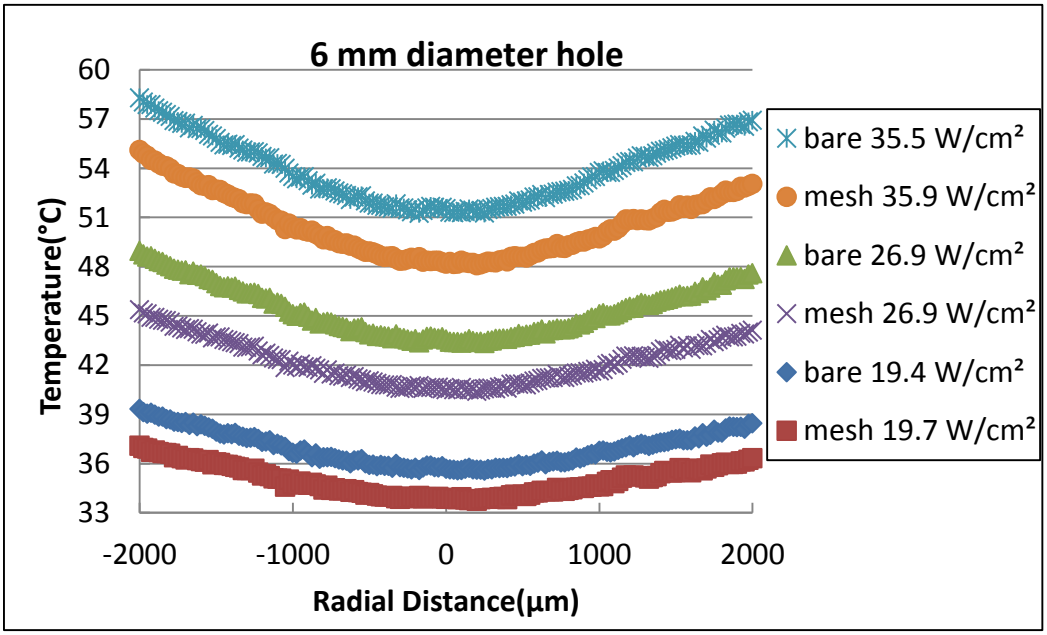

Figure 63. Temperature distribution of triangulated droplet steam with Copper meshes with a center hole at 6 mm, size at 100x100 and gap distance at 0.2 mm, flowrate at 480 ml/hr, frequency at 5000 Hz, spacing of 500 µm and different heat fluxes

From Figure 58, all the temperature profiles overlap with each other at all three heat fluxes. Figure 58 shows that the bare surface temperature profile is lower or equal to the 2.5 mm center hole mesh temperature profile at different heat flux conditions. This indicates that the 2.5 mm center hole mesh does not enhance cooling performance. However, for the 4.5 mm center hole temperature profile in Figure 59 and 6 mm center hole temperature profile in Figure 60, the temperature distribution profiles are lower than the bare surface temperature profile, which indicates that the boiling phenomena on heating surface with screen laminates was suppressed and the cooling performance was enhanced. Moreover, the 6 mm hole size mesh temperature profile appears to be more effective than the 4.5 mm hole size mesh because surface was able to reach the lower (or lowest temperature difference between mesh and bare surface, $T_{min,mesh}$-$T_{min,bare}$), which indicates that the bigger hole size leads to better performance. For Figures 61-63, the results of 500 μm cases are consistent with the 1000 μm results.

Figure 64 and 65 show the minimum temperature with different mesh center hole sizes under different heat flux conditions. In Figure 64, the slope of 6 mm center hole trend line is 6.3 % more than the slope of bare surface trend line, the intersection of the 6 mm center hole trend line is 0.73 % larger than the intersection of bare surface trend line. Moreover, in Figure 65, the slope of 6 mm center hole trend line is 0.42 % less than the slope of bare surface trend line, the intersection of 6 mm center hole trend line is 8.64 % smaller than the intersection of bare surface trend line. From Figure 64, it is evident that

the screen laminate enhances the convection process as the surface temperature increases at small droplet stream spacing (500 μm). On the other hand, at larger droplet stream spacing (1000 μm) the enhancement in convection is independent of temperature as seen in Figure 65.

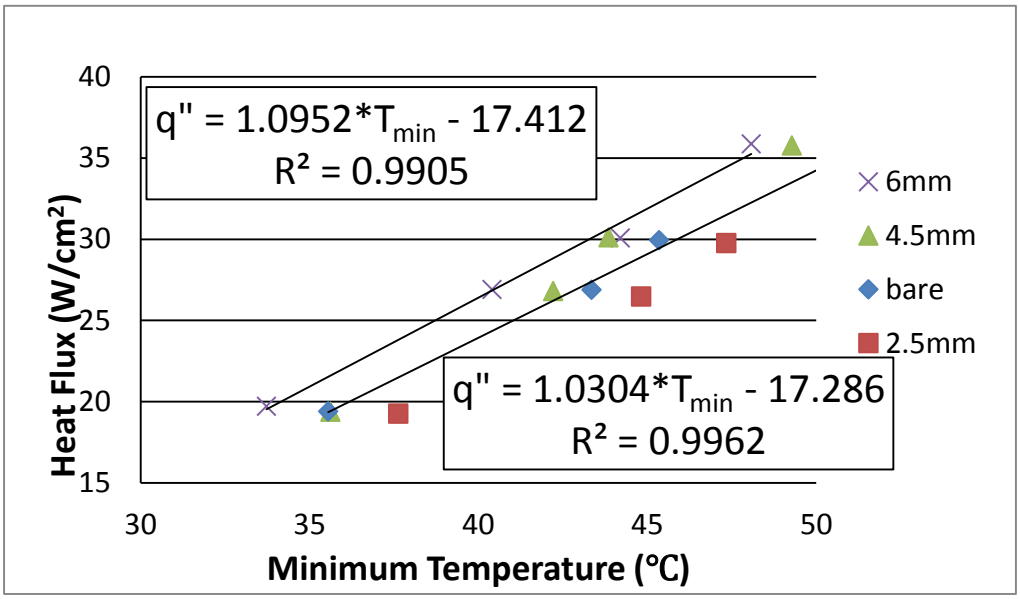

Figure 64. Minimum temperature for triple droplets stream with and without copper mesh under 500 μm spacing and different heat flux conditions

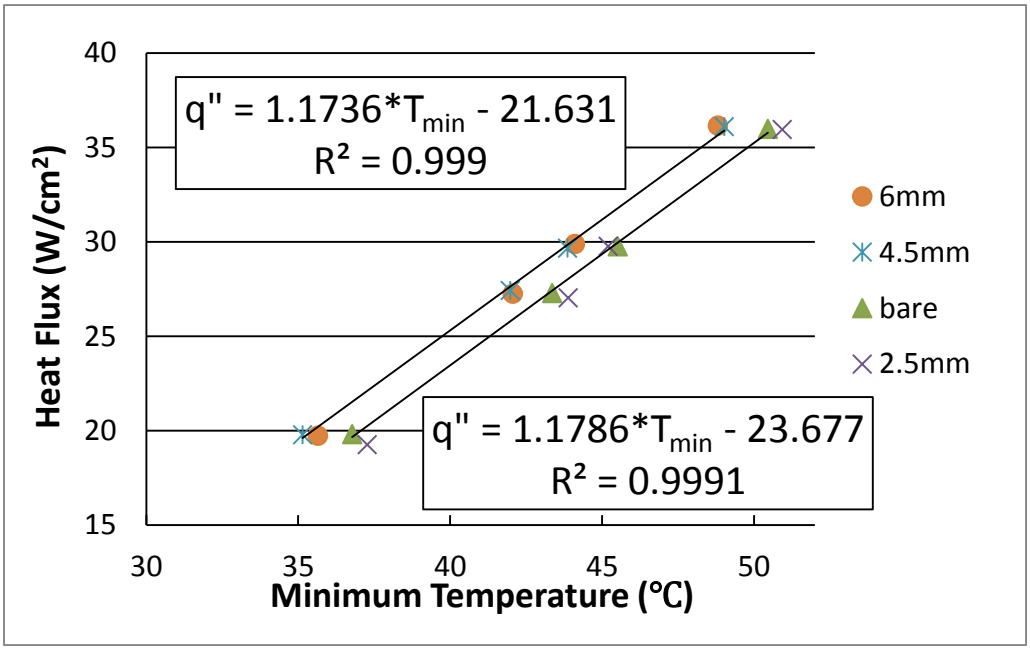

Figure 65. Minimum temperature for triple droplets stream with and without copper mesh under 1000 µm spacing and different heat flux conditions

Figure 66-71 show the High Speed Camera (HSC) images taken from a 45º degree angle for all the 1000 µm spacing experiments. Through these figures, the effect of using screen laminates can be appreciated a bit more. HSC figures were compared between the no heat flux and the highest heat flux (36 W/cm^2) conditions.

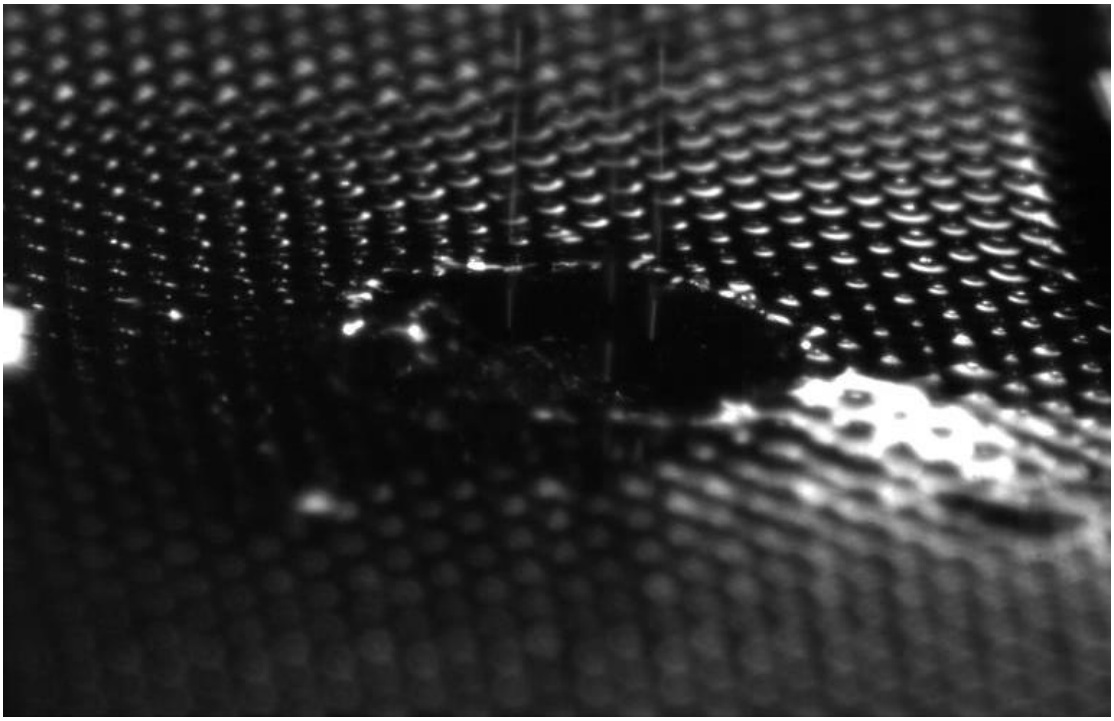

Figure 66. Triple stream droplets at 1000 µm spacing, with 100x100 copper mesh with 2.5 mm center hole with no heat flux

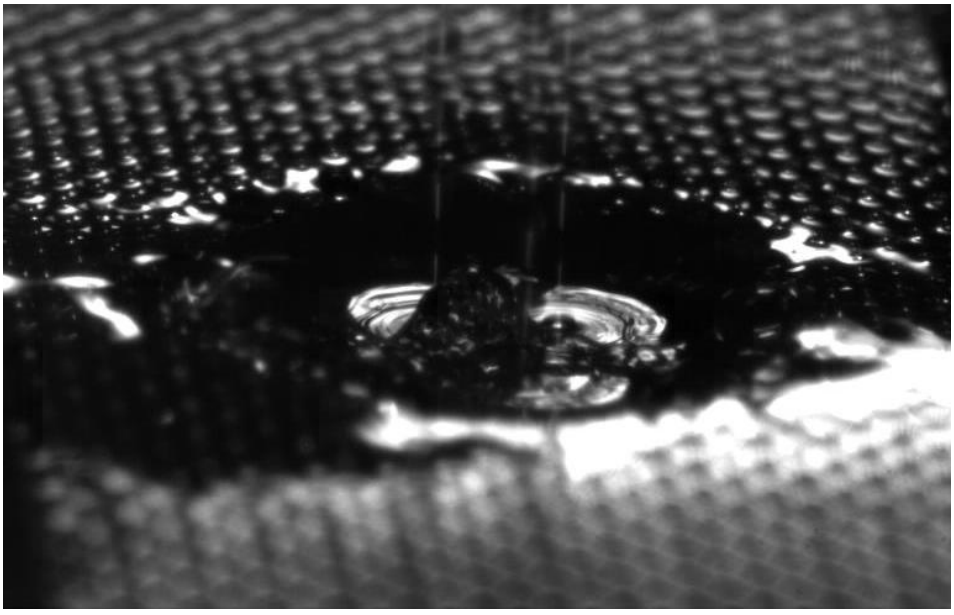

Figure 67. Triple stream droplets at 1000 µm spacing, with 100x100 copper mesh with 4.5 mm center hole with no heat flux

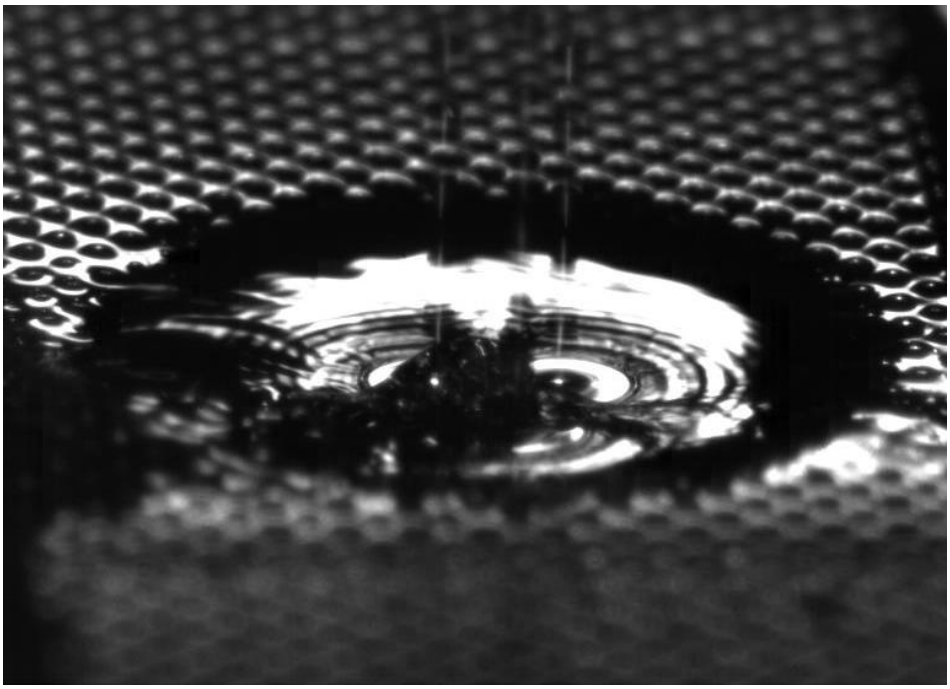

Figure 68. Triple stream droplets at 1000 μm spacing, with 100x100 copper mesh with 6 mm center hole with no heat flux

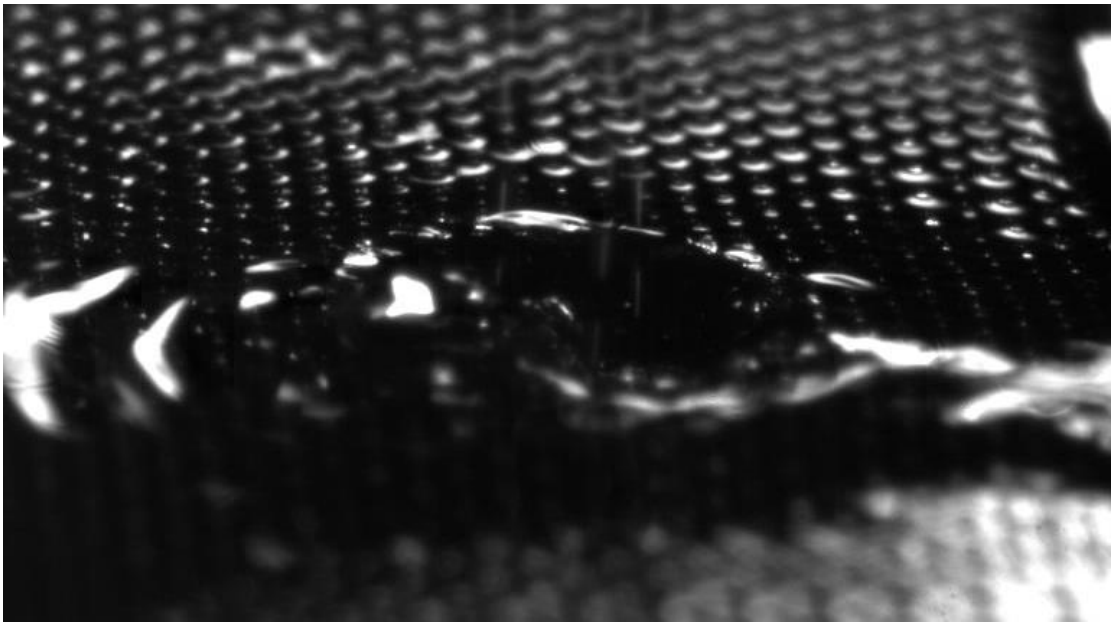

Figure 69. Triple stream droplets at 1000 μm spacing with 100x100 copper mesh with 2.5 mm center hole with heat flux at 36 W/cm^2

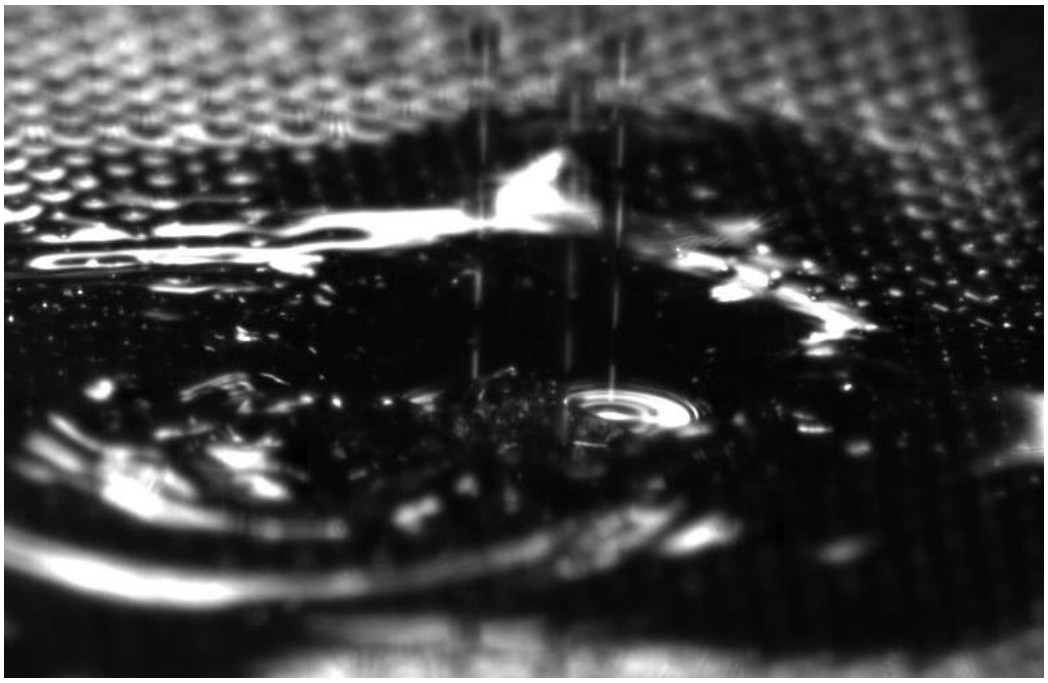

Figure 70. Triple stream droplets at 1000 µm spacing with 100x100 copper mesh with 4.5 mm center hole with heat flux at 36 W/cm^2

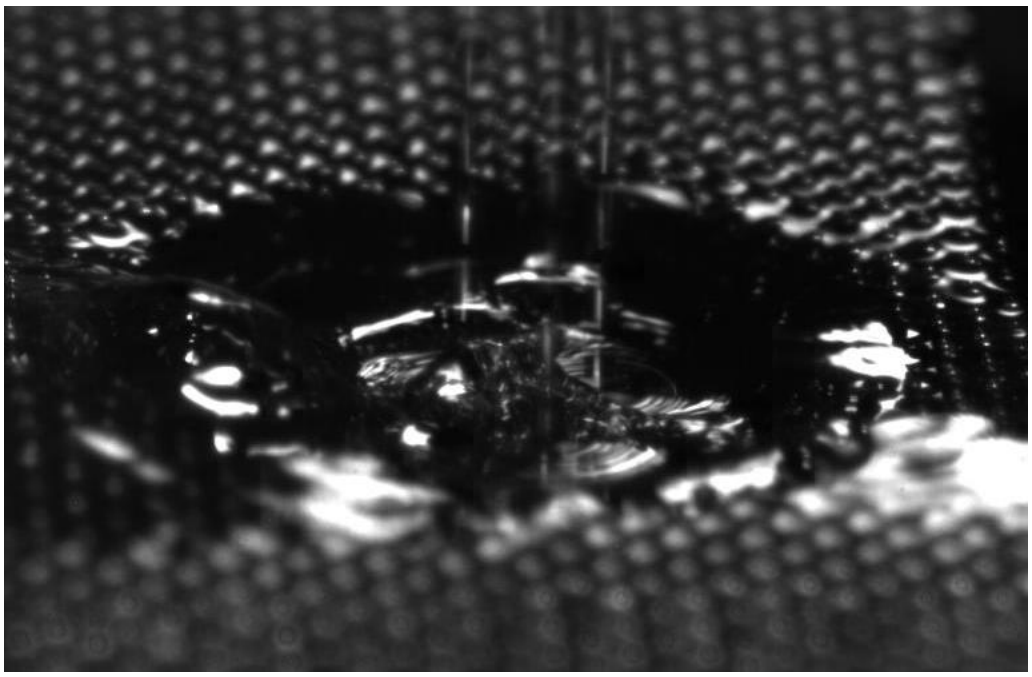

Figure 71. Triple stream droplets at 1000 µm spacing with 100x100 copper mesh with 6 mm center hole with heat flux at 36 W/cm^2

Liquid accumulation can be observed at 2.5 mm and 4.5 mm center hole cases (Figures 66 and 67), which indicates that the cooling fluid formed a relatively large liquid film between the mesh and heating surface which reduce cooling efficiency. So when the surface was heated, the liquid accumulation phenomenon should have taken place as observed through Figures 69 and 70 for the 2.5 mm and 4.5 mm center hole cases. When the center hole size approached 6 mm in Figure 71, the liquid film had no contact with the mesh, which means that the cooling fluid evaporates downstream from the impact crater, which could have improved cooling efficiency. Furthermore, increased contact between the mesh layers and the heater surface led to an increased in effective thermal conductivity, which also contributed to improve heat transfer.

Figure 72 shows the High Speed Camera images for the 500 μm spacing cases. Splashing is observed which indicates that 500 μm impact craters spacing is too small for cooling enhancement. Although the temperature distribution profiles show that the cooling performance is still enhanced with 6 mm center hole mesh, but splashing still affect the cooling efficiency somewhat.

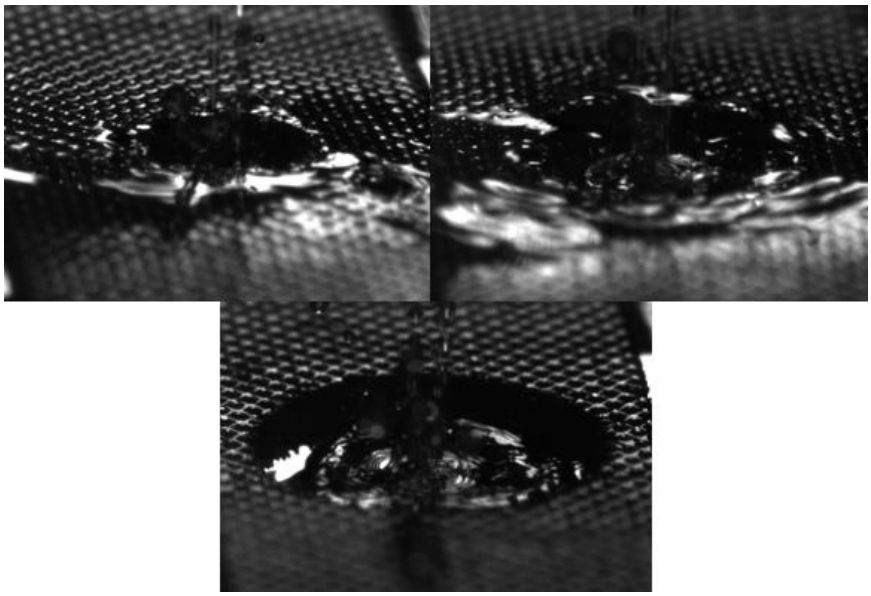

Figure 72. Triple stream droplet at 500 µm spacing with 100x100 copper mesh with 2.5mm, 4.5mm and 6mm center hole and heat flux at 36 W/cm^2

Figure 73 – 76 present IR images under conditions at 1000 µm spacing, 480 ml/hr flowrate and 5000 Hz droplet impingement frequency with and without mesh. The isotherm circle shown in the images corresponds for the boiling point of HFE-7100 (61 ^{o}C), which increases with the mesh hole size. From the figures, it is evident that the effective cooling area (area encircled by the isotherm) increases with mesh hole size.

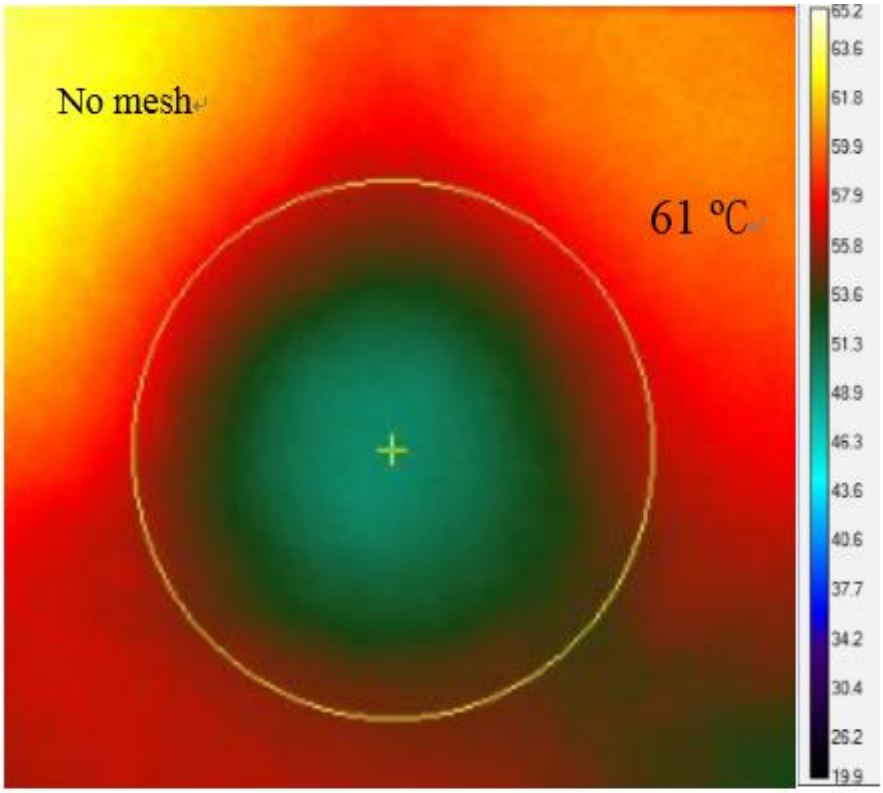

Figure 73. Triple stream droplets at 1000 µm spacing, 480 ml/hr flowrate and 5000 Hz frequency without mesh

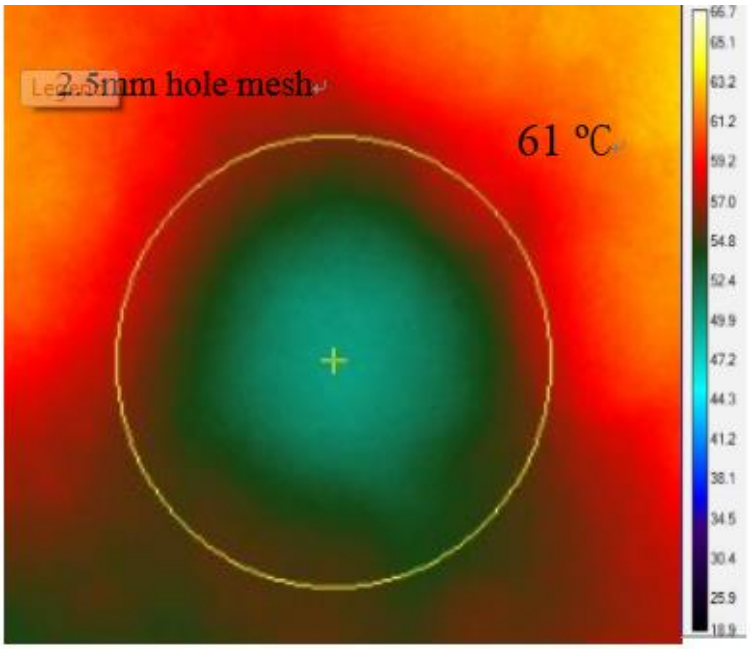

Figure 74. Triple stream droplets at 1000 µm spacing, 480 ml/hr flowrate and 5000 Hz frequency with 2.5 mm diameter center hole mesh

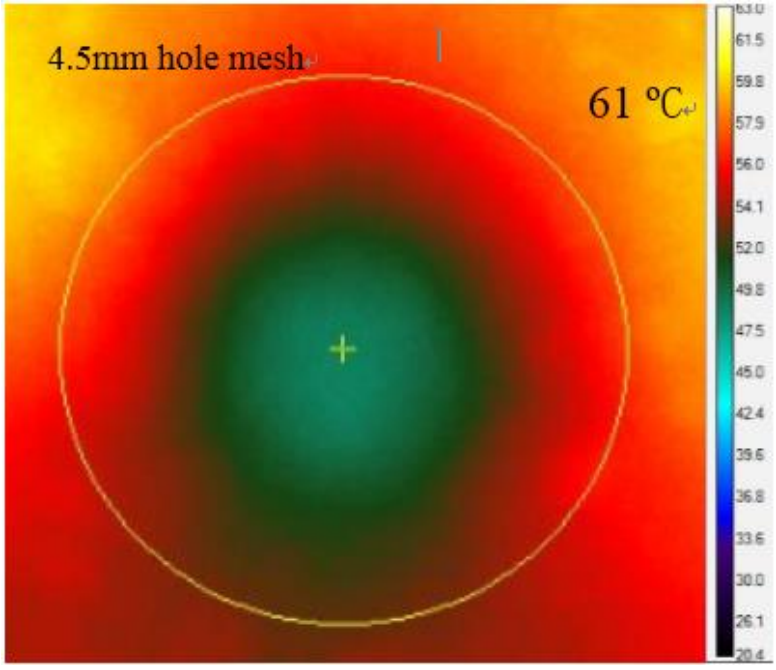

Figure 75. Triple stream droplets at 1000 µm spacing, 480 ml/hr flowrate and 5000 Hz frequency with 4.5 mm diameter center hole mesh

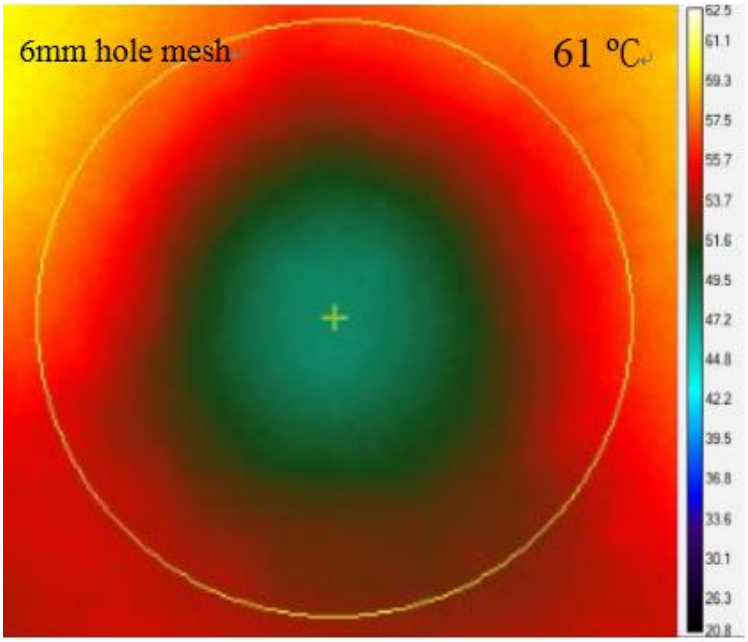

Figure 76. Triple stream droplets at 1000 µm spacing, 480 ml/hr flowrate and 5000 Hz frequency with 6 mm diameter center hole mesh

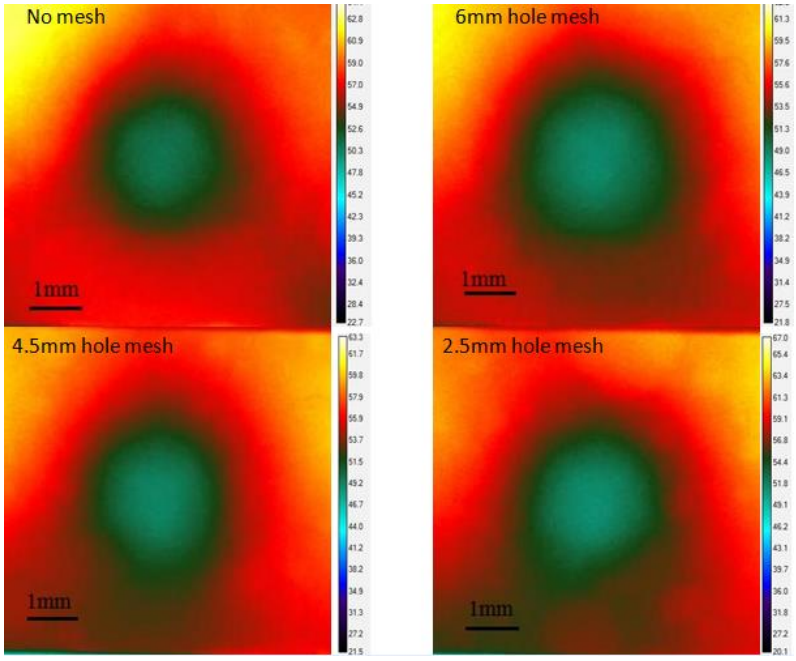

Figure 77. IR image comparison of impact craters for triple droplets streams with 1000 µm spacing, 480 ml/hr flowrate and 5000Hz frequency

Figure 77 shows the original images taken by IR camera without the isotherm lines. The impact craters appears to be enlarged by the screen laminates, especially when using the 6 mm center hole mesh, which indicates that the screen laminates has the effect of enlarging the cooling area by as much as 44.8% and 68.2% for the 4.5 mm and 6 mm hole size, respectively. When the center hole was 6 mm, the cooling area was the biggest with the lowest surface temperature among all the cases. All experimental data suggest that screen laminates or meshes lead to an increase in the effective cooling area. The exact mechanism by which the area increases is not clearly understood; however, the meshes seem to increase the bubble departure rate where the surface temperature exceeds the boiling point of HFE-7100 as seen in other studies [21]. As the experimental data suggest, the larger holes are more effective in terms of heat transfer enhancement, which can be attributed to the departure of bubbles at an optimal radial distance from the impingement zone. It can be implied that enhanced bubble departure induced by the copper mesh help drive the impinged liquid film away from the impingement zone resulting in a thinner liquid film and enhanced convection.

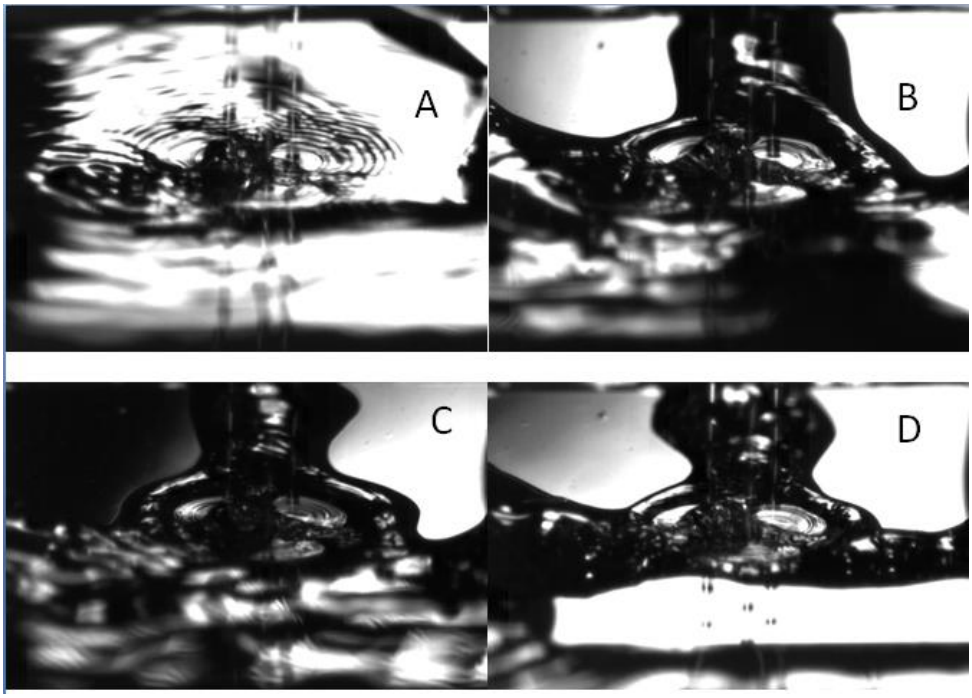

Figure 78. Triple streams at 1000 µm spacing, 5000 Hz frequency, 480 ml/hr flowrate and different heat fluxes, without mesh

From Figure 78, dryout was observed when sample was heated at different heat fluxes. The dryout area increases with heat flux, which leads to a temperature gradient along the surface. From Figures 69 - 71, dryout was not observed for the tests with mesh. With triple droplets stream, the impinged liquid film seems to spread more easily with the mesh which helps cool the surface uniformly.

5. CONCLUSION

Single stream droplet impingement cooling at different flowrates and frequencies was performed to investigate the effect of them on heat transfer. Triple stream droplet impingement cooling at different flowrates, frequencies and spacing was performed to investigate the effect of them on heat transfer. Single streams droplet impingement with screen laminates at different height between mesh and heating surface and material were also tested to understand their effects on surface cooling. Triple streams droplet impingement with screen laminates at center hole sizes and impact craters spacing were also tested to understand their effects on surface cooling. The droplet and impact crater images were captured using a high speed imaging system. An infrared thermal imaging technique was used to measure surface temperature within the heat transfer area.

From single stream thermal images results, the temperature curve shifts upwardly when the heat flux increases. Furthermore, the temperature within the impact crater at high heat flux is below the boiling point of HFE (60 °C), indicating that the droplet streams impinging on the surface suppresses the onset of boiling within the impact crater. Moreover, the results suggest that the interaction between larger impinging droplets and the fluid at the surface could be playing a significant role in terms of surface cooling. Pointedly, it could be inferred that larger droplets lead to greater microscale capillary waves at the solid-liquid interface.

From triple streams thermal images results, ejection phenomenon was observed in the adjacent area between two impact craters which led to the lower and stable temperature distribution. Furthermore, impact craters spacing was presented to be a significant parameter in the triangulated fashion spray cooling considered the effect of splashing. In addition, the effect of flowrate and frequency consisted with the single stream droplets experiments results.

From single stream droplets experiments with screen laminates or meshes, it is inferred that aluminum meshes interrupt the evaporation of cooling fluid on the heating surface. Moreover, it appears that the relatively high specific heat of aluminum (903 J/kg-k) which is comparable to the specific heat of HFE-7100, reduce the fluids ability to dissipate heat effectively. Furthermore, the thermal conductivity of aluminum is about 237 W/m-K which is 40% than for copper. In general, aluminum is not the right material which can suppress the boiling in impact craters. Furthermore, the results also show that coarse meshes at close proximity to the heater surface are detrimental in terms of heat transfer. Moreover, the copper mesh with size of 100x100 and the gap distance at 0.2 mm worked the best, which indicates that the finest filaments could provide the best cooling performance.

From triple streams droplets experiments with screen laminates or meshes, size of center hole is a significant parameter which indicates that the boiling phenomena on heating surface with screen laminates was suppressed and the cooling performance was

enhanced. Moreover, the screen laminate enhances the convection process as the surface temperature increases at small droplet stream spacing (500 μm). On the other hand, at larger droplet stream spacing (1000 μm) the enhancement in convection is independent of temperature. Furthermore, increased contact between the mesh layers and the heater surface led to an increased in effective thermal conductivity, which also contributed to improve heat transfer. Furthermore, the larger holes are more effective in terms of heat transfer enhancement, which can be attributed to the departure of bubbles at an optimal radial distance from the impingement zone. It can be implied that enhanced bubble departure induced by the copper mesh help drive the impinged liquid film away from the impingement zone resulting in a thinner liquid film and enhanced convection.

REFERENCES

[1] Mudawar, I., 2001, "Assessment of high-heat-flux thermal management schemes," IEEE Transactions on Components and Packaging Technologies, 24(2) pp. 122-141.

[2] Monde, M., 1979, "Critical heat flux in the saturated forced convection boiling on a heated disk with impinging droplets," Heat Transfer - Japanese Research, 8(2) pp. 54-64.

[3] Mudawar, I., and Deiters, T. A., 1994, "Universal approach to predicting temperature response of metallic parts to spray quenching," International Journal of Heat and Mass Transfer, 37(3) pp. 347-362.

[4] I. A. Kopchikov, G. I. Voronin, T. A. Kolach, D. A. Labuntsov and P. D. Lebedev, 1969, "Liquid boiling in a thin film", International Journal of Heat and Mass Transfer, 12 (7) pp. 791-796.

[5] S. Toda, 1972. "Study of mist cooling: 1st report: investigation of mist cooling," Heat Transfer - Japanese Research, 1(3) pp. 39–50,

[6] S. Toda, 1974. "Study of mist cooling 2: Theory of mist cooling and its fundamental experiments," Heat Transfer – Japanese Research, 1(3) pp. 1–44.

[7]D. E. Tilton, "Spray cooling," Ph.D. dissertation, University of Kentucky, Lexington, 1989.

[8]J. E. Navedo, "Parametric effects of spray characteristics on spray cooling heat transfer," Ph.D. dissertation, University of Central Florida, Orlando, 2000.

[9] L. Ortiz and J. E. Gonzalez, 1999. “Experiments on steady-state high heat fluxes using spray cooling,” Experimental Heat Transfer, 12(3) pp. 215-233

[10] K. A. Estes and I. Mudawar, 1995. “Correlation of sauter mean diameter and critical heat flux for spray cooling of small surfaces,” International Journal of Heat and Mass Transfer, 38(16) pp. 2985-2996

[11] C. Cho and R. Ponzel, “Experimental study on the spray cooling of a heated solid surface,” in Proceedings of the 1997 ASME International Mechanical Engineering Congress and Exposition, November 16 – 21, 1997, vol. 244, pp. 265–272, ASME.

[12] Y. Tao, X. Huai, Lei Wang, Z. Guo, 2011. "Experimental characterization of heat transfer in non-boiling spray cooling with two nozzle," Applied Thermal Engineering, 31 (10) pp. 1790 -1797

[13] Z. Zhang, J. Li, P. Jiang, 2013. "Experimental investigation of spray cooling on flat and enhanced surfaces," Applied Thermal Engineering 51(2) pp. 102-111

[14] Z. B. Yan, F. Duan, T. N. Wong, K. C. Toh, K. F. Choo, P. K. Chan, Y. S. Chua, L. W. Lee, 2013. "Large area impingement spray cooling from multiple normal and inclined spray nozzles," Heat Mass Transfer, 49 (2) pp, 985–990

[15] D. Fabris, S. Escobar-Vargas, J E. Gonzalez, R. Sharma and C. Bash, " 2012, Monodisperse spray cooling of small surface areas at high heat flux," Heat Transfer Engineering, 33(14) pp, 1161–1169,

[16] H. Tsai, “Study of the effects of single and double droplets impingement on surface cooling,” MS. dissertation, Texas A&M University, College Station. 2011.

[17] A. G. Pautsch, and T. A. Shedd, 2005. “Spray impingement cooling with single and multiple nozzle arrays. Part I: Heat transfer data using FC-72,” Int. J. Heat Mass Transfer, 48(15) pp 3167-3175.

[18] Y. Hou, Y. Tao, X. Huai, Z. Guo, 2012. "Numerical characterization of multi- nozzle spray cooling", Applied Thermal Engineering, 39(1) pp. 163-170

[19] G. Soriano, "Study the physics of droplet impingement cooling," Ph.D. dissertation, Texas A&M University, College Station, 2011.

[20] Y.Lin, "Doplets impingement cooling experiments on nano-structured surfaces", MS. Dissertation, Texas A&M University, College Station. 2010.

[21] B. Holland, N. Ozman, R.A. Wirtz, 2008, "Flow boiling of FC-72 from a screen laminate extended surface matrix," Microelectronics Journal, 39 (7) pp. 1001 – 1007.

[22] Sloan A., S. Penley and R. A. Wirtz, “Sub-Atmospheric pressure pool boiling of water on a screen laminate-enhanced surface,” 25th Annual IEEE Semiconductor Thermal Measurement and Management Symposium [1065-2221], 2009 pp. 246 -253

[23] Li, C. and G.P. Peterson, 2007. “Parametric study of pool boiling on horizontal highly conductive microporous coated surfaces”, ASME JHT, 129(11) pp. 1465 – 1475.

[24] M F. Trujillo, J. Alvarado, E. Gehring, G S. Soriano, “Numerical simulations and experimental characterization of heat transfer from a periodic impingement of droplets,” Journal of Heat Transfer 133(12), 122201.

[25] T. Zhang, H. Tsai, J L. Alvarado, “Effects of single and double streams of droplet impingements on surface cooling,” Atomization and Sprays, Accepted for publication in 2014.

APPENDIX A

A. Emissivity measurement and uncertainty analysis

In this project research, Standard ASTM E1933 "Standard test methods for measuring and compensating for emissivity using infrared imaging radiometers " was used.

The procedure indicated in the standard was followed using the experimental setup shown in Figure 79. Firstly, an aluminum foil was attached as the reflective foil (as shown in Figure 80). Secondly, the black tape was attached onto the ceramic sample with the heater sample just besides it (as shown in Figure 81). In the end, both the reflective foil and the ceramic sample was heated so their temperature is at least 30 ℃ above the surrounding temperature, then measured the irradiance counts from the target and aluminum foil. Infrared imaging of the target was shown in Figure 82.

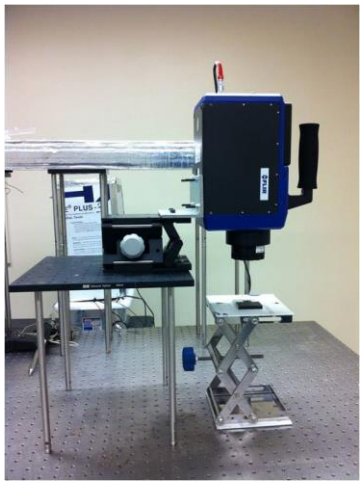

Figure 79. Experimental setup

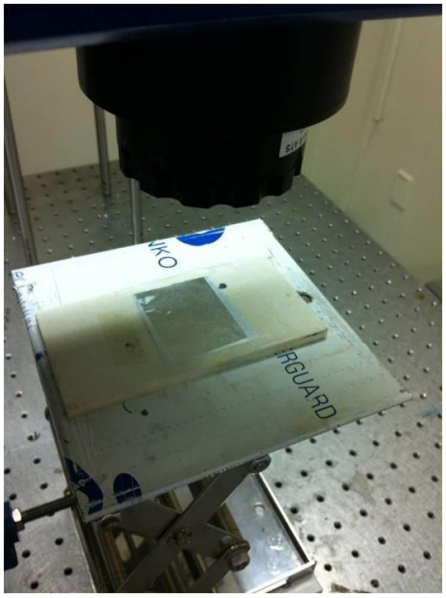

Figure 80. Reflective foil

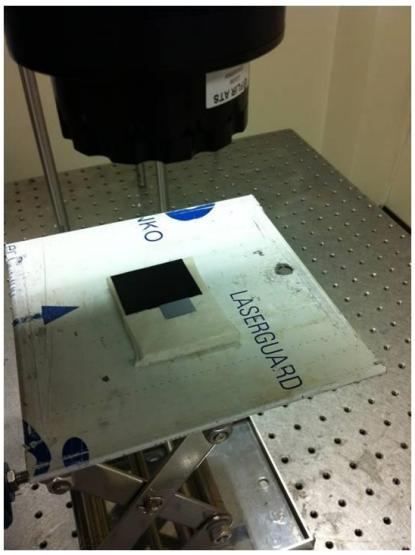

Figure 81. Black tape and heater sample

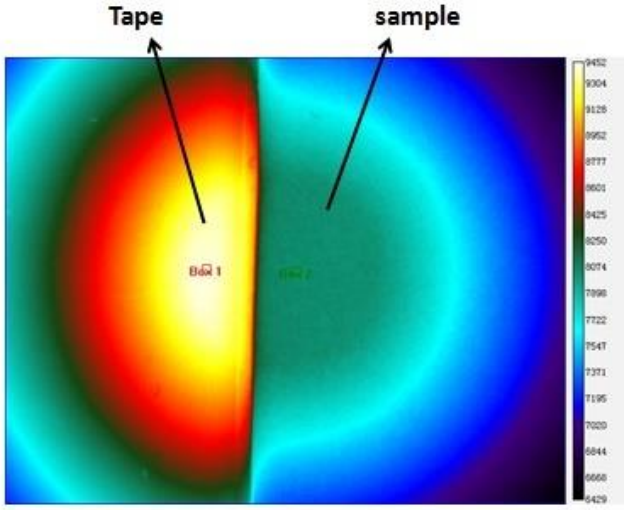

Figure 82. IR image

According to the ASTM Standard, the emissivity was calculated with following equation:

$$\varepsilon_{obj} = \frac{D_{obj} - D_{sur}}{D_{ref} - D_{sur}} * \varepsilon_{ref} \quad (1)$$

Where D represents the digital reading of the camera in number of counts. The reference used for this measurement was an electrical vinyl tape Super 88 with a known emissivity value of ε=0.95±0.05. The calculated emissivity values at different temperatures are listed at Table 11:

Table 11. Emissivity measurement

Temperature(℃)	D_{obj}	D_{ref}	D_{sur}	Emissivity	Error propagation
62	8276.9	9484.7	2916	0.775	0.0408
61.6	8229.9	9429.8	2940	0.774	0.0407
61.3	8187.7	9375	2957	0.774	0.0407
66.5	9017	10508.3	2826	0.766	0.0403
67	9103.2	10622.8	2842.3	0.764	0.0402
66.2	8987.4	10444.4	2891.2	0.767	0.0403
71.6	9997.6	11776.7	2891.8	0.76	0.04
71.3	9922.2	11687.9	2981.5	0.757	0.0398
71.9	10081	11855.9	2955.4	0.761	0.04
74.8	10626	12610	2966.5	0.755	0.0397
75.2	10728	12722.4	2978.2	0.756	0.0397
75.3	10718.2	12755.9	3020	0.751	0.0395

From this table, the objects emissivity vs. objective irradiance counts was plotted as follows (Figure 83), and also the trace line to get a function which can be used to calculate the emissivity at different temperatures. The function was shown as follows:

$$\varepsilon = -0.07 \ln(D_{obj}) + 1.473 \qquad (2)$$

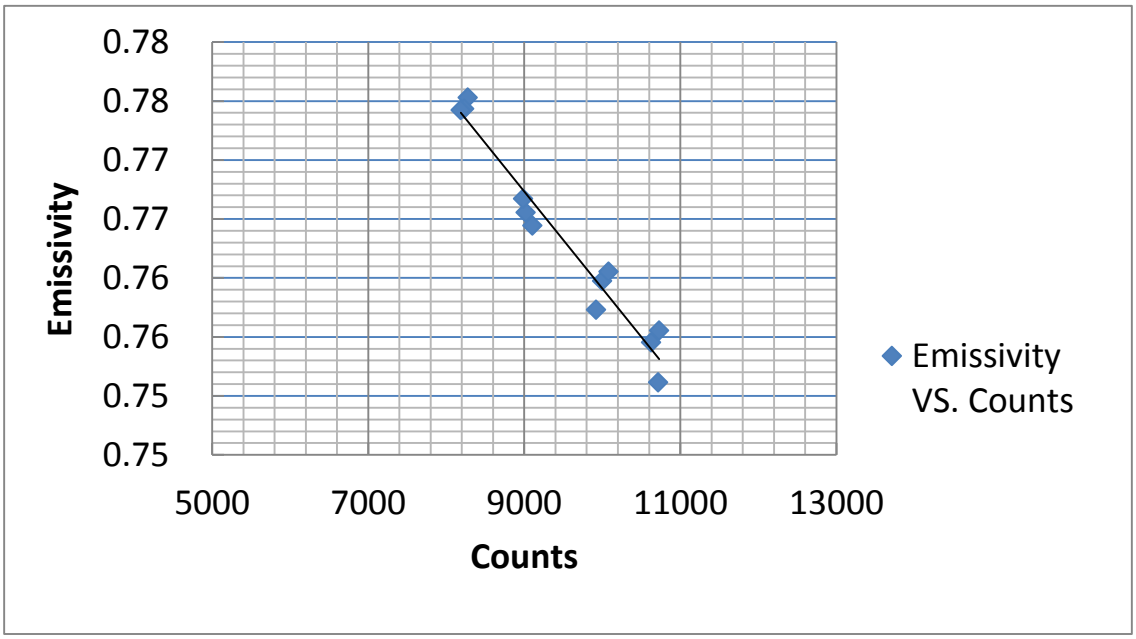

Figure 83. Emissivity vs. counts

B. Droplet diameter and droplet velocity measurement

1. Droplet diameter measurement

The droplet diameter was measured using the image analysis tool from National Instrument Vision Assistant software. The projected vertical surface area of each droplet was obtained first and then used to compute the droplet diameter. A scale of 1.5μm/pixel was used for the measurement. The uncertainty of the diameter measurement was as follows:

$$u_{d_d} = \frac{\partial d_d}{\partial A} u_A \qquad (3)$$

The droplet diameter uncertainty was found to be ±7.5μm.

2. Droplet velocity measurement

The droplet velocity was calculated through equation 4

$$v_d = L \times f \tag{4}$$

Where L is the distance between droplets and f is the frequency of the function generator. The uncertainty of the velocity measurement was given by:

$$u^2{}_{v_d} = (\frac{\partial v_d}{\partial L} u_L)^2 + \left(\frac{\partial v_d}{\partial f} u_f\right)^2 \tag{5}$$

The distance of each droplet was measured using a magnification of 4.5μm/pixel with a corresponding uncertainty of ± 20μm. Uncertainty of frequency for signal generator (BK Precision Model 4011A) was ± 10Hz. By substituting these values into Equation 5, the uncertainty of the droplet velocity was found to be ± 0.14 m/s.